creative commons

COMMONS DEED

저작자표시 **2.0** 대한민국

이용자는 아래의 조건을 따르는 경우에 한하여 자유롭게

- 이 저작물을 복제, 배포, 전송, 전시, 공연 및 방송할 수 있습니다.
- 이차적 저작물을 작성할 수 있습니다.
- 이 저작물을 영리 목적으로 이용할 수 있습니다.

다음과 같은 조건을 따라야 합니다:

저작자표시. 귀하는 원저작자를 표시하여야 합니다.

- 귀하는, 이 저작물의 재이용이나 배포의 경우, 이 저작물에 적용된 이용허락조건을 명확하게 나타내어야 합니다.
- 저작권자로부터 별도의 허가를 받으면 이러한 조건들은 적용되지 않습니다.

저작권법에 따른 이용자의 권리는 위의 내용에 의하여 영향을 받지 않습니다.

이것은 이용허락규약(Legal Code)을 이해하기 쉽게 요약한 것입니다.

Disclaimer

dCollection

A THESIS

FOR THE DEGREE OF DOCTOR OF PHILOSOPHY

Metal-Organic Frameworks (MOFs) Incorporated Polymeric Membranes for the Removal of Hazardous Materials from Wastewater

GNANASELVAN GNANASEKARAN

MAJOR OF ENERGY & CHEMICAL ENGINEERING

FACULTY OF APPLIED ENERGY SYSTEM

GRADUATE SCHOOL

JEJU NATIONAL UNIVERSITY

August - 2021

Metal-organic frameworks (MOFs) incorporated polymeric membranes for the removal of hazardous materials from wastewater

GNANASELVAN GNANASEKARAN

(Supervised by Professor Young Sun Mok)

A thesis submitted in partial fulfillment of the requirement for the degree of

Doctor of Philosophy

2021. 05

The thesis has been examined and approved.

Prof. **Howon Lee** Thesis Director		Department of Chemical and Biological Engineering, Jeju National University
Prof. **Heonju Lee** Thesis Committee Member		Department of Nuclear and Energy Engineering, Jeju National University
Prof. **Hyomin Lee** Thesis Committee Member		Department of Chemical and Biological Engineering, Jeju National University
Dr. **Duy Khoe Dinh** Thesis Committee Member		Department of Industrial Plasma Engineering, Korea Institute of Machinery and Materials
Prof. **Young Sun Mok** Thesis Committee Member & Supervisor	목 영 선	Department of Chemical and Biological Engineering, Jeju National University

May - 2021

MAJOR OF ENERGY & CHEMICAL ENGINEERING
FACULTY OF APPLIED ENERGY SYSTEM
GRADUATE SCHOOL
JEJU NATIONAL UNIVERSITY

My humble effort
I Dedicate
To
My Beloved Family and Friends
&
Respected
Teachers and Professors

ACKNOWLEDGMENTS

First of all, I would like to express my sincere gratitude to the many individuals who helped and supported me during my doctoral course. It gives me pride and pleasure to express my deep gratitude to my research supervisor, **Professor Young Sun Mok,** for his supervision, advice and guidance, and extraordinary support throughout the work. He has been supportive since the day I began working in this laboratory. He always tells us to try nonstop to achieve the higher goals in our life and gives more motivation for achieving the goal. During some of my initial critical times in the research, he is the actual guardian for overcoming the issues.

I would like to express my sincere gratitude to **Professor Arthanareeswaran Gangasalam** for recommending me to this lab for the doctoral course. Without his help, I couldn't get such an excellent opportunity to work in this lab. I also thank him for his support and guidance during my doctoral course.

I extend my sincere thanks to the thesis evaluation director, **Professor Howon Lee**, and thesis committee members, **Professor Heonju Lee, Professor Hyomin Lee, and Dr. Duy Khoe Dinh,** for their time, interest, excellent suggestions, and support finish my thesis.

I would like to express my sincere gratitude to **Dr. Anand Sebastian** for recommending me to this lab for this doctoral course and for his constant support during the Ph.D. course.

I would like to express my soulful gratitude to my brother to **Mr. John David**, for supporting us continuously in all our critical situations to overcome. The First angel identified me and facilitated me in all professional and personal life and gave moral support to my family and me.

I feel gratitude to thank my friends **Mr. Sasikumar Balaguru, Mr. Dhilep Vignesh, Mr. Arun Prabakaran**, **Dr. Santhoshkumar, Mrs. Keerthika, and Ms. Sathya Bharathi,** who give me continuous support in my personal and professional life.

I also want to thank my lab colleagues and friends, **Dr. MSP Sudhakaran, Dr. Dilafruz, Dr. Ba, Dr. Mokther, Dr. Kim, Mr. Toan, Mr. Roshan, Mr. Nosir, Mrs. Shirjana, Mr. Yoon, Mr. Sosi.** I am glad to have my Indian friends, who are very supportive and made a homely environment. Thanks to **Dr. Anil Khambampati Anna, Dr. Karthi Sir, Dr. Natarajan Maams (Roommate (501)), Dr. Karthikeyan Aadhimoolam Anna. Dr. Sunny Kumar Poguluri, Dr. Nagmalleswar Rao Anna, Dr. Parthiban Pazhamalai Anna, Dr. Yuvasree, Dr. Vivek, Dr. Sravan Kumar, Dr.Surjit**

Sahoo, Dr.Gaurav, Mr. Daniel Prem, Ms. Sindhuja Manoharan (Anbu Akka), Dr.Vimal Kumar Nanban, Dr. Vijayakumar, Dr. Nirmal Prashanth, Dr.Karthika, Mr. Vineet Singh, Mr. Jithin Joy, Mr. Abisega Priyan Nanban (Roommate (102)), Mr. Divakar Ravi Nanban, Mr. Dhanasekar Kesavan Nanban (Roommate (101)) and Mrs. Sathya Dhanasekar (Sister), Mr. Prashanth Kannan, Mr. Swapnil Nardekar, Mr. Arun George, Mrs.Priyanka, Mr. Mohanraj Machan & Abitha Mohanraj Sister, Ms. Debapriya Hazra, Mr. Abdul, Mr. Vikran Prathab Mr. Arun Prasath, Mrs. Aparna, Mr. Noor, and Mr. Prasanna and I would like to thank my dear Annas. They stayed out of Jeju national university and gave supportive brotherhood during my Jeju life, **Mr. Selvakumar, Mr. Muthaia, Mr. Senthil, and Mr. Anamuthu**.

I would like to thank my friends **Mr. Karthik Ji (SKKU), Mr. Ashok, Dr. Soundar, Dr. Seeni, Mr. Amarnath (Anbu Thampi), Dr. Inamul Hasan Madar, Dr.Manivannan, and Dr. Govindan,** who stays at the mainland of South Korea.

I would like to thank my NITT seniors and friends who gave moral support to me at all times., **Dr. Sathish Kumar, Mr. Sudhan, Ms. Elakkiya, Ms. Deepa, Mr. Basker, Mr. Revanth, Mr. Rathnavel, Mr. Akash, Mr. Akhilan, Mr. Joel, Ms. Priya, Ms. Kasthuri, Ms. Narkavi, Ms. Ragavi, Mrs. Divya, all NITT Tamil Pasanga, and ADRASTOS.**

I must thank the university administration for providing me a full tuition fee waiver. I also thank the university administration and BK21 plus fellowship for providing me sufficient funds for my living. I would like to thank the chemical and biological engineering department personnel for their kindness and help in official issues. I am grateful to the staff at the center for research facility (CRF) at this university to provide the instrument facilities to carry out our research.

Last but certainly not least, I would like to express my deepest gratitude to our parents **Late Mr. Gnanasekaran Avidai and Mrs. Vijalakshmi Aagan**. They have sacrificed their entire life for the betterment of my tomorrow with love and thankfulness. I also thank **our sister Late Ms. Gnanaselvi Gnanasekaran** has love and support for us. Finally, I also thank my brother come son into my life, **Mr. Gnanakumar Gnanasekaran**, who continuously supports achieving great success to give proud names to our parents.

Words can hardly substitute the thankful that I owe to my inspiring teachers and friends who stood behind in all possible ways to complete this work successfully. Without the above, I might not finish this research work as a great full one. I thank one and all who have helped me, directly and indirectly, to complete my research works.

Finally, I'm heartfully respecting the real heroes in our society (Social reformers), **Dr. Bhimrao Ramji Ambedkar, Thanthai Periyar, Karmaveerar Kamarajar, Peraringar Anna, Dr. Kalaingar Karunanidhi, Dr. M. G. Ramachandran, Dr. Vallal Alagappa, Dr. APJ Abdul Kalam, and all the Social Justice Fighters.** They are the reason for an ordinary rural man to become a doctorate (Dr. Gnanaselvan Gnanasekaran).

Thanks & Regards,
Gnanaselvan Gnanasekaran

TABLE OF CONTENTS

PAGE

TABLE OF CONTENTS **I**

NOMENCLATURE **VIII**

LIST OF TABLES **X**

LIST OF FIGURES **XI**

ABSTRACT **XVI**

CHAPTER 1 INTRODUCTION AND LITERATURE REVIEW 1

1.1 Background.. 1

1.2 Membrane separation 3

1.3 List of polymeric membrane used for wastewater treatment 4

1.3.1 Polyethersulfone.. 4

1.3.2 Chitosan... 5

1.3.3 Polysulfone.. 6

1.4 Membrane flow configurations 7

1.5 Types of membranes process... 8

1.5.1 Microfiltration 8

1.5.2 Ultrafiltration.. 8

1.5.3 Nanofiltration 9

1.5.4 Reverse osmosis 9

1.6 Metal-organic framework (MOFs) 10

1.6.1 MOFs applications 11

1.7 MOFs incorporated polymeric membranes 11

1.8 Hazardous pollutants 12

1.8.1 Dye 12

1.8.2 Methylene blue dye 12

1.8.3 Methyl Orange.. 13

1.8.4 Indigo Carmine.. 13

1.8.5 Salts 13

1.8.6 Microplastics 14

1.9 The scope of this present work 15

1.10 References 17

CHAPTER 2 MATERIALS AND METHODS 26

2.1 Introduction 26

2.2 Materials 26

2.2.1 Chemicals 26

2.3 Apparatus... 30

2.4 MOF synthesis 30

2.5 Membrane preparation.. 31

2.6 Material characterization 31

  2.6.1 Fourier transform infrared spectroscopy 31

  2.6.2 X-ray diffraction.. 32

  2.6.3 Brunauer–Emmett–Teller (BET) surface area analysis 32

  2.6.4 Field-emission scanning electron microscopy 32

  2.6.5 Field-emission transmission electron microscopy 33

  2.6.6 Energy dispersive X-ray spectroscopy.. 33

  2.6.7 X-ray photoelectron spectroscopy.. 33

  2.6.8 Zeta potential measurement 33

  2.6.9 3D nanoprofiller 34

  2.6.10 Contact angle measurement 34

2.7 Nanofiltration... 35

2.8 Flux recovery ratio... 36

2.9 References 37

CHAPTER 3 PERFORMANCE OF COMPOSITE PES/MOF-5 MEMBRANES FOR THE REMOVAL OF HAZARDOUS TEXTILE DYES 39

3.1 Introduction 39

3.2 Preparation and characterization of MOF-5 41

3.3 Membrane preparation.. 42

3.4 Permeation studies 43

3.5 Rejection of textile dye... 44

3.6 Results and Discussion 44

3.6.1 FTIR characterization of MOF-5 44

3.6.2 XRD analysis of MOF-5 45

3.6.3 Surface Morphology of MOF-5 46

3.6.4 Energy Dispersive X-ray Spectroscopy of MOF-5 47

3.6.5 XRD analysis of membranes 48

3.6.6 Surface morphology of membranes 49

3.6.7 EDX analysis of membranes 50

3.6.8 Contact angle measurement of membranes 51

3.6.9 Porosity and pore size of membranes 52

3.6.10 Permeability of membranes 52

3.6.11 Dye rejection 53

3.6.12 Effect of pH... 54

3.7 Conclusion 56

3.8 References 57

CHAPTER 4 EFFICIENT REMOVAL OF ANIONIC, CATIONIC TEXTILE DYES AND SALT MIXTURE USING A NOVEL CHITOSAN/MIL-100 (FE) BASED NANOFILTRATION MEMBRANE 63

4.1 Introduction 63

4.2 Preparation of MIL-100 (Fe) 66

4.3 Preparation of CS/MIL-100 (Fe) membranes 67

4.4 Nanofiltration 69

4.5 Result and discussion 69

4.5.1 MIL-100 (Fe) characterizations 69

4.5.2 Membrane characterization 73

4.5.2.1 XRD and FTIR analysis of membranes 73

4.5.2.2 Morphological analyses of membranes 73

4.5.2.3 Surface roughness of membranes 75

4.5.2.4 Elemental analysis of membranes 77

4.5.2.5 Surface charge of membranes 79

4.5.3 Membrane performances 83

4.5.3.1 Permeability of membranes 83

4.5.3.2 Dye rejection of membranes 84

4.5.3.3 Antifouling performance of membranes 88

4.5.3.4 Salt rejection of membranes 88

4.5.3.5 Dye/salt mixture rejection of membrane 91

4.5.3.6 Reusability of membranes 95

4.6 Conclusion 100

4.7 References 101

CHAPTER 5 NOVEL MIL-100 (FE) INCORPORATED HIGH-FLUX POLYSULFONE NANOFILTRATION MEMBRANE AND ITS EXCELLENT REMOVAL PERFORMANCE OF MICROPLASTIC ADSORBED DYE CONTAMINANT FROM TEXTILE WASTEWATER 113

5.1 Introduction 113

5.2 Preparation of PSF/MIL-100 (Fe) membranes 117

5.3 Characterization of PSF/MIL-100 (Fe) membranes 118

5.4 Nanofiltration 118

5.5 Result and discussion 119

5.5.1 XRD analysis of membranes 119

5.5.2 Cross-sectional view of the membrane 121

5.5.3 EDS analysis of membrane 123

5.5.4 Pure water flux of membranes 123

5.5.5 Porosity and mean pore size of membranes 125

5.5.6 Contact angle of membranes 126

5.5.7 Work of adhesion and wetting energy 127

5.5.8 Filtration performance of membranes 128

5.5.8.1 Effect of pH on the membrane performances 129

5.5.8.1.1 MB rejection 129

5.5.8.1.2 Rejection of MPs adsorbing MB 133

5.5.8.2 Effect of concentration on membrane performances 137

5.5.8.2.1 MB rejection 137

5.5.8.2.2 Rejection of MPs adsorbing MB 139

5.5.8.3 Effect of pressure on the membrane 141

5.5.9 Salt rejection of membranes 143

5.5.10 Cycling performance 145

5.6 Conclusions 147

5.7 References 148

CHAPTER 6 SUMMARY AND RECOMMENDATIONS 156

6.1 Summary 156

6.2 Recommendation 157

NOMENCLATURE

NF	Nanofiltration
MOF	Metal-organic framework
CS	Chitosan
PES	Polyethersulfone
CA	Cellulose acetate
PSF	Polysulfone
MB	Methylene blue
MO	Methyl orange
rpm	Revolutions per minute
PEG	Polyethylene glycol
PVDF	Polyvinylidene fluoride
$\omega 1$	The wet weight of the membranes (g)
$\omega 2$	The dry weight of the membranes (g)
ε	Porosity
d_p	Density of polymer
d_w	Density of water
l	The membrane thickness (m),
η	Water viscosity (8.9×10^{-4} Pa s)
Q	The permeate flow rate (m^3/s)
Δt	The permeation time (h)
ΔP	The operating pressure (Mpa/bar)

A	The active membrane area (m^2)
J_w	Permeability (L/m^2h)
V	The permeate volume (m^3)
ppm	Parts per million
UV-vis	Ultraviolet-visible
C_f	Feed concentration (ppm)
C_p	Permeate concentration (ppm)
FRR	Flux recovery ratio
R_{real}	Real rejection (%)
R_{actual}	Actual rejection (%)
MPs	Microplastics
DI	De-ionized

LIST OF TABLES

Table 2.1 Specifications of chemicals used in this study 26

Table 2.2 List of equipment used for materials preparation and filtration study. 30

Table 3.1 The membranes composition.. 43

Table 3.2 The membranes properties. 52

Table 4.1 The membrane surface properties. 76

Table 4.2 Elemental compositions of membranes... 79

Table 4.3 Hydrated radius, Stokes radius, and rejection % of ions................................. 94

LIST OF FIGURES

Figure 1.1 The structure of polyethersulfone. 5

Figure 1.2 The structure of chitosan. 6

Figure 1.3 The structure of polysulfone. 7

Figure 3.1 Structures of (a) Methylene blue (b) Indigo carmine. 41

Figure 3.2 FTIR spectra of MOF-5. 45

Figure 3.3 XRD spectra of MOF-5. 46

Figure 3.4 SEM image of MOF-5. 47

Figure 3.5 EDX spectra of MOF-5 48

Figure 3.6 XRD spectra of membranes. 48

Figure 3.7 Cross-sectional images of membranes. 50

Figure 3.8 EDX spectra of membranes. 51

Figure 3.9 Permeate flux rate of membranes. 53

Figure 3.10 Rejection percentage of methylene blue. 54

Figure 3.11 Rejection (%) of indigo carmine. 55

Figure 4.1 The schematic representation. MIL-100 Fe synthesis (a); nanofiltration setup (b). 67

Figure 4.2 Schematic diagram of CS/MIL-100 (Fe) membrane fabrication by the film casting method. 68

Figure 4.3 Characterization of as-synthesized MIL-100 (Fe). XRD pattern (a); FTIR spectrum (b); N_2 adsorption-desorption isotherms with inset image of pore size distributions (c); FESEM image (d); FETEM images (e)-(f); XPS survey spectrum (g); Fe 2p (h); C 1s (i); O 1s spectrums (j). 71

Figure 4.4 EDS Spectra of MIL-100 (Fe) (a); EDS mapping of MIL-100 (Fe) (b)-(e). ... 72

Figure 4.5 XRD (a) and FTIR (b) spectra of C0-C1 membranes and MIL-100 (Fe)....... 74

Figure 4.6 Membrane morphology and surface roughness. FESEM images of top surface (a)-(d); cross-sectional view (e)-(h); 2D and contact angle images (i)-(l); 3D images (m)-(p).. 77

Figure 4.7 EDS Spectra of pure CS and CS/MIL-100 (Fe) membranes. 80

Figure 4.8 Elemental and surface charge characterization. Survey spectra (a); C 1s of CS (b) and CS/MIL-100 (Fe) (c); zeta potential (d) and mobility (e); Effect of sample position at various pH for zeta potential (f)-(g) and mobility (h)-(i). 81

Figure 4.9 EDS mapping of pure CS membrane. 82

Figure 4.10 EDS mapping of CS/MIL-100 (Fe) membrane. 82

Figure 4.11 XPS spectrum of Fe 2p of the CS/MIL-100 (Fe) membrane........................ 83

Figure 4.12 The rejection performances of dyes through the membranes. The effect of TMP on PWF (a); effect of MB and MO rejection, PWF at 0.4 MPa (b); effect of pH (c); effect of dye concentration on MB (d); MO (e). 85

Figure 4.13 UV-vis absorption spectra of feed and permeate of MB at various pH (a); UV-vis absorption spectra of feed and permeate of MO at different pH (b). 86

Figure 4.14 Schematic representation of the dye molecule separation mechanism by CS/MIL-100 (Fe) membrane at the acidic and alkaline environment............................... 87

Figure 4.15 UV-vis absorption spectra with the inset images of feed and permeate solution (a) MB and (b) MO. 88

Figure 4.16 The rejection performances of dye/salt mixture through membranes. Salts (a); ions in salts (b); MB+salts (c); ions in MB+salts (d); MO+salts (e); ions in MO+salts (f). Cyclic stability of MB (g); MO (h); MB+$MgSO_4$ (i). CS/MIL-100 (Fe) rejection (%) comparison with reported membranes. MB (j); MO (k); $MgSO_4$ (l). 90

Figure 4.17 The images of feed, permeate, and retentate of MB dye/salt mixture (a); UV-vis absorbance spectrum of MB dye/salt mixture at 665 nm for permeate and feed solution (b). 93

Figure 4.18 Schematic representation separation performances of CS/MIL-100 (Fe) membrane. 95

Figure 4.19 The feed and permeate images of MB solutions for six cycles. 96

Figure 4.20 UV-vis absorbance spectrum of feed and permeate for six cycles MB (a); MO (b). 96

Figure 4.21 Reusability of C3 membrane for MB/$MgSO_4$ mixture. (a) UV-vis absorbance spectrum of feed and permeate of MB/$MgSO_4$ salt mixer solutions at 665 nm for six cycles; (b) The images of permeate and feed solutions of MB/$MgSO_4$ salt for six cycles. 98

Figure 5.1 Schematic representation of the fabrication process of PSF/MIL-100 (Fe) membranes. 117

Figure 5.2 XRD patterns of membranes and MIL-100 (Fe). 120

Figure 5.3 Cross-sectional view of the membranes 122

Figure 5.4 EDS mapping of pristine PSF membrane 124

Figure 5.5 EDS mapping of PSF/MIL-100 (Fe) membrane. 124

Figure 5.6 (a) PWF, porosity, and pore size; (b) contact angle, wetting energy, and work of adhesion; (c) rejection (%), flux, and FRR (%). 126

Figure 5.7 UV-vis absorption spectra (a), visual images of feed, and permeate MB solutions (b). 130

Figure 5.8 Rejection performance at various pH: (a) rejection (%), flux and FRR % of MB solution; (b) MB rejection (%), flux, and FRR % of PVC+MB solution; (c) MB rejection (%), flux, and FRR % of PE+MB solution. 131

Figure 5.9 UV-vis absorption spectra and images of feed and permeate solutions of MB at various pH. 132

Figure 5.10 Image of untreated and treated membranes at various pH. 132

Figure 5.11 UV-vis absorption spectra of feed, permeate, and retentate solutions at alkaline pH (9 and 11). 134

Figure 5.12 UV-vis absorption spectra of feed, permeate, and retentate solutions at neutral pH (7). 136

Figure 5.13 UV-vis absorption spectra of feed, permeate, and retentate solutions at acidic pH (3 and 5). 137

Figure 5.14 Rejection performance at various concentration: (a) rejection (%), flux and FRR % of MB solution; (b) MB rejection (%), flux, and FRR % of PVC+MB solution; (c) MB rejection (%), flux, and FRR % of PE+MB solution. 138

Figure 5.15 UV-vis absorption spectra and visual images of feed and permeate solutions of MB at various concentrations. 139

Figure 5.16 UV-vis absorption spectra of feed, permeate, and retentate solutions with MB solution at various PVC concentrations (0.5, 1, 1.25, and 1.5 g/L). 140

Figure 5.17 UV-vis absorption spectra of feed, permeate, and retentate solutions with MB solution at various PE concentrations (0.5, 1, 1.25, and 1.5 g/L). 141

Figure 5.18 Membrane performance: (a) PWF at various TMPs, (b) MB rejection (%), flux, and FRR % at various TMPs, (c) rejection (%), flux, and FRR % of various salts solution, (d) reusability performance of the membrane. 142

Figure 5.19 UV-vis absorption spectra (a), visual images of feed and permeate of MB solutions for M0.5 membrane at various TMP (b). 144

Figure 5.20 UV-vis absorption spectra (a), visual images of feed and permeate of MB solutions for reusability of 1-6 cycles of M0.5 membrane (b). 146

ABSTRACT

Rapid industrial development, urbanization, and population growth have given rise to an immense responsibility to address increasing water scarcity and environmental pollution issues. Currently, the volume of textile wastewater discharged into the aquatic environment is rising enormously. The purification of harmful textile dyeing wastewater has unveiled several challenges since it comprises a complex mixture, counting dyestuff, additives, microplastics, salts, etc. Moreover, these large quantities of textile wastewater with colored chemicals are non-biodegradable and highly harm humans and creatures living in aqueous environments. Therefore, it is essential to remove the contaminants from textile wastewater. Many conventional techniques, including adsorption, advanced oxidation processing, distillation, flocculation, and membrane separation, have been extensively used for textile wastewater treatment.

Recently, membrane separation has attracted extensive interest for wastewater treatment owing to its excellent benefits of low energy consumption yet higher separation efficiency combined with a convenient operating procedure. Several membrane separation techniques were established, such as microfiltration, ultrafiltration, nanofiltration, and reverse osmosis. Specifically, nanofiltration (NF) technologies offer the highest potential as the most potent candidate for separating organic molecules and inorganic salts. However, developing an innovative NF membrane capable of rejecting almost 100 % of contaminants with high water flux is highly desirable. Numerous studies have focused on fabricating novel composite NF membranes composed of nanofillers and a polymer matrix for selective contaminant removal from wastewater. More recently, synthetic and natural polymers have become the dominant raw materials for fabricating separation membranes. However, polymeric membranes facing several disadvantages, including lack of hydrophilicity, low anti-fouling ability, limited mechanical stability, and

insufficient chemical stability. Therefore, they significantly restrict their use in wide-reaching applications.

Membrane modification is a superior technique to overcome these obstacles. Incorporating novel nanomaterials into polymers has impressively contributed to developing renewable composite membranes for wastewater treatment. Metal-organic frameworks (MOFs) have been widely utilized as novel candidates to fabricate futuristic composite membranes due to their high porosity, superior surface area, tunable pore structure, suitable polymers affinity, an abundance of functional groups, and high adsorption capacity. Consequently, in this work, the fabricated PES/MOF-5 membrane was primarily studied to remove hazardous indigo carmine (IC) and methylene blue (MB) dyes. MOF-5 incorporation enhances the permeability and hydrophilicity of the PES membrane with the values of pure water flux (PWF) of 20.5 to 77.1 L/m^2 h and contact angle of 73.1 to 60.3°, respectively, even though PES/MOF-5 membrane sustained 97% and 89% rejection of MB and IC, respectively.

Likewise, an Eco-friendly MOF membrane was fabricated with hazardous free MOFs (MIL-100 (Fe)) incorporated into the chitosan (CS) biopolymer. MIL-100 (Fe) incorporation enhances the CS membrane properties, including pore size, surface charge, structural morphology, and hydrophilicity. The CS/MIL-100 (Fe) membrane exhibited the improved pure water flux from 5 to 52 L/m^2 h and 99% rejection of cationic methylene blue and anionic methyl orange. The CS/MIL-100 (Fe) membrane rejects the salts in the following trend of $MgSO_4$ (R_{real} - 67% and R_{actual} - 64.2%) > Na_2SO_4 (R_{real} - 59.4% and R_{actual} - 58.1%) > $CaCl_2$ (R_{real} - 49.1% and R_{actual} - 48.3%) > NaCl (R_{real} - 32.6% and R_{actual} - 32.1%). The CS/MIL-100 (Fe) membrane exhibited excellent rejection and anti-fouling performances with outstanding recycling stability.

Moreover, the removal of harmful dye adsorbed microplastics (MPs) was studied by the PSF/MIL-100 (Fe) membrane. Compared to the pristine PSF membrane (M0), incorporation of the hydrophilic MIL-100 (Fe) nanoparticles significantly modified the morphology, hydrophilicity (water contact angle reduced to 63.2º ±1.2 from 83.6º ±1), porosity, and pore size. Incorporating a 0.5 wt% loading of MIL-100 (Fe) particles into the PSF matrix (M0.5) was initiated to deliver the highest performance relative to the membranes with other loadings. M0.5 membrane includes superior pure water flux (10.3 times higher than M0) with a high methylene blue (MB) rejection rate of more than 99% and excellent anti-fouling properties of MB dye, microplastics (MPs)+MB dye feed solutions. Besides, the M0.5 membrane was sustained with outstanding performances at various concentrations of MB dye, MPs, and a range of transmembrane pressures (TMPs). Furthermore, the membrane exhibited good salt rejection capability and reusability for as many as six cycles of MB dye rejection without compromising the permeability and anti-fouling performance. This study highlights MOFs incorporated polymeric composite membrane offers excellent potential for efficiently removing contaminants from the actual textile wastewater.

CHAPTER 1 INTRODUCTION AND LITERATURE REVIEW

1.1 Background

Water is a precious natural resource and essential to human life. The rapid development of the human population and industrialization enormously demand freshwater. Hence, more than 71% of our earth occupied by water; among them, about 97% is ocean water, and only 3% is fresh water. Moreover, in freshwater, about 98.8% are frozen icecaps and under groundwater, which not easy to access. In addition, the fast development of industrial and human activities causes massive water pollutions, which adversely affects our lives. Notably, the hazardous materials in the discharged wastewater cause various diseases, adversely affect aquatic lives, and many health issues. The growing industrial technology and populations, and the deterioration of water resources, increase the demand for purified water. In the current situation, water scarcity and water contamination are severe problems worldwide [1].

In particular, wastewater from the textile industry processes (dyeing, bleaching, printing, and finishing) significantly impacts the atmosphere due to extreme water consumption and producing abundant hazardous effluents. It is a dangerous risk to our lives, triggering groundwater pollution, defeating the human immune structure, causing various illnesses, blocking sunlight penetration, and adversely affecting aquatic life [2,3]. The textile coloring process required water, dyestuff, additives (surfactants and dispersing agents), and salts (retarding and exhausting agents). Especially, a significant amount of salt is essential to quicken the exhaustion and fixation of colors on the fabrics. In the dyeing process, 1 kg of cotton needs 0.6–0.8 kg of sodium chloride (NaCl) and 30-60 g of dyes with 70-150 L of freshwater [4]. However, the added massive amount of inorganic salts (NaCl, Na_2SO_4, $MgCl_2$, $MgSO_4$, etc.) are discharged from the dyeing process [1]. The salts in the textile effluents add to the pollutants load and increase the decoloration time [5], making more trouble for water purification. However, almost 700,000 tons /year of dyes are produced worldwide, and the textile dyeing industry pays to a massive quantity of dyeing waste release with intense coloration [6]. Besides, based on the coloring process and various manufacturing plans, the generated waste may be in acidic or alkaline environments, adding more water purification challenges [7]. Removing dyes from textile wastes is essential because they are carcinogenic, mutagenic, and hazardous [8]. Therefore, we urgently need an effective treatment method to separate dye and salts from textile wastewater.

Many conventional methods are active for wastewater treatment, including adsorption, coagulation, chemical precipitation, advanced oxidation processes, electrochemical treatment, membrane technologies, etc. In wastewater treatment, membrane technology has been recognized as adequate for separating pollutants from contaminated sources and purifying the water [9]. Membranes are selective barricades that separate two distinct segments, permitting specific components and retaining other parts. Membrane processes depend on a physical separation, typically through no chemicals in the feed and no phase modification; therefore, membrane technology positions high as substitutions to other conventional techniques. In addition, low energy consumption, reduced processing steps, superior separation efficiency, besides enhanced ultimate product quality are the main attractions of membrane technology.

Further enhancements and novelties are desirable for wastewater treatment membranes, mainly morphological structure, functional group enrichments, high permeability, superior separation, high anti-fouling performances, and high stability and reusability. In addition, Membrane technology owns some characteristic features which demonstrate effective technique than other conventional techniques. Thus, the excellent benefits are a modular and compact design, continuous operation, no regeneration step, suitable scale-up, and convenient operation at less maintenance.

1.2 Membrane separation

Membranes can be used excellently in diverse applications, which are specified as follows [10],

- The pore channel in the membrane surface can act as a barrier preventing the specified matters from traveling, including bacteria, viruses, salts, contaminants, and permeating the passage of air and water.
- Reserve osmosis is a well-developed technique to get drinking water from sea and wastewater. In the RO process, the membrane active in the primary role as a filter to purify the water.
- Membranes are not only functional for filtration, distillation, and extraction; they can also be used for gas storage in biogas plants or act as catalysts in syntheses, sensors, and electrodes for energy storage and generation applications.

1.3 List of polymeric membrane used for wastewater treatment

Many polymeric materials were widely used for the development of membrane for the wastewater treatment, which are followed by,

- Cellulose Acetate (CA) [11],
- Chitosan (CS) [12],
- Polysulfone (PSF) [13],
- Polyethersulfone (PES) [14],
- Polyacrylonitrile (PAN) [15],
- Polyamide (PA) [16],
- Polyvinylidene Fluoride (PVDF) [17],
- Polyimide (PI) [18],
- Polyethylene (PE) [19],
- Polypropylene (PP) [20],
- Polytetrafluoroethylene (PTFE) [21],
- Polyvinylchloride (PVC) [22].

Our research work, PES, CS, and PSF polymeric membranes, were selected to remove hazardous material from wastewater.

1.3.1 Polyethersulfone

Polyethersulfone (PES) is one of the vital polymeric materials and which widely explored in separation applications. Specifically, PES and composite PES-based membranes display excellent properties, including hydrolytic stability, oxidative, high mechanical, and thermal stability. Furthermore, the PES membranes constantly demonstrate the asymmetric structure and which fabricated using phase inversion techniques. Additionally, the ultimate design of the PES membrane has been influenced by the effect of composition in terms of solvent, additives, concentrations, temperatures, coagulation bath, non-solvent, and environment. However, PES membranes are limited in real applications due to the hydrophobic character, which leads to fouling formation, less permeability, a short lifetime, and erratic separation performances. Therefore, developing a new membrane with attractive properties, including high stability, supreme anti-fouling nature, high permeability, and excellent separation performances. The modification of the PES membrane is an effective technique to achieve a membrane with outstanding properties for wastewater treatments. Hence, three approaches followed to modify membranes, such as surface modification, bulk modification, and blending with additives. In our study, we followed the blending technique to prepare the modified PES membranes [23]. Figure 1.1 illustrates the PES structure.

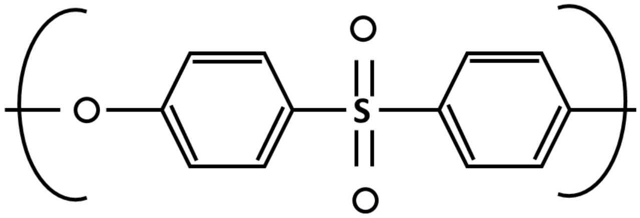

Figure 1.1 The structure of polyethersulfone.

1.3.2 Chitosan

Recently utilizing biopolymers to fabricate membrane for wastewater treatment has attracted because of their fascinating features, including easy availability, inexpensive, and earth-friendly [24]. In addition, Chitosan (CS) is a hopeful polymeric membrane for textile wastewater treatment because of its strong hydrophilicity, toxic-free, excellent film-forming ability, outstanding anti-bacterial activity and, characteristic biomedical properties. Responsive amino and hydroxyl groups on the chitosan provide multifunctional action [25–27]. Additionally, those functional groups offer hydrophilic CS, which influences high water diffusion and superior sorption [28]. However, it has some limitations, including less mechanical strength, less stability, and low porosity. Modification of the CS membrane by incorporating explicit fillers such as SiO_2 [29], TiO_2 [30], Graphene oxide [31], and polyethylene glycol [32] enhances the properties of water treatment [33]. Figure 1.2 shows the structure of the chitosan.

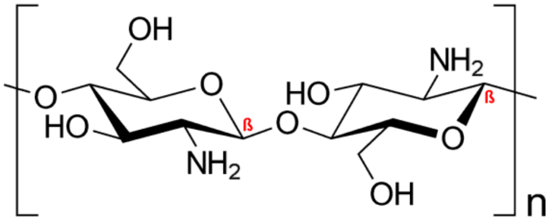

Figure 1.2 The structure of chitosan.

1.3.3 Polysulfone

Polysulfone (PSF) membranes have mainly been active for wastewater treatment. PSF is a desired material for developing membranes due to its excellent properties, including availability, effortlessness of modification, high mechanical and chemical stability, surface charge, operated at wide pH and temperatures. In addition, the presence of aryl or alkyl sulfone functional groups in the PSF compositions offers inherent biocompatibility [34]. Moreover, PSF is commonly used as an appropriate material for wastewater treatment; subsequently, it provides outstanding tensile strength and mechanical stability at a pressure range of 70-83 MPa. However, the hydrophobic surface of PSF is a significant disadvantage which contributes to the fouling formation on the membrane surface. Modifying PSF membranes with hydrophilic functional groups is an excellent way to overcome the issues and enhance PSF membranes' performance [13,34]. Figure 1.3 shows the structure of polysulfone.

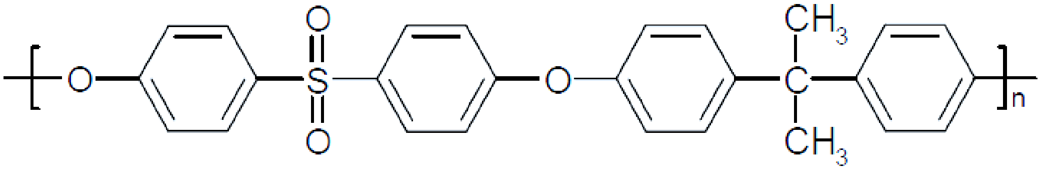

Figure 1.3 The structure of polysulfone.

1.4 Membrane flow configurations

Two flow arrangements of membrane processes were commercially applicable, including dead-end and cross-flow filtrations. The fluid movement is perpendicular to the membrane surface in a separation scheme, including gaseous or liquid substances. In a dead-end system, concentrate does not recirculate, which more likely to deposit on the membrane surface, and the permeate pass through membrane pores. In a cross-flow system, the feed passes tangential to the surface of the membrane and is divided into two streams. At that point, the concentrate or retentate is recirculated and mixed with the feedwater. Indifference, the permeate flows through the membrane and collected in other portions. The both, dead-end and cross-flow system provides many benefits and drawbacks. The dead-end membrane system is comparatively inexpensive to develop, and the process is very convenient to operate. The main shortcoming of the dead-end system is massive fouling formation and concentration polarization, which necessitates periodic pauses to clean or remove the membrane filter.

1.5 Types of membranes process

Membrane separation processes play a vital character in the separation industry. In membrane separation, four pressure-driven membrane processes are used for wastewater treatment such as microfiltration (MF), ultrafiltration (UF), nanofiltration (NF), and reverse osmosis (RO). These processes are eminent by the application of hydraulic pressure as the driving force for mass transport.

1.5.1 Microfiltration

MF is a filtration technique to remove substances in the range of 0.025 to 10 μm at an applied pressure less than 0.2 MPa using membranes. Additionally, the pore size of the MF membranes characterized between 0.1 to 10 μm. MF techniques are involved in various applications, including the cell separation process in biotechnology, the dairy and food industry, oil treatments, separation of protein solution in the pharmaceutical process, and plasma separation in blood treatments.

1.5.2 Ultrafiltration

Historically, Ultrafiltration (UF) has been stated to MF membranes regarding the pore size (μm). In contrast, UF membranes could reject the substance based on its molecular weight. In addition, higher than 1 MPa pressure was applied in UF to separate the substances in the range of 1 to 300 kDa. Furthermore, UF membranes potentially retain the solutes and suspended solids with more than 300 kDa; meanwhile, the low molecular weight matters and water transport through membrane pores. Typical applications of UF comprise food materials purification and protein separation in the dairy and food industries. In addition, they are removing hazardous heavy metal ions and harvesting cells, lysozyme, liposome in biotechnology, and many wastewater treatments.

1.5.3 Nanofiltration

Nanofiltration (NF) is a pressure-driven membrane-based separation process with an applied pressure range of 4 to 20 MPa to reject the particles or molecules in the value of 350 to 1000 Da of molar mass. The properties of the NF membranes were well-thought-out in between the RO and UF. Based on the molecular weight cut-off of 300-500 Da, the membrane's pore size is characteristically 1 nm. Therefore, the NF membranes can effectively remove inorganic salts and small organic molecules comparable with RO. However, high divalent ion rejection, less monovalent rejection without compromise, the higher flux shows the significant benefits of NF in wastewater treatment. In addition, NF is often used in surface water and fresh groundwater treatment to soften and remove disinfection by-product precursors such as organic and synthetic organic matter (herbicides, pharmaceuticals, etc.) [35,36].

1.5.4 Reverse osmosis

Dissimilar MF and UF membranes, Reverse osmosis (RO) membranes are dense membranes that do not consist of distinct pores. It is pressure-driven filtration (between 20 and 80 MPa), which rejects the minutest contaminants and monovalent ions (<350 Da) from the feed solutions. The mass transfer in RO is owing to the solution-diffusion mechanism, charge exclusion, size exclusion, and physical-chemical interactions between solute, solvent, and the membrane. RO is greatest frequently known for its usage in water purification from seawater, removing the salt and other substances from water. This technology has been long-established to be helpful for water treatments. In addition, it could offer high elimination efficiencies in treating an extensive diversity of effluents from textile, chemical, pulp and paper, petroleum and petrochemical, food, metal finishing, and tanning industries [37].

1.6 Metal-organic framework (MOFs)

Metal-Organic Frameworks (MOFs) are mixtures containing metal clusters/ions corresponding to carbon-based molecules. Specifically, MOFs are a coordinated network including the organic molecules act as ligands typically bi, tri-dentate carboxylic acids, and metal atom. Hence, MOFs are synthesized mainly by solvothermal or hydrothermal methods, where crystals gradually grow from the solution. The high adsorption capacity of MOFs favors removing harmful entities through the adsorption mechanism. Newly, scientists developed several MOFs to remove hazardous pollutants from wastewater, specified below [38].

- MOF-5
- MIL-100 (Fe)
- MIL-101(Cr),
- MIL-53(Al, Cr, Fe),
- UiO-66.

1.6.1 MOFs applications

The emerging MOFs are active in various advanced applications due to their attractive properties, including ultrahigh porosity, well-defined pore channel, high surface area, structural diversity, and enriched functionalities. In addition, versatile MOFs play an active role in gas/liquid separation, storage, sensing, catalysis, and other fields [39,40].

1.7 MOFs incorporated polymeric membranes

In general, polymeric membranes have been extensively applied for water purification applications. However, the trade-off issue between permeability and selectivity has inadequate usage in numerous applications. Incorporating inorganic fillers improves the membrane properties for effective water treatment, but inorganic fillers create other problems, including less dispersibility, accumulation, poor compatibility, and aggregation. In addition, inorganic particle accumulation originates pore blockage, flux decrease, structural flaw, and weaken fouling resistance [41,42].

The introduction of metal-organic framework (MOFs) as an innovative filler for membrane fabrication is more effective than inorganic fillers. The synergistic possessions of organic ligands and inorganic metal clusters or ions in MOFs provide extraordinary properties to the membranes [43]. Additionally, the properties of the membranes are enhanced by increasing the interface compatibility between the polymeric matrix and nano-fillers. In addition, MOF materials with intrinsic properties that could increase the properties of the membrane for effective removal of hazardous pollutants from wastewater: In MOFs, the existence of metal or metal clusters and functionalized organic molecules including pyridines, amines phosphonates, carboxylates, and sulphonates offering an inclusive variability of crystalline porous materials, The porous MOFs structures can perform as molecular sieves, and the excellent surface area and free pore volume provide enormous contact area to remove the contaminant and high stability [9].

1.8 Hazardous pollutants

The discharged wastewater from the textile industry consists of various hazardous pollutants including, dyes, salts, additives, and microplastics. The hazardous pollutants are necessary to remove from the wastewater. In this study, methylene blue, methyl orange, indigo carmine, various salt solutions, and microplastics were selected to simulate the natural textile wastewater to examine the performance of MOF incorporated membranes.

1.8.1 Dye

Dyes are carbon-based compounds that are extensively applied for imparting color to textiles. They are shaped either chemically or by plants. An exciting point about them is that different paint does not build on the fiber's surface but is absorbed into the material's pores due to the size of the dye molecules being smaller than the size of the pores in the fabric thread. As a result, the dye molecules are designed like narrow strips of paper with length and breadth but relatively little thickness. This planar shape assists them in slipping into the polymer structure when the fabric or yarn is introduced into the dye bath.

1.8.2 Methylene blue dye

Methylene blue (MB), a cationic dye, is the generally used dyeing substance for cotton, silk, and wool. Although MB is not considered a very toxic contaminant, it can cause harmful effects such as vomiting, increased heart rate, diarrhea, shock, cyanosis, jaundice, quadriplegia, and tissue necrosis. Consequently, MB containing wastewater should be treated before discharge.

1.8.3 Methyl Orange

Methyl orange (MO) is a very common water-soluble azo dye (generally identified as a pH indicator) extensively used in several industries, including the textile, paper, printing, and food industries. Regrettably, the treated wastewater is highly poisonous to our health, including the inhalation of MO causes gastrointestinal irritation with nausea, vomiting, and diarrhea and may cause central nervous system effects.

1.8.4 Indigo Carmine

Indigo Carmine (IC) is a water-soluble blue acid dye to benefit an easy dyeing process. However, disadvantages are poor lightfastness and wash fastness. Indigo Carmine is widely used in numerous industries, including the textile, printing, food, paper, and pulp industries. However, the treated wastewaters are mostly discharged into water sources, which severely affect our health. Specifically, it may cause skin irritation, gastrointestinal irritation with nausea, diarrhea, and vomiting. In addition, inhalation of IC may cause respiratory tract irritation.

1.8.5 Salts

In the textile dyeing process, various parameters contributing to enlightening the quality of dyeing. Among them, the concentration of salts is the most necessary parameter. The industrial textile dyeing process essentially required dyestuff, water, salts (retarding and exhausting agents), and additives (surfactants and dispersing agents). Notably, a considerable amount of salt is needed to accelerate the exhaustion and fixation of dyes on fabric. In the dyeing process, 1 kg of cotton required 0.6–0.8 kg of NaCl and 30-60 g of dyestuff with 70-150 L of water consumption [4]. NaCl and Na_2SO_4 salts are mainly utilized as exhausting and retarding agents in the dyeing process. The added vast amount of inorganic salts (NaCl, Na_2SO_4, $MgCl_2$, $MgSO_4$, etc.) are discharged from the dyeing process as a by-product [1]. The salt content in the textile effluent creates additional pollutants and increases the decoloration time [5]. Extreme salt concentration (0-100 g/L) is desired for the reactive dyeing process [44].

1.8.6 Microplastics

The manufacture and trading events of textile industries contribute to most microplastics (MPs) in the wastewater. More than 5.4 million tons of synthetic textile fibers were manufactured worldwide in 2016, which can contact the aquatic environment and contribute 90% of microplastic pollution [45]. Furthermore, MPs are highly moveable and omnipresent in the discharged wastewaters due to insolubility and lightweight characteristics. Based on the physical structures, MPs are categorized as fibers, microbeads, sheets, and fragments. In chemically, MPs are polymers, which include polystyrene (PS), polypropylene (PP), polyvinyl chloride (PVC), polyethylene (PE), polyethylene terephthalate (PET), and polyamide (PA) [46].

In textile industries, numerous dye molecules, salts, and additives have been intensively utilized in the textile dyeing process. The precarious dyestuff existence in the wastewater from the dyeing process would harm humans and creatures living in aqueous environments. Therefore, it is essential to remove the dye contaminants from textile wastewater [47–49].

1.9 The scope of this present work

As a result, the principal goal of this study was to improve the membrane properties by incorporating MOFs for the treatment of wastewater. Nanofiltration (NF) technologies are the most hopeful and powerful tool for separating organic dye molecules and inorganic salts [50]. Unfortunately, though, low usage in numerous applications has raised the trade-off issue between selectivity and permeability. Incorporating inorganic additives boost the membrane properties for effective water treatment; nonetheless, it has other problems, including aggregation, insufficient compatibility accumulation, and less dispersibility [42,51–53]. [41,42]. The metal-organic framework (MOFs) introduction as a novel filler for the polymeric membrane is more efficient than inorganic fillers. The synergetic properties of inorganic metal clusters and organic ligands in MOFs offer extraordinary properties to the membranes. According to the literature survey, MOF-5 and MIL-100 (Fe) widely utilized for wastewater treatment. MOFs (MOF-5 and MIL-100 (Fe)) are incorporated into polymeric membranes (CA, PES, PVDF, CS, and PSF) to improve the properties of the membrane.

- Specifically, the objectives of this thesis are as follows:
- To synthesis novel MOF using a sustainable method.
- To investigate and analyse the crystalline phase, functional groups, surface morphology, structural properties, and elemental identification of the prepared samples by X-ray diffraction (XRD), Fourier-transform infrared spectroscopy

(FT-IR), X-ray photoelectron spectroscopy (XPS), Brunauer–Emmett–Teller (BET) method, and Field-emission scanning electron microscopy (FESEM) and Field-emission transmission electron microscopy (FETEM).

- To incorporate the synthesized MOFs into polymeric membranes and fabricate the composite membranes.
- Investigate the effect of MOFs in the polymeric membranes in terms of crystalline phase, functional groups, surface morphology, structural properties, and elemental identification, surface roughness, surface charge, and hydrophilicity.
- To study the filtration performances of membranes, including permeability, rejection efficiency, fouling resistance, reusability for wastewater treatment.

1.10 References

[1] J. Jin, X. Du, J. Yu, S. Qin, M. He, K. Zhang, G. Chen, High performance nanofiltration membrane based on SMA-PEI cross-linked coating for dye/salt separation, J. Memb. Sci. 611 (2020) 118307. https://doi.org/10.1016/j.memsci.2020.118307.

[2] A. Malik, R. Akhtar, E. Grohmann, Environmental Deterioration and Human Health, Springer Netherlands, Dordrecht, 2014. https://doi.org/10.1007/978-94-007-7890-0.

[3] J. Huang, K. Zhang, The high flux poly (m-phenylene isophthalamide) nanofiltration membrane for dye purification and desalination, Desalination. 282 (2011) 19–26. https://doi.org/10.1016/j.desal.2011.09.045.

[4] P. Colindres, H. Yee-Madeira, E. Reguera, Removal of Reactive Black 5 from aqueous solution by ozone for water reuse in textile dyeing processes, Desalination. 258 (2010) 154–158. https://doi.org/10.1016/j.desal.2010.03.021.

[5] M. Muthukumar, Studies on the effect of inorganic salts on decolouration of acid dye effluents by ozonation, Dye. Pigment. 62 (2004) 221–228. https://doi.org/10.1016/j.dyepig.2003.11.002.

[6] S. Ma, S. Lee, K. Kim, J. Im, H. Jeon, Purification of organic pollutants in cationic thiazine and azo dye solutions using plasma-based advanced oxidation process via submerged multi-hole dielectric barrier discharge, Sep. Purif. Technol. 255 (2021) 117715. https://doi.org/10.1016/j.seppur.2020.117715.

[7] S. Leaper, A. Abdel-Karim, T.A. Gad-Allah, P. Gorgojo, Air-gap membrane distillation as a one-step process for textile wastewater treatment, Chem. Eng. J. 360 (2019) 1330–1340. https://doi.org/10.1016/j.cej.2018.10.209.

[8] I. Mantasha, S. Hussain, M. Ahmad, M. Shahid, Two dimensional (2D) molecular frameworks for rapid and selective adsorption of hazardous aromatic dyes from aqueous phase, Sep. Purif. Technol. 238 (2020) 116413. https://doi.org/10.1016/j.seppur.2019.116413.

[9] X. Li, Y. Liu, J. Wang, J. Gascon, J. Li, B. Van Der Bruggen, Metal-organic frameworks based membranes for liquid separation, Chem. Soc. Rev. 46 (2017) 7124–7144. https://doi.org/10.1039/c7cs00575j.

[10] E. Obotey Ezugbe, S. Rathilal, Membrane Technologies in Wastewater Treatment: A Review, Membranes (Basel). 10 (2020) 89. https://doi.org/10.3390/membranes10050089.

[11] G. Arthanareeswaran, P. Thanikaivelan, K. Srinivasn, D. Mohan, M. Rajendran, Synthesis, characterization and thermal studies on cellulose acetate membranes with additive, Eur. Polym. J. 40 (2004) 2153–2159. https://doi.org/10.1016/j.eurpolymj.2004.04.024.

[12] E. S., A. G., I. A.F., G. P.S., L.T. Y., Review on characteristics of biomaterial and nanomaterials based polymeric nanocomposite membranes for seawater treatment application, Environ. Res. 197 (2021) 111177. https://doi.org/10.1016/j.envres.2021.111177.

[13] T. Matsuura, G. Arthanareeswaran, A.F. Ismail, A. Pagidi, R. Saranya, Enhanced oil–water separation using polysulfone membranes modified with polymeric additives, Desalination. 344 (2014) 280–288. https://doi.org/10.1016/j.desal.2014.03.033.

[14] G. Gnanasekaran, S. Balaguru, A. Gangasalam, D.B. Das, Removal of hazardous material from wastewater by using metal organic framework (MOF) -embedded polymeric membranes Removal of hazardous material from wastewater by using metal organic framework (MOF) -embedded polymeric membranes, Sep. Sci. Technol. 00 (2018) 0–13. https://doi.org/10.1080/01496395.2018.1508232.

[15] R. Saranya, G. Arthanareeswaran, S. Sakthivelu, P. Manohar, Preparation and Performance Evaluation of Nanokaolinite- Particle-Based Polyacrylonitrile Mixed-Matrix Membranes, (2012).

[16] T.A. Saleh, V.K. Gupta, Synthesis and characterization of alumina nano-particles polyamide membrane with enhanced flux rejection performance, Sep. Purif. Technol. 89 (2012) 245–251. https://doi.org/10.1016/j.seppur.2012.01.039.

[17] H.P. Srivastava, G. Arthanareeswaran, N. Anantharaman, V.M. Starov, Performance of modified poly(vinylidene fluoride) membrane for textile wastewater ultrafiltration, Desalination. 282 (2011) 87–94. https://doi.org/10.1016/j.desal.2011.05.054.

[18] D.Y. Zhang, J. Liu, Y.S. Shi, Y. Wang, H.F. Liu, Q.L. Hu, L. Su, J. Zhu, Antifouling polyimide membrane with surface-bound silver particles, J. Memb.

Sci. 516 (2016) 83–93. https://doi.org/10.1016/j.memsci.2016.06.012.

[19] Q.-M. Li, H.-Y. Ma, Y.-N. Hu, Y.-F. Guo, L.-J. Zhu, Z.-X. Zeng, G. Wang, Polyamide thin-film composite membrane on polyethylene porous membrane: Fabrication, characterization and application in water treatment, Mater. Lett. 287 (2021) 129270. https://doi.org/10.1016/j.matlet.2020.129270.

[20] Y. Wang, G. He, Y. Shao, D. Zhang, X. Ruan, W. Xiao, X. Li, X. Wu, X. Jiang, Enhanced performance of superhydrophobic polypropylene membrane with modified antifouling surface for high salinity water treatment, Sep. Purif. Technol. 214 (2019) 11–20. https://doi.org/10.1016/j.seppur.2018.02.011.

[21] A. Lin, S. Shao, H. Li, D. Yang, Y. Kong, Preparation and characterization of a new negatively charged polytetrafluoroethylene membrane for treating oilfield wastewater, J. Memb. Sci. 371 (2011) 286–292. https://doi.org/10.1016/j.memsci.2011.01.052.

[22] A. Behboudi, Y. Jafarzadeh, R. Yegani, Polyvinyl chloride/polycarbonate blend ultrafiltration membranes for water treatment, J. Memb. Sci. 534 (2017) 18–24. https://doi.org/10.1016/j.memsci.2017.04.011.

[23] C. Zhao, J. Xue, F. Ran, S. Sun, Modification of polyethersulfone membranes - A review of methods, Prog. Mater. Sci. 58 (2013) 76–150. https://doi.org/10.1016/j.pmatsci.2012.07.002.

[24] A.J. Sanjari, M. Asghari, A Review on Chitosan Utilization in Membrane Synthesis, (2016) 134–158. https://doi.org/10.1002/cben.201500020.

[25] A. Kovtun, E. Campodoni, L. Favaretto, M. Zambianchi, A. Salatino, S. Amalfitano, M.L. Navacchia, B. Casentini, V. Palermo, M. Sandri, M. Melucci, Multifunctional graphene oxide/biopolymer composite aerogels for microcontaminants removal from drinking water, Chemosphere. 259 (2020) 127501. https://doi.org/10.1016/j.chemosphere.2020.127501.

[26] Z. Jiang, Y. Yu, H. Wu, Preparation of CS/GPTMS hybrid molecularly imprinted membrane for efficient chiral resolution of phenylalanine isomers, J. Memb. Sci. 280 (2006) 876–882. https://doi.org/10.1016/j.memsci.2006.03.006.

[27] Q. Long, Z. Zhang, G. Qi, Z. Wang, Y. Chen, Z.-Q. Liu, Fabrication of Chitosan Nanofiltration Membranes by the Film Casting Strategy for Effective Removal of Dyes/Salts in Textile Wastewater, ACS Sustain. Chem. Eng. 8 (2020) 2512–2522. https://doi.org/10.1021/acssuschemeng.9b07026.

[28] A.M. Sajjan, H.G. Premakshi, M.Y. Kariduraganavar, Synthesis and characterization of GTMAC grafted chitosan membranes for the dehydration of low water content isopropanol by pervaporation, J. Ind. Eng. Chem. 25 (2015) 151–161. https://doi.org/10.1016/j.jiec.2014.10.027.

[29] M.M.A. Nikje, Z.M. Tehrani, Novel Hybrid Membranes Based on Chitosan and Organically-Modified Nano-SiO2, Des. Monomers Polym. 12 (2009) 315–322. https://doi.org/10.1163/156855509X448280.

[30] D. Yang, J. Li, Z. Jiang, L. Lu, X. Chen, Chitosan/TiO2 nanocomposite pervaporation membranes for ethanol dehydration, Chem. Eng. Sci. 64 (2009)

3130–3137. https://doi.org/10.1016/j.ces.2009.03.042.

[31] X. Qian, N. Li, Q. Wang, S. Ji, Chitosan/graphene oxide mixed matrix membrane with enhanced water permeability for high-salinity water desalination by pervaporation, Desalination. 438 (2018) 83–96. https://doi.org/10.1016/j.desal.2018.03.031.

[32] S.B. Rekik, S. Gassara, J. Bouaziz, A. Deratani, S. Baklouti, Enhancing hydrophilicity and permeation flux of chitosan/kaolin composite membranes by using polyethylene glycol as porogen, Appl. Clay Sci. 168 (2019) 312–323. https://doi.org/10.1016/j.clay.2018.11.029.

[33] F. Khoerunnisa, W. Rahmah, B. Seng Ooi, E. Dwihermiati, N. Nashrah, S. Fatimah, Y.G. Ko, E.-P. Ng, Chitosan/PEG/MWCNT/Iodine composite membrane with enhanced antibacterial properties for dye wastewater treatment, J. Environ. Chem. Eng. 8 (2020) 103686. https://doi.org/10.1016/j.jece.2020.103686.

[34] S.C. Mamah, P.S. Goh, A.F. Ismail, N.D. Suzaimi, L.T. Yogarathinam, Y.O. Raji, T.H. El-badawy, Recent development in modification of polysulfone membrane for water treatment application, J. Water Process Eng. 40 (2021) 101835. https://doi.org/10.1016/j.jwpe.2020.101835.

[35] W.-J. Lau, A.F. Ismail, Polymeric nanofiltration membranes for textile dye wastewater treatment: Preparation, performance evaluation, transport modelling, and fouling control — a review, Desalination. 245 (2009) 321–348.

https://doi.org/10.1016/j.desal.2007.12.058.

[36] A.G.T. Fane, R. Wang, Y. Jia, Membrane and Desalination Technologies, Humana Press, Totowa, NJ, 2011. https://doi.org/10.1007/978-1-59745-278-6.

[37] B. Van Der Bruggen, C. Vandecasteele, T. Van Gestel, W. Doyen, R. Leysen, A review of pressure-driven membrane processes in wastewater treatment and drinking water production, Environ. Prog. 22 (2003) 46–56. https://doi.org/10.1002/ep.670220116.

[38] U. Mueller, M. Schubert, F. Teich, H. Puetter, K. Schierle-Arndt, J. Pastré, Metal-organic frameworks - Prospective industrial applications, J. Mater. Chem. 16 (2006) 626–636. https://doi.org/10.1039/b511962f.

[39] I. Ahmed, S.H. Jhung, Adsorptive desulfurization and denitrogenation using metal-organic frameworks, J. Hazard. Mater. 301 (2016) 259–276. https://doi.org/10.1016/j.jhazmat.2015.08.045.

[40] Challenges and recent advances in MOF–polymer composite membranes for gas separation.pdf, (n.d.).

[41] R.Y. Hong, Q. Chen, Dispersion of Inorganic Nanoparticles in Polymer Matrices: Challenges and Solutions, in: Adv. Polym. Sci., 2014: pp. 1–38. https://doi.org/10.1007/12_2014_286.

[42] M. Baghbanzadeh, D. Rana, C.Q. Lan, T. Matsuura, Effects of Inorganic Nano-Additives on Properties and Performance of Polymeric Membranes in Water Treatment, Sep. Purif. Rev. 45 (2016) 141–167.

https://doi.org/10.1080/15422119.2015.1068806.

[43] A. Elrasheedy, N. Nady, M. Bassyouni, A. El-Shazly, Metal organic framework based polymer mixed matrix membranes: Review on applications in water purification, Membranes (Basel). 9 (2019). https://doi.org/10.3390/membranes9070088.

[44] B. Van der Bruggen, E. Curcio, E. Drioli, Process intensification in the textile industry: the role of membrane technology, J. Environ. Manage. 73 (2004) 267–274. https://doi.org/10.1016/j.jenvman.2004.07.007.

[45] H. Deng, R. Wei, W. Luo, L. Hu, B. Li, Y. Di, H. Shi, Microplastic pollution in water and sediment in a textile industrial area, Environ. Pollut. 258 (2020) 113658. https://doi.org/10.1016/j.envpol.2019.113658.

[46] H. Hidayaturrahman, T. Lee, A study on characteristics of microplastic in wastewater of South Korea: Identification, quantification, and fate of microplastics during treatment process, Mar. Pollut. Bull. 146 (2019) 696–702. https://doi.org/10.1016/j.marpolbul.2019.06.071.

[47] X.L. Cao, Y.N. Yan, F.Y. Zhou, S.P. Sun, Tailoring nanofiltration membranes for effective removing dye intermediates in complex dye-wastewater, J. Memb. Sci. 595 (2020) 117476. https://doi.org/10.1016/j.memsci.2019.117476.

[48] Y.-F. Mi, G. Xu, Y.-S. Guo, B. Wu, Q.-F. An, development of antifouling nanofiltration membrane with zwitterionic functionalized monomer for efficient dye/salt selective separation, J. Memb. Sci. 601 (2020) 117795.

https://doi.org/10.1016/j.memsci.2019.117795.

[49] G. Gnanaselvan, B. Sasikumar, G. Arthanareeswaran, Y.S. Mok, performance of composite PES/MOF-5 membranes for the treatment of textile wastewater, Desalin. WATER Treat. 156 (2019) 220–228. https://doi.org/10.5004/dwt.2019.23777.

[50] B. Van der Bruggen, C. Vandecasteele, Removal of pollutants from surface water and groundwater by nanofiltration: overview of possible applications in the drinking water industry, Environ. Pollut. 122 (2003) 435–445. https://doi.org/10.1016/S0269-7491(02)00308-1.

[51] S.-L. Wu, F. Liu, H.-C. Yang, S.B. Darling, Recent progress in molecular engineering to tailor organic–inorganic interfaces in composite membranes, Mol. Syst. Des. Eng. 5 (2020) 433–444. https://doi.org/10.1039/C9ME00154A.

[52] D. Qadir, H. Mukhtar, L.K. Keong, Mixed Matrix Membranes for Water Purification Applications, Sep. Purif. Rev. 46 (2017) 62–80. https://doi.org/10.1080/15422119.2016.1196460.

[53] P.S. Goh, B.C. Ng, W.J. Lau, A.F. Ismail, Inorganic nanomaterials in polymeric ultrafiltration membranes for water treatment, Sep. Purif. Rev. 44 (2015) 216–249. https://doi.org/10.1080/15422119.2014.926274.

CHAPTER 2 MATERIALS AND METHODS

2.1 Introduction

This chapter explains the detailed information regarding the materials, preparation, characterizations, and fabrication techniques adapted for the present investigation of this work. Initially, to accomplishes the research objective; experimental work was done in the laboratory, followed by physicochemical characterization, evaluation of properties of the obtained materials. This chapter describes the experimental details, including the materials, chemicals, and apparatus used in the research project. Next, typical materials synthesis methods were followed, such as solvothermal, hydrothermal processes to prepare metal-organic frameworks synthesis. The film casting and phase inversion techniques were followed to fabricate the membranes, and finally, the filtration study is discussed in detail.

2.2 Materials

2.2.1 Chemicals

Table. 2.1 displayed the list of chemicals used in this study and respective grades and were used without any further purifications and applications.

Table 2.1 Specifications of chemicals used in this study

Chemicals	Application	Supplier
N, N-dimethylformamide (DMF)	MOF-5/Membrane fabrication	Merck specialties Pvt Ltd

Terephthalic acid	MOF-5 synthesis	Merck specialties Pvt Ltd
Zinc nitrate hexahydrate	MOF-5 synthesis	Loba Chemie Pvt Ltd. India
Copper sulphate pentahydrate	Filtration study	Merck specialties Pvt Ltd
Cobalt sulfate hexahydrate	Filtration study	Merck specialties Pvt Ltd
Polyethersulfone (PES, veradel 13000 p)	Membrane fabrication	Solvay Solexis Ltd., India
N, N-dimethylformamide (DMF)	Membrane fabrication	Merck specialties Pvt Ltd
Polyvinylidene fluoride (PVDF, Solef® 6010)	Membrane fabrication	Solvay Solexis Ltd., India
Cellulose Acetate (CA)	Membrane fabrication	Mysore Acetate and Chemicals Company Ltd., India
Indigo carmine (M.W: 466)	Filtration study	SRL Pvt Ltd, Mumbai, India.
Methylene blue (M.W: 319)	Filtration study	Sigma-Aldrich, South Korea

Trimesic acid (TA)	MIL-100 (Fe) synthesis	Sigma-Aldrich, South Korea
Chitosan (CS, medium molecular weight)	Membrane fabrication	Sigma-Aldrich, South Korea
Acetic acid (AA)	Membrane fabrication	Sigma-Aldrich, South Korea
Polyethylene glycol (PEG, MW=10,000)	Membrane fabrication	Sigma-Aldrich, South Korea
Sodium chloride (NaCl)	Filtration study	Sigma-Aldrich, South Korea
Sodium sulfate (Na_2SO_4)	Filtration study	Sigma-Aldrich, South Korea
Calcium chloride ($CaCl_2$)	Filtration study	Sigma-Aldrich, South Korea
magnesium sulfate ($MgSO_4$)	Filtration study	Sigma-Aldrich, South Korea
Iron (II) chloride tetrahydrate ($FeCl_2 \cdot 4H_2O$), and	MIL-100 (Fe) synthesis	Daejung Chemicals Ltd, South Korea

Sodium hydroxide (NaOH),	MIL-100 (Fe) synthesis	Daejung Chemicals Ltd, South Korea
Hydrochloric acid (HCl)	Filtration study	Daejung Chemicals Ltd, South Korea
Ethanol (C_2H_5OH)	Filtration study	Daejung Chemicals Ltd, South Korea
Methyl orange (MO)	Filtration study	Fisher Scientific Korea Ltd., Seoul, Korea
Polysulfone (PSF, average Mw~ 35000	Membrane fabrication	Sigma-Aldrich, South Korea
poly(vinylpyrrolidone) (PVP, average Mw 10000)	Membrane fabrication	Sigma-Aldrich, South Korea
N-methyl-2-pyrrolidone (NMP)	Membrane fabrication	Sigma-Aldrich, South Korea
Polyvinyl chloride (PVC)	Filtration study	Sigma-Aldrich, South Korea
Polyethylene (PE)	Filtration study	Sigma-Aldrich, South Korea

2.2.2 Gas

Nitrogen gas used for filtration study to maintain the constant pressure inside the nanofiltration stirred cell.

2.3 Apparatus

Table 2.2 List of equipment used for materials preparation and filtration study.

Apparatus	Model or specifications	Manufacturer
Hotplate & magnetic stirrer	MGH-320	SIBATA
Oven	OF-02 GW	ISUZU
Balance	DRAGON	Mettler Toledo
Nanofiltration stirred cell	HP4750	Sterlitech
pH meter	STARTER 3100	OHAUS
Thermally insulated shaker	SSI-501	Finetech

2.4 MOF synthesis

Several techniques were followed for the MOFs synthesis. Specifically, slow diffusion [1], hydrothermal, solvothermal [2], electrochemical [3], mechanochemical [4], microwave-assisted heating, and ultrasound [5]. However, based on the structures and properties, MOFs may be prepared using several distinct synthetic methods.

2.5 Membrane preparation

The phase inversion methods and film casting and solvent evaporation methods have been used to fabricate membranes. MOFs were mixed with polymers at solvent and placed at stirring for homogeneous solution formation. The above-prepared dope solution cast a smooth glass plate by a film applicator. After releasing, the thin film was instantly immersed in the distilled water at 10°C. The synthesized membrane was submerged into Deionised water for 24 hr to remove the residual solvent.

2.6 Material characterization

The synthesized MOFs and membranes were analyzed using several characterization techniques to identify the crystal phase, morphology, micro and nanostructure, size, composition, surface area, and surface charge. The detailed experimental conditions are specified below.

2.6.1 Fourier transform infrared spectroscopy

To characterize the change in chemical structure and functional group identification of MOFs and membranes were analyzed Fourier transform infrared (FTIR) spectrophotometer (Thermo Scientific Nicolet iS5 FT-IR spectrometer). The change in chemical structure can be observed through wavenumber drift against the percentage transmittance, and the samples were collected over the spectral region of wavelengths from 400 to 4000 cm^{-1}.

2.6.2 X-ray diffraction

X-ray diffraction (XRD) is an essential analytical technique to determine the phase purity, the phase of crystal, structure, and crystal size. The synthesized samples were performed using (XRD, PANanalytical's Empyrean) X-ray diffractometer operated at the power of 40 kV and current of 40 mA with Cu Kα radiation in the range 2θ angle of 5−80° with the step of 0.02°.

2.6.3 Brunauer–Emmett–Teller (BET) surface area analysis

Nitrogen (N_2) adsorption-desorption isotherm measurement was carried out to determine the surface area, pore-volume, and pore size distribution of the as-prepared samples. The Brunauer–Emmett–Teller (BET) analysis was performed with Quantachrome Autosorb-1, Quantachrome instrument v2.11, and nitrogen gas was used as an adsorptive to determine the above parameters. The specific surface area of samples calculated by using the multiple-point BET model. The pore size distribution obtained from the isotherm's adsorption/ desorption branch by Barrett-Joyner-Halenda (BJH) method. The total pore volume was calculated from the volume of nitrogen adsorbed at a relative pressure of P/P_o= 0.95.

2.6.4 Field-emission scanning electron microscopy

Field-emission scanning electron microscopy (FESEM) analysis can provide information on surface morphology (size and shape) with three-dimensional images. The MOFs and membrane (surface and cross-sectional) morphology were observed by field-emission scanning electron microscope (FESEM, TESCAN, MIRA3, Center for Research

Facilities (CRF), Jeju National University, Jeju, Republic of Korea) at 15 kV. The membrane samples were dried and cut into small pieces at room temperature. The samples were cryogenically fractured by immersed into liquid nitrogen to observe the cross-sectional morphology. Before analysis, Pt sputter-coated on the samples using a sputter coater (quorum rotary-pumped sputter coater-Q150R).

2.6.5 Field-emission transmission electron microscopy

Nano-structural morphology of MIL-100 (Fe) examined by field-emission transmission electron microscopy (FETEM, JEOL TEM: JEM 2011, KBSI Busan center, South Korea).

2.6.6 Energy dispersive X-ray spectroscopy

The elemental composition of membrane samples was examined by energy-dispersive X-ray spectroscopy (EDS, TESCAN, MIRA3, Center for Research Facilities (CRF), Jeju National University, Jeju, Republic of Korea) with element mapping measurements at 15 kV.

2.6.7 X-ray photoelectron spectroscopy

The atomic composition and chemical state of samples were examined by X-ray photoelectron spectroscopy (XPS) techniques using ESCA-2000, VG Microtech Ltd (Korea Basic Institute of Science (KBSI), Busan Center, Korea).

2.6.8 Zeta potential measurement

The surface potential of membranes investigated by zeta potential and nanoparticle analyzer (ELSZ-2000, KAIST, Energy Environment Research Center, South

Korea). Surface and pore parameters measured by particle and pore size analysis system (UPA-150, ASAP2010, AutoporeIV, KBSI, Jeonju Center, South Korea).

2.6.9 3D nanoprofiller

3D nano-profiling system (3D Optical Surface Profiler, NV-2400, Nanosystem, Korea) is performed to characterize membranes' surface roughness. The 3D nanoprofillers provide the 2D and 3D surface roughness of the membrane surface, average roughness (Ra), and root means squared roughness (Rq).

2.6.10 Contact angle measurement

The contact angle measurements examined the hydrophilicity/hydrophobicity characteristics of the membrane surface. The contact angle of the prepared membranes was performed by a sessile drop method using a goniometer (Phonix 300, Surface & Electro-Optics Co., Ltd., Korea). Contact angle readings were calculated by placing 5 µl of water in drops on dried membrane samples at five different regions. The average contact angle readings were reported [6].

2.6.11 Pore size and porosity measurement

The porosity (ε) of all the membrane samples was calculated by the gravimetric method, as the following Eq. (1) [7].

$$\varepsilon = \left(\frac{\frac{\omega_1 - \omega_2}{d_w}}{\frac{(\omega_1 - \omega_2)}{d_w} + \left(\frac{\omega_2}{d_p}\right)} \right) \qquad (1)$$

where, ω_1, ω_2, d_w, and d_p are wet, dry weight of the membranes (g), the density of water and polymer, respectively.

The membranes mean pore radius calculated by Guerout-Elford-Ferry Eq. (2).

$$r_m = \sqrt{\left(\frac{(2.9 - 1.75\varepsilon)\ 8Ql\eta}{\varepsilon\ A\ \Delta P}\right)} \qquad (2)$$

where η is the water viscosity (8.9×10^{-4} Pa s), l is the membrane thickness (m), ε is the porosity of the membrane (%), Q is the permeate flow rate (m^3/s), ΔP is the operating pressure (0.1 MPa), and A is the active membrane area (m^2).

2.7 Nanofiltration

The filtration study was carried out in dead-end nanofiltration (Sterlitech HP4750 stirred cell [8]) with an active membrane area of 14.6 cm^2 (Figure 4.1(b)). The pre-compaction of membranes was employed by using pure DI water at constant pressure for 60 min. The separation performances of the membranes were examined by the filtration experiments using simulated wastewater, with the various concentration and pH of cationic MB and anionic MO dyes, microplastics, NaCl, Na_2SO_4, $CaCl_2$, and $MgSO_4$ salts solutions. The permeability value was calculated by following Eq. (3).

$$J_w = \frac{V}{A \times \Delta t} \qquad (3)$$

where J_w is permeability (L/m^2h), V is the permeate volume (m^3), A is the active membrane area (m^2), and Δt is the permeation time (h).

The rejection percentage (R) of the membrane was calculated by the Eq. (4)

$$\mathrm{R}\ (\%) = \frac{\mathrm{C_f} - \mathrm{C_p}}{\mathrm{C_f}} \times 100\% \qquad (4)$$

where C_f (ppm) and C_p (ppm) are feed and permeate concentrations of synthetic textile wastewater solutions (dyes, ions, and salts), respectively. We measured the concentration values of feed, permeate, and retentate solutions in terms of salt rejection. R_{actual} calculated from Eq. (4), and R_{real} estimated from the retentate concentration after the filtration. The dye concentration was measured by an Ultraviolet-visible (UV-vis) spectrophotometer (MEGA-2100- SCINCO Company–Korea) at a wavelength of 460 nm for MO and 665 nm for MB. The salt concentration is determined by a conductivity meter (DiST 3 by Hanna instruments, South Korea). The pH of the dye solutions was adjusted by 0.1 M NaOH and 0.1 M HCl. The ion presence in the feed and permeate solution was characterized by ion chromatography (Model: ICS-1600, Thermo Scientific. (Dionex Corp.)).

2.8 Flux recovery ratio

The membrane reusability and antifouling performance were calculated by the percentage of flux recovery ratio (FRR) by the following Eq. (5).

$$\mathrm{FRR}\ (\%) = \left(\frac{\mathrm{J_{w.2}}}{\mathrm{J_{w.1}}}\right) \times 100 \qquad (5)$$

where, $J_{w.1}$ is initial pure water flux, and $J_{w.2}$ is pure water flux after dye and salt filtration [9].

2.9 References

[1] J.-Y. Wu, T.-C. Chao, M.-S. Zhong, Influence of Counteranions on the Structural Modulation of Silver–Di(3-pyridylmethyl)amine Coordination Polymers, Cryst. Growth Des. 13 (2013) 2953–2964. https://doi.org/10.1021/cg400363e.

[2] Y. Zhang, X. Bo, A. Nsabimana, C. Han, M. Li, L. Guo, Electrocatalytically active cobalt-based metal–organic framework with incorporated macroporous carbon composite for electrochemical applications, J. Mater. Chem. A. 3 (2015) 732–738. https://doi.org/10.1039/C4TA04411H.

[3] N. Campagnol, E.R. Souza, D.E. De Vos, K. Binnemans, J. Fransaer, Luminescent terbium-containing metal–organic framework films: new approaches for the electrochemical synthesis and application as detectors for explosives, Chem. Commun. 50 (2014) 12545–12547. https://doi.org/10.1039/C4CC05742B.

[4] M.Y. Masoomi, A. Morsali, P.C. Junk, Rapid mechanochemical synthesis of two new Cd(<scp>ii</scp>)-based metal–organic frameworks with high removal efficiency of Congo red, CrystEngComm. 17 (2015) 686–692. https://doi.org/10.1039/C4CE01783H.

[5] N.A. Khan, S.H. Jhung, Synthesis of metal-organic frameworks (MOFs) with microwave or ultrasound: Rapid reaction, phase-selectivity, and size reduction, Coord. Chem. Rev. 285 (2015) 11–23. https://doi.org/10.1016/j.ccr.2014.10.008.

[6] A. Pagidi, R. Saranya, G. Arthanareeswaran, A.F. Ismail, T. Matsuura, Enhanced oil–water separation using polysulfone membranes modified with polymeric additives, Desalination. 344 (2014) 280–288. https://doi.org/10.1016/j.desal.2014.03.033.

[7] G. Gnanasekaran, S. Balaguru, G. Arthanareeswaran, D.B. Das, Removal of hazardous material from wastewater by using metal organic framework (MOF) embedded polymeric membranes, Sep. Sci. Technol. 54 (2019) 434–446. https://doi.org/10.1080/01496395.2018.1508232.

[8] Y.T. Chung, L.Y. Ng, A.W. Mohammad, Sulfonated-polysulfone membrane surface modification by employing methacrylic acid through UV-grafting: Optimization through response surface methodology approach, J. Ind. Eng. Chem. 20 (2014) 1549–1557. https://doi.org/10.1016/j.jiec.2013.07.046.

[9] G. Arthanareeswaran, P. Thanikaivelan, Fabrication of cellulose acetate-zirconia hybrid membranes for ultrafiltration applications: Performance, structure and fouling analysis, Sep. Purif. Technol. 74 (2010) 230–235. https://doi.org/10.1016/j.seppur.2010.06.010.

CHAPTER 3 PERFORMANCE OF COMPOSITE PES/MOF-5 MEMBRANES FOR THE REMOVAL OF HAZARDOUS TEXTILE DYES

3.1 Introduction

The treatment of the discharged hazardous wastewater from various dye-utilizing industries is a global issue in the environmental concern. In addition, manufacturing units like textile, plastic, paper, leather, food processing, and cosmetics contributed majorly to the discharge of dyes [1]. The effluent from textile industries contains organic and inorganic salts, heavy metals, and organic dyes. The release of dye to aquatic sources can cause a severe problem because of its toxicity and carcinogenic effect on marine and human life. Thus, it is essential to treat dye effluent before discharging them into the environment.

Numerous methods have been adopted for dye removal, namely coagulation, adsorption [2], ion exchange [3], electrochemical [4], oxidation, and membrane separation [5]. Membrane separation is more efficient for treating dye effluent than conventional methods because of its less energy consumption, effective removal percentage, higher selectivity, and easy handling process [6]. Nanofiltration (NF) was proven to be a promising technique for removing dyes from wastewater [5-7]. So, consistent attempts have been made to fabricate novel membranes for wastewater treatment with high selectivity, permeability, and increased membrane stability. The performance of membranes could be heightened by improving the interface compatibility of polymeric matrix and fillers. Cheng et al. Studied the incorporation of potential nanomaterials into membranes matrix enhanced the ultrafast molecular separation (UMS) membranes [7].

The properties of the poly vinylidene fluoride (PVDF) membrane have been improved by the addition of mussel-inspired sticky catechol with functionalized polyethylene glycol (Cate-PEG) [8]. Ma X H et al. [9] synthesized NF membranes by the incorporation of MOFs (NH_2-MIL-101(Al) and NH_2-MIL-101(Cr)) into chitosan polymeric matrix for the effective removal of multivalent cations. The Metal-Organic Frameworks (MOFs) is a good alternative compared to Nano-fillers. Using MOFs as fillers for enhancing the performance of polymeric membranes is a promising research area.

MOFs are primarily used in gas separation, storage, drug delivery, and catalysis [10]. MOFs exposed a potential adsorbent for water pollutants such as malachite green, methylene blue [11], copper ions [12], etc. MOFs have an advantage over other porous materials due to their high surface area, tunability, high porosity, open metal sites, etc. [13]. Adsorptive removal of methyl orange and methylene blue dye has been examined using MOF-235. It shows that MOF can adsorb many dyes via electrostatic interaction between dyes and adsorbents [14]. Echaide et al. studied the performance of MOFs embedded nanocomposite membranes to remove dye with different solvents [15]. However, studies on MOFs as adsorbents and their effects on membranes synthesis for liquid phase separation are limited. Polyethersulfone (PES) is nominated for nanofiltration membrane due to its good chemical, thermal and mechanical stability, commercial availability, adequate selectivity, and permeability [3].

Following those above, in the present work, a detailed investigation was carried out for the removal of methylene blue (MB) and indigo carmine (IC) using MOF-5 incorporated PES nanofiltration membranes. We have studied the incorporation of MOF-

5 into polymeric membranes as an active material for the removal of hazardous materials like Cu (II) and Co (II) from wastewater [16]. The effect of MOF-5 on the membrane morphology and performance was evaluated. The efficiency of MOF-5 incorporated membranes for dye removal was studied through a nanofiltration study of MB and IC. Chemical structures of dye used for adsorption and filtration studies are shown in Figure 3.1.

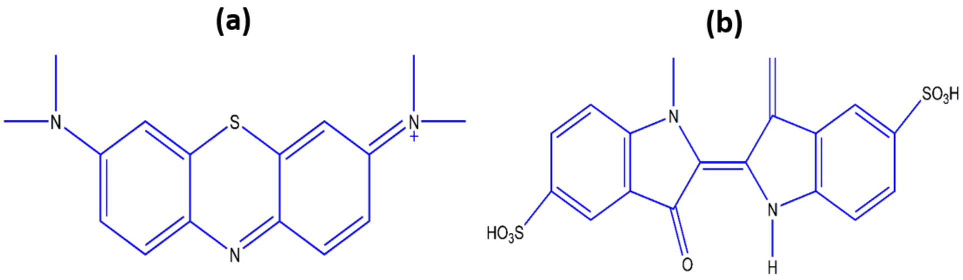

Figure 3.1 Structures of (a) Methylene blue (b) Indigo carmine.

3.2 Preparation and characterization of MOF-5

MOF-5 was synthesized in a glass reactor equipped with a reflux condenser following the procedure reported in the literature. [9,15] 2 g of terephthalic acid and 9.31 g of zinc nitrate hexahydrate were dissolved in 60 ml of DMF solution under stirring at atmospheric conditions and heated up to 150°C for 4h. After 2 hr, white crystals of MOF-5 were formed, and the product was cooled down to room temperature. The white crystals were separated by filtration and washed with 100 ml acetone, and finally, solid crystals were dried at 60°C for 3 hr in a vacuum oven.

3.3 Membrane preparation

The phase inversion methods have been used in the fabrication of neat and MOF-5 incorporated PES membranes. MOF-5 loading was kept at 0.25%, 0.5% and 0.75% of PES. The casting solutions contain 17.5% of PES and MOF-5 and 21.7 ml (82.5%) of DMF solvent. The composition of the membrane casting solution is listed in Table. 3.1. For composite membranes, the MOF-5 particles were added into DMF solution and well dispersion by ultra-sonication for 1 hr, followed by stirring at room temperature. The PES powder was added to the mixture solution and stirred for 3-5 hours until a uniform dispersion occurred. After the complete dispersion, the dope solution was placed for 30 min in ultra-sonication to prepare a homogenous casting solution. For neat PES, a similar procedure was followed to prepare dope solution without adding the MOF-5 particles. The above-prepared dope solution was cast by 400 μm thickness of casting knife at smooth glass plate. After casting, the thin film was instantly immersed in the distilled water at 10°C. The synthesized PES membrane was submerged into fresh distilled water for 24 hr to remove the residual solvent.

Table 3.1 The membranes composition.

Membrane code	PES and MOF-5 composition (17.5 wt. %)	Solvent (wt %)	
	PES	MOF-5	DMF
M0	100%	-	82.5%
M1	99.75%	0.25%	82.5%
M2	99.50%	0.50%	82.5%
M3	99.25%	0.75%	82.5%

3.4 Permeation studies

The permeation of composite PES/MOF-5 and neat PES membranes were studied with pure water and 50 mg/l of textile dye (methylene blue and indigo carmine) at 10 bar pressure. Furthermore, the effect of different pH) were studied by using a dead-end Nanofiltration cell (model HP4750 STIRRED CELL, USA) with an effective membrane area of 13.6 cm^2. Initially, membranes were compacted to collect steady-state permeate volume. Once a steady-state was achieved. The membrane permeates volume was collected every 10 min.

3.5 Rejection of textile dye

The rejection percentage (R) of a textile dye such as methylene blue (λ=665 nm) and indigo carmine (λ = 610 nm) for both neat PES and PES/MOF-5 membranes was calculated by the following equation (2). The feed and permeate concentration of textile dye solution has been analyzed by a UV visible spectrophotometer (Model: spectroquant prove 600).

$$R = \left(1 - \frac{C_f}{C_p}\right) \times 100 \qquad (2)$$

C_f is feed concentrations of the dye solutions; C_p is the permeate concentrations of the dye solutions.

3.6 Results and Discussion

3.6.1 FTIR characterization of MOF-5

The FTIR spectra of MOF-5 are shown in Figure 3.2 the peaks of 1381 and 1573 cm^{-1} show the Asymmetric stretching of C-O bonded to Zn has been identified by the attachment of carboxylate ligand to Zn_4O Centre. In addition, the small peak presence between 900 to 1250 cm^{-1} specifies the benzene dicarboxylate linker's C-H stretching. The broad peak in the range of 3161 cm^{-1} shows the O-H group IR bands at 1502, and 653 cm^{-1} indicated random dimethylformamide (DMF) distribution in the MOF-5 framework structure [17].

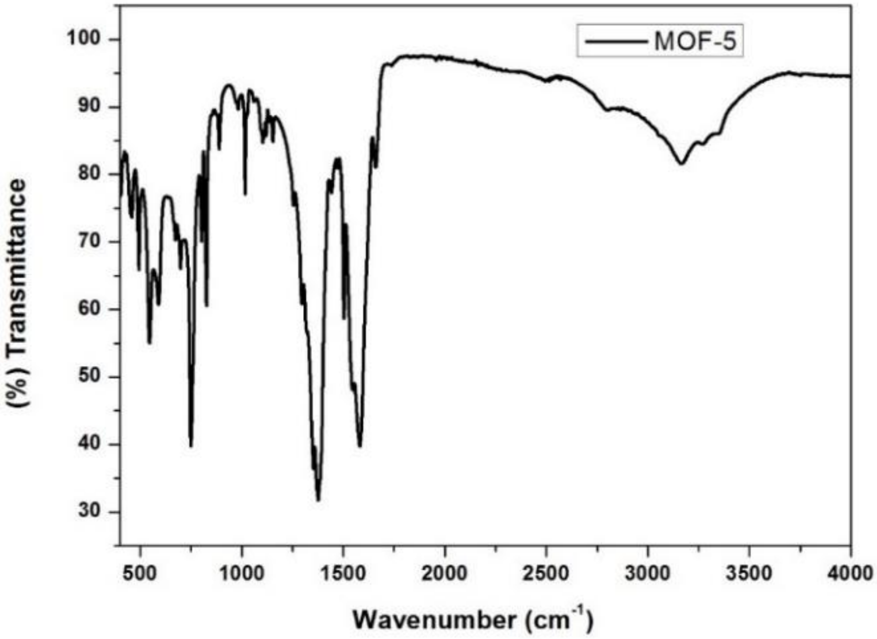

Figure 3.2 FTIR spectra of MOF-5.

3.6.2 XRD analysis of MOF-5

X-ray diffraction analysis of MOF-5 is shown in Figure 3.6. The peaks at 6.8°, 9.7°, 14° and 15.8° in 2θ which indicates the formation of a crystalline structure [17]. The inconsistency peaks appear due to the framework interpenetration and pore occupation. The intensities of the two peaks were upturned, which can be attributed to some alterations of atomic orientations in the crystal planes by absorbed species (solvent and water molecules), unreacted zinc centers, and framework interpenetration.

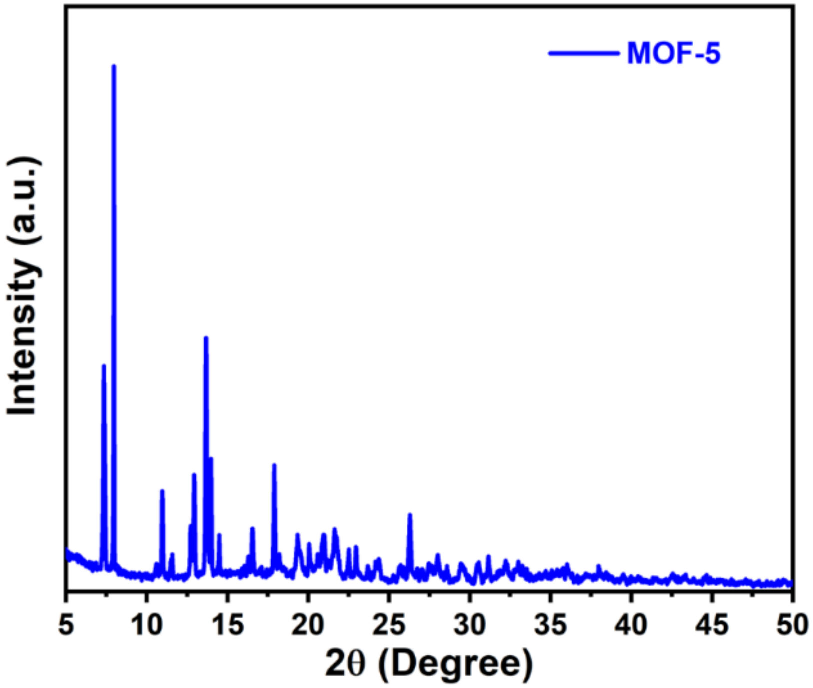

Figure 3.3 XRD spectra of MOF-5.

3.6.3 Surface Morphology of MOF-5

The surface morphology of MOF-5 has shown using SEM images in Figure 3.6. Irregularly shaped, the majority had the cubic shape with crystal structure and porous nature, present in the (Figure 3.4(a) and Figure 3.4(d) [17]. The cubical structure has occurred more, and some cluster-like arrangement also presents which shows the adsorption property of MOF-5, its shows in (Figure 3.4(b) and Figure 3.4(c). The organic cluster and inorganic moiety interaction have occurred in MOF-5.

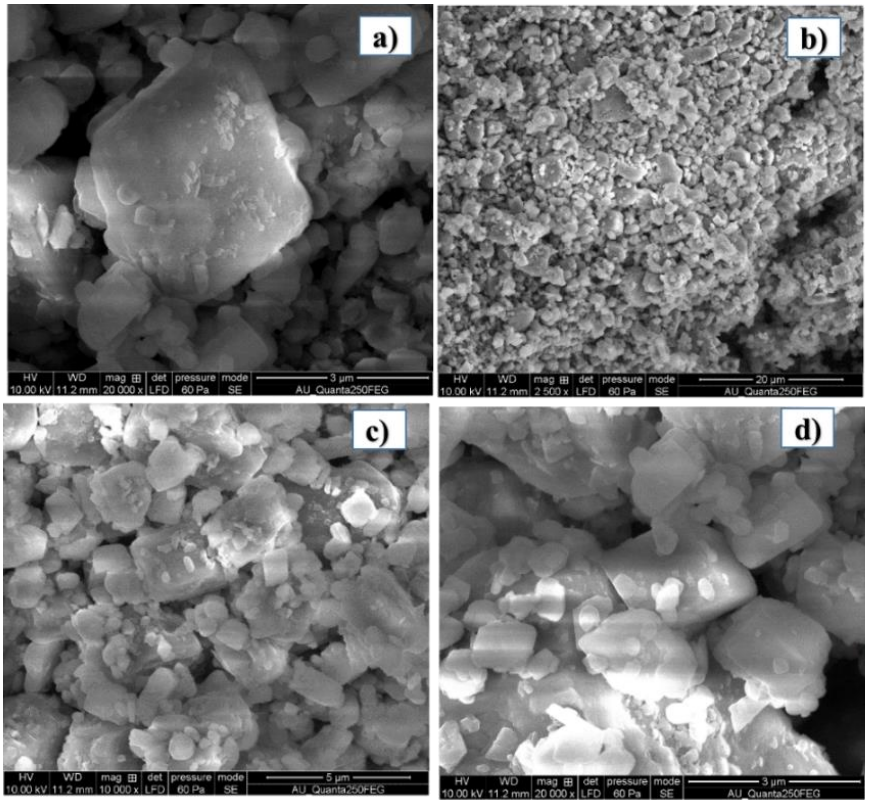

Figure 3.4 SEM image of MOF-5.

3.6.4 Energy Dispersive X-ray Spectroscopy of MOF-5

The elemental composition of the MOF-5 was characterized by EDX (Figure3.5), revealing the expected elemental constituents (C, Zn, and O) are detected. Furthermore, the peak appearance indicates the Zn metal ion attaches with carboxylate ligand, and it proves the formation of MOF-5 by the interaction of metal ion and organic cluster [17].

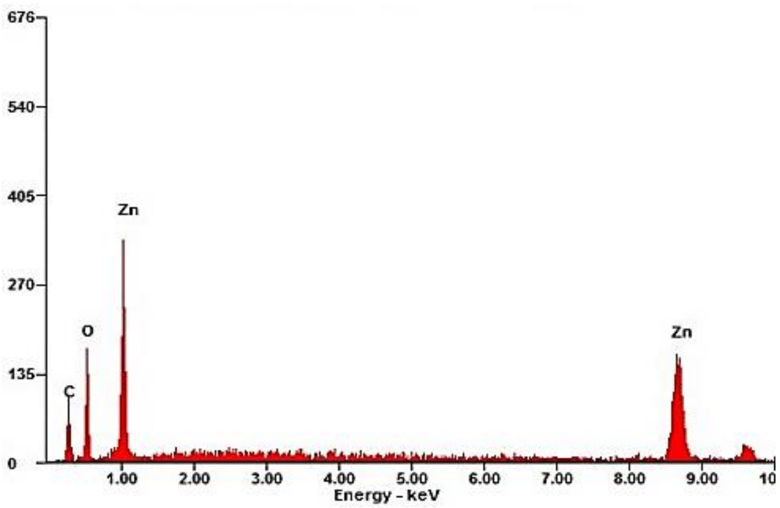

Figure 3.5 EDX spectra of MOF-5

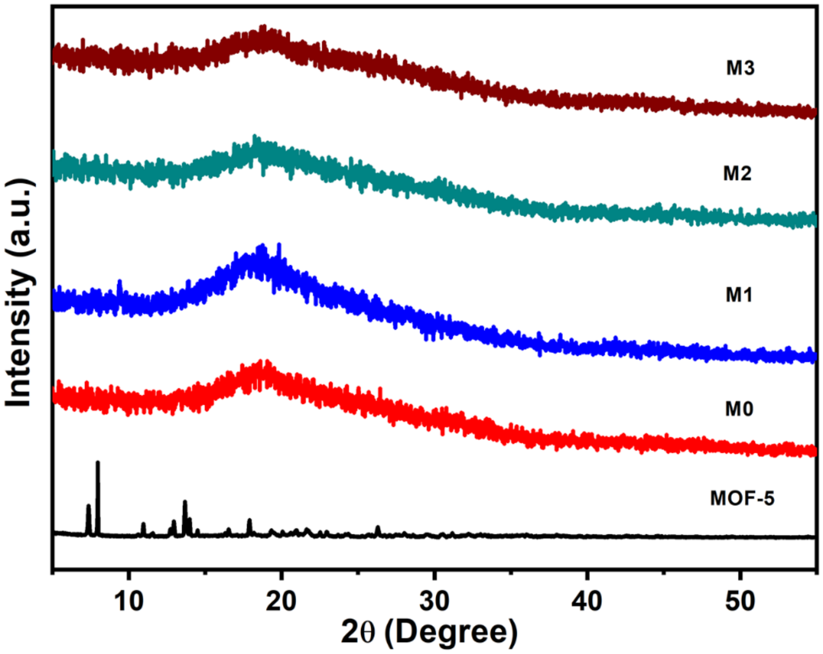

Figure 3.6 XRD spectra of membranes.

3.6.5 XRD analysis of membranes

Figure 3.6 shows the XRD patterns of neat and MOF-5 embedded PES membranes and MOF-5. Both neat and PES/MOF-5 membranes have a peak occurrence at 2Θ = 18°, which indicates the amorphous characteristic of PES, confirming the successful fabrication of PES membranes [20]. The XRD spectra of MOF-5 at 6.9° and 9.8° at 2ϴ indicate the successful MOF-5 synthesis [21]. The peak at 2ϴ = 6.9° in the PES/ MOF-5 membranes shows a slight shift, indicating the distribution of MOF-5 in the PES matrix. The appearance of these peaks clearly shows that MOF-5 acts as a surface modifying agent for PES membranes and proves the MOF-5 and PES matrix interaction [18].

3.6.6 Surface morphology of membranes

Cross-section images of composite PES/MOF-5 and neat PES and membranes are shown in Figure 3.7 The asymmetry with a finger-like structure occurred in both neat PES and PES/MOF-5 membranes. In addition, the interconnection between the bottom layer and skin top layer was upgraded for PES/MOF-5 membranes. Finger-like substructures and thin skin layers were observed with the addition of MOF-5. The permeability and pore radius was improved. The wide finger-like pore size and macro voids of membranes were enlarged in the bottom layer by increasing the concentration of MOF-5 into the PES matrix. In addition, the pore size and permeability of PES/MOF-5 membranes were improved [22].

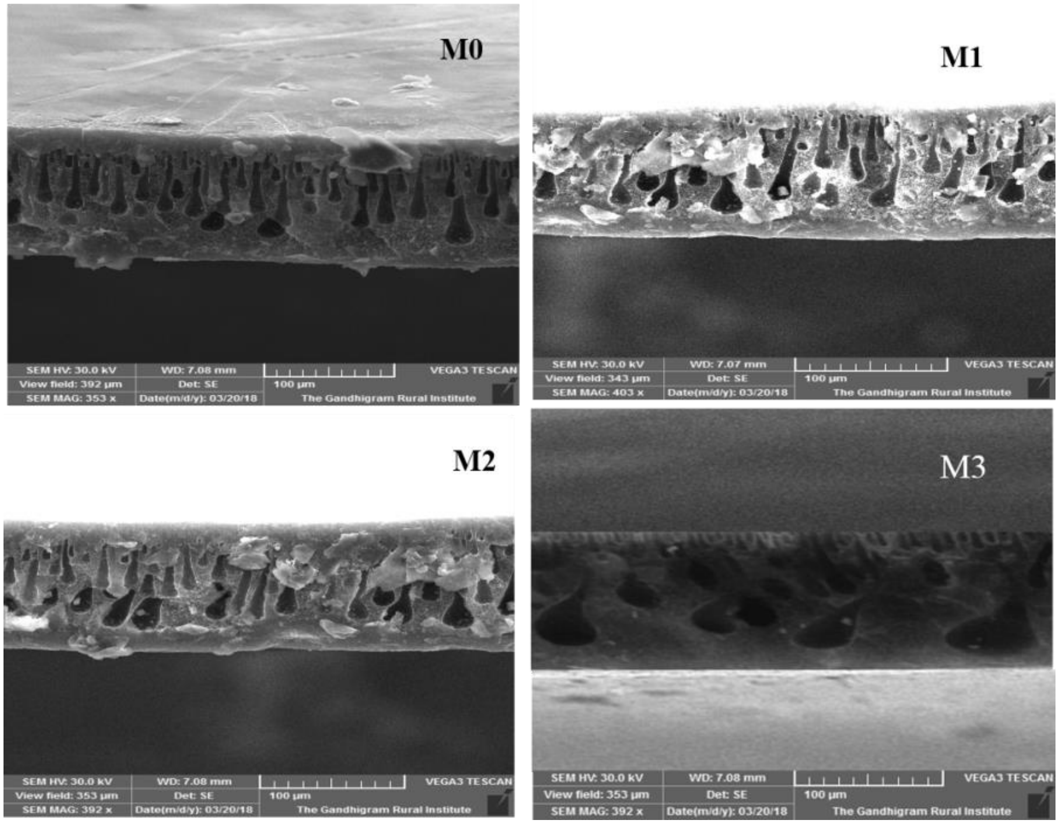

Figure 3.7 Cross-sectional images of membranes.

3.6.7 EDX analysis of membranes

Figure 3.8 shows the EDX spectra of hybrid PES/MOF-5 and neat PES membranes. It shows that all the organic compound has been present in neat PES membrane and PES/MOF-5 membranes and MOF-5 distribution on PES matrix. The presence of the Zn element has proved the impact of MOF-5 on the PES/MOF-5. The minor percentage of Zn in the PES/MOF-5 membranes due to the low loading of MOF-5 into the PES matrix [23].

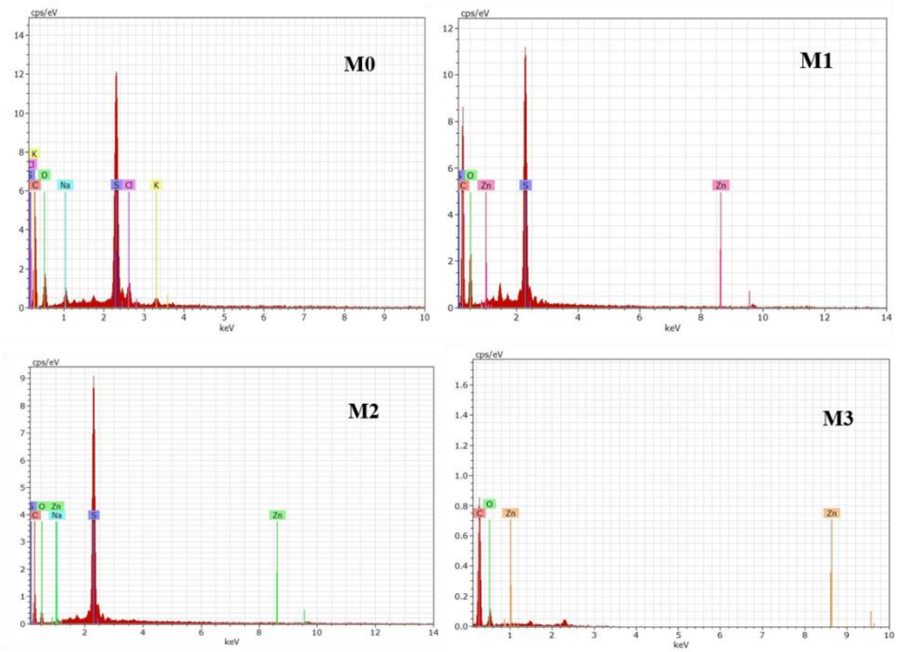

Figure 3.8 EDX spectra of membranes.

3.6.8 Contact angle measurement of membranes

The membrane permeability and antifouling property always depended upon the hydrophilic nature of membranes, which is commonly investigated via contact angle measurement. Contact angle measurements of neat PES and PES/MOF-5 membranes are summarized in Table. 3.2. When increasing the loading percentage of MOF-5 into the PES matrix, the water contact angle decreased from 73.1° to 60.3°, which indicates that PES membranes' hydrophilicity and pore radius increased. The hydrophilicity of PES/MOF-5 membranes has enhanced with the hydrophilic hydroxyl (-OH) functional group (MOF-5) incorporation into the polymer matrix (PES membranes) [24]. It proves that incorporating MOF-5 has enhanced the antifouling property and permeability of the PES matrix [25].

Table 3.2 The membranes properties.

Sl.no	**Name of the Membranes**	**Porosity (%)**	**Pore Radius (nm)**	**Water Contact Angle (°)**
1	M0	63.40	6.45	73.1 ±2.3
2	M1	63.96	6.91	70.6 ± 1.7
3	M2	66.67	7.74	66.7 ± 2.1
4	M3	67.40	8.05	60.3 ± 2.5

3.6.9 Porosity and pore size of membranes

The porosity and pore size of the membranes were listed in Table. 3.2. The porosity increases from 63.4% to 67.4%, increasing the concentration of MOF-5 into the PES membranes. Rising porosity for the impact of the membrane on the antifouling properties of membranes [27]. The pore size of the membranes is gradually increasing from 6.45 nm to 8.05 nm with the increasing concentration of MOF-5. The formation of a pore on the surface of the membrane enhances the permeability and adsorption of membranes [28].

3.6.10 Permeability of membranes

Figure 3.9 shows the permeability of pure water and dye solution of membranes. The pure water permeation of PES/MOF-5 membranes was increasing from 20.5 to 77.1 L/m^2 hr compared to neat PES membranes. The permeability of PES membranes was influenced by the concentration of MOF-5 into the PES matrix. It confirms that the addition of MOF-5 effectively enhanced the hydrophilicity and pore formation of PES membranes. The permeate flux of dye solution also increased compared to neat PES membranes, but the pure water flux is high compared to dye solution flux due to the fouling formation on the membranes. The particle accumulation occurred in the PES/MOF-5 membranes when increasing the concentration of the MOF-5 particles more than 0.75%, which leads to the particle's irregular distribution in the composite membranes [29]. The enhanced membrane permeability shows that incorporating MOF-5 into the PES matrix improves the membranes' hydrophilicity and anti-fouling properties [30].

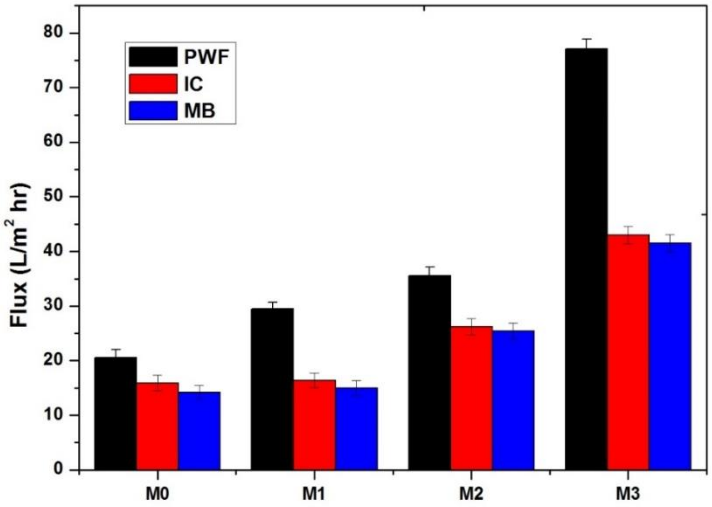

Figure 3.9 Permeate flux rate of membranes.

3.6.11 Dye rejection

The percentage rejection of textile dye (Methylene Blue and Indigo Carmine) has been studied for both neat PES and PES/MOF-5. Figure 3.10 and Figure 3.11 show the rejection percentage of methylene blue and indigo carmine, respectively, at various pH. The MOF-5 incorporated PES membranes have a higher rejection percentage of methylene blue and indigo carmine than neat PES membranes. In addition, the modified PES membranes have higher rejection rates, such as 97% and 89% for MB and IC. The selectivity for dye removal has been enhanced due to the coordination interactions between polymeric matrix (PES) functional groups and organic ligands and Zn (II) [29]. The high rejection percentage of IC dyes due to the size exclusion and charge repulsion [31]. The rejection performance of MB and IC for PES/MOF-5 membranes increased with the increasing concentration of MOF-5 into the PES matrix [30]. The presence of metal oxide in the MOF-5 has enhanced the higher adsorption of dye on PES membranes. MB dye has a higher rejection percentage due to the electrostatic attraction of positively charged MB with a negatively charged PES matrix [32].

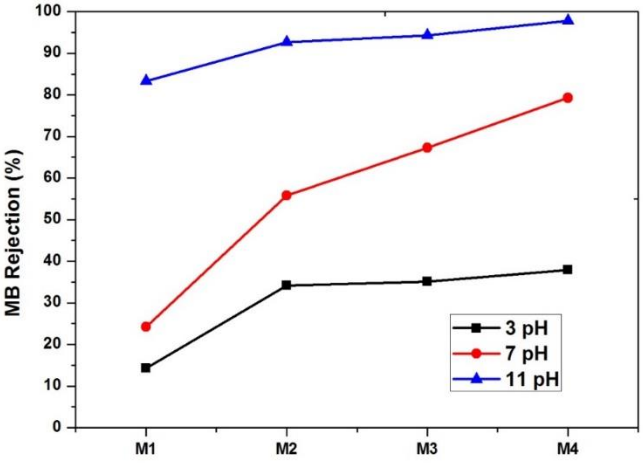

Figure 3.10 Rejection percentage of methylene blue.

3.6.12 Effect of pH

Changing the pH of the textile dye's feed solution plays a vital role in rejecting textile dyes. At three pH, the rejection percentage of methylene blue increasing from

13.2% to 37.8%. At seven pH, the rejection is rising from 23.2 to 2%. For 11 pH, the rejection of effluent rising from 83% to 97%. For indigo carmine, the rejection percentage increasing from 67.7% to 80% for three pH. For seven pH, the rejection is rising from 78.8% to 83.7%. For 11 pH, the rejection of effluent increasing from 81% to 89%. When increasing the pH of the sewage, the rejection percentage also increasing for MOF-5 incorporated PES membranes. The metal oxide of MOF-5 provides an effective binding site, which enhances the adsorption of Methylene blue and Indigo carmine on PES/MOF-5 membranes. Therefore, when increasing the pH, the textile dye highly adsorbed on the membranes, improving the rejection percentage [32].

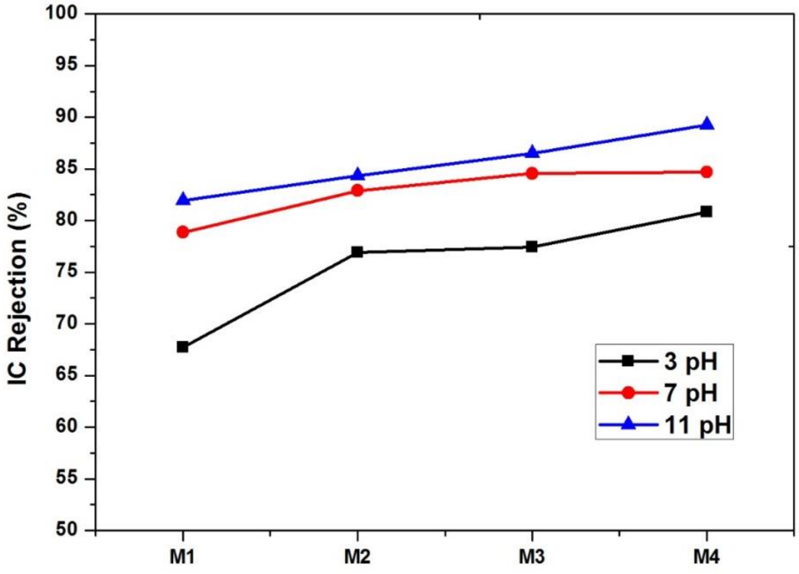

Figure 3.11 Rejection (%) of indigo carmine.

3.7 Conclusion

The prepared neat PES and MOF-5 incorporated PES membranes were characterized by FTIR, XRD, SEM with EDX, and TGA. All the results confirm the impact of MOF-5 on the PES matrix. The incorporation of MOF-5 in the PES matrix influenced the porosity and pore size of the fabricated composite PES/MOF-5 membranes. Further, the contact angle of composite membranes decreased from 73.1° to 60.3° due to improved hydrophilicity. This result favors the permeability enhancement (20.5 to 77.1 L/m^2 hr) of composite PES/MOF-5 membranes. The PES/MOF-5 nanofiltration membranes effectively removed 97% and 89% for methylene blue (MB) and indigo carmine (IC) dyes, respectively. In addition, the PES/MOF-5 membranes have a high rejection percentage of textile dye compared to neat PES membranes. Therefore, the PES/MOF-5 membrane is a potential material for the treatment of textile wastewater.

3.8 References

[1] S. Yu, M. Liu, M. Ma, M. Qi, Z. Lü, C. Gao, Impacts of membrane properties on reactive dye removal from dye/salt mixtures by asymmetric cellulose acetate and composite polyamide nanofiltration membranes, J. Memb. Sci. 350 (2010) 83–91. doi:10.1016/j.memsci.2009.12.013.

[2] N.M. Mahmoodi, Synthesis of core-shell magnetic adsorbent nanoparticle and selectivity analysis for binary system dye removal, J. Ind. Eng. Chem. 20 (2014) 2050–2058. doi:10.1016/j.jiec.2013.09.030.

[3] L. Xu, L.S. Du, C. Wang, W. Xu, Nanofiltration coupled with electrolytic oxidation in treating simulated dye wastewater, J. Memb. Sci. 409–410 (2012) 329–333. doi:10.1016/j.memsci.2012.03.001.

[4] V.S. Antonin, S. Garcia-Segura, M.C. Santos, E. Brillas, Degradation of Evans Blue diazo dye by electrochemical processes based on Fenton's reaction chemistry, J. Electroanal. Chem. 747 (2015) 1–11. doi:10.1016/j.jelechem.2015.03.032.

[5] A. Akbari, S. Desclaux, J.C. Rouch, J.C. Remigy, Application of nanofiltration hollow fibre membranes, developed by photografting, to treatment of anionic dye solutions, J. Memb. Sci. 297 (2007) 243–252. doi:10.1016/j.memsci.2007.03.050.

[6] S.S. Shenvi, A.M. Isloor, A.F. Ismail, S.J. Shilton, A. Al Ahmed, Humic Acid Based Biopolymeric Membrane for Effective Removal of Methylene Blue and Rhodamine B, Ind. Eng. Chem. Res. 54 (2015) 4965–4975. doi:10.1021/acs.iecr.5b00761.

[7] X.Q. Cheng, Z.X. Wang, X. Jiang, T. Li, C.H. Lau, Z. Guo, J. Ma, L. Shao,

Towards sustainable ultrafast molecular-separation membranes: From conventional polymers to emerging materials, Prog. Mater. Sci. 92 (2018) 258–283. doi:10.1016/j.pmatsci.2017.10.006.

[8] H. Sun, X. Yang, Y. Zhang, X. Cheng, Y. Xu, Y. Bai, L. Shao, Segregation-induced in situ hydrophilic modification of poly (vinylidene fluoride) ultrafiltration membranes via sticky poly (ethylene glycol) blending, J. Memb. Sci. 563 (2018) 22–30. doi:10.1016/j.memsci.2018.05.046.

[9] X.H. Ma, Z. Yang, Z.K. Yao, Z.L. Xu, C.Y. Tang, A facile preparation of novel positively charged MOF/chitosan nanofiltration membranes, J. Memb. Sci. 525 (2017) 269–276. doi:10.1016/j.memsci.2016.11.015.

[10] H. Ting, H.Y. Chi, C.H. Lam, K.Y. Chan, D.Y. Kang, High-permeance metal-organic framework-based membrane adsorber for the removal of dye molecules in aqueous phase, Environ. Sci. Nano. 4 (2017) 2205–2213. doi:10.1039/c7en00639j.

[11] E. Haque, J.E. Lee, I.T. Jang, Y.K. Hwang, J.S. Chang, J. Jegal, S.H. Jhung, Adsorptive removal of methyl orange from aqueous solution with metal-organic frameworks, porous chromium-benzenedicarboxylates, J. Hazard. Mater. 181 (2010) 535–542. doi:10.1016/j.jhazmat.2010.05.047.

[12] N. Bakhtiari, S. Azizian, Adsorption of copper ion from aqueous solution by nanoporous MOF-5: A kinetic and equilibrium study, J. Mol. Liq. 206 (2015) 114–118. doi:10.1016/j.molliq.2015.02.009.

[13] J. Abdi, M. Vossoughi, N.M. Mahmoodi, I. Alemzadeh, Synthesis of metal-

organic framework hybrid nanocomposites based on GO and CNT with high adsorption capacity for dye removal, Chem. Eng. J. 326 (2017) 1145–1158. doi:10.1016/j.cej.2017.06.053.

[14] E. Haque, J.W. Jun, S.H. Jhung, Adsorptive removal of methyl orange and methylene blue from aqueous solution with a metal-organic framework material, iron terephthalate (MOF-235), J. Hazard. Mater. 185 (2011) 507–511. doi:10.1016/j.jhazmat.2010.09.035.

[15] C. Echaide-Górriz, S. Sorribas, C. Téllez, J. Coronas, MOF nanoparticles of MIL-68(Al), MIL-101(Cr) and ZIF-11 for thin film nanocomposite organic solvent nanofiltration membranes, RSC Adv. 6 (2016) 90417–90426. doi:10.1039/c6ra17522h.

[16] G. Gnanasekaran, S. Balaguru, A. Gangasalam, D.B. Das, Removal of hazardous material from wastewater by using metal organic framework (MOF) -embedded polymeric membranes Removal of hazardous material from wastewater by using metal organic framework (MOF) -embedded polymeric membranes, Sep. Sci. Technol. 00 (2018) 0–13. doi:10.1080/01496395.2018.1508232.

[17] N. Bakhtiari, S. Azizian, Adsorption of copper ion from aqueous solution by nanoporous MOF-5 : A kinetic and equilibrium study, 206 (2015) 114–118.

[18] J.F. Li, Z.L. Xu, H. Yang, L.Y. Yu, M. Liu, Effect of TiO2nanoparticles on the surface morphology and performance of microporous PES membrane, Appl. Surf. Sci. 255 (2009) 4725–4732. doi:10.1016/j.apsusc.2008.07.139.

[19] A. Rahimpour, UV photo-grafting of hydrophilic monomers onto the surface of

nano-porous PES membranes for improving surface properties, 265 (2011) 93–101. doi:10.1016/j.desal.2010.07.037.

[20] A. Ananth, G. Arthanareeswaran, H. Wang, The influence of tetraethylorthosilicate and polyethyleneimine on the performance of polyethersulfone membranes, Desalination. 287 (2012) 61–70. doi:10.1016/j.desal.2011.11.030.

[21] S. Ahmad, A. Badshah, H. Muhammad, M. Jawad, S. Mustansar, U. Ali, S.U. Khan, Synthesis of highly stable MOF-5 @ MWCNTs nanocomposite with improved hydrophobic properties, (2017).

[22] F. Gholami, S. Zinadini, A.A. Zinatizadeh, A.R. Abbasi, TMU-5 metal-organic frameworks (MOFs) as a novel nanofiller for flux increment and fouling mitigation in PES ultrafiltration membrane, Sep. Purif. Technol. 194 (2018) 272–280. doi:10.1016/j.seppur.2017.11.053.

[23] L. Shen, X. Bian, X. Lu, L. Shi, Z. Liu, L. Chen, Z. Hou, K. Fan, Preparation and characterization of ZnO / polyethersulfone (PES) hybrid membranes, 293 (2019) 21–29. doi:10.1016/j.desal.2012.02.019.

[24] F. Gholami, S. Zinadini, A.A. Zinatizadeh, A.R. Abbasi, Separation and Purification Technology TMU-5 metal-organic frameworks (MOFs) as a novel nanofiller for flux increment and fouling mitigation in PES ultrafiltration membrane, 194 (2018) 272–280.

[25] V. Vatanpour, S.S. Madaeni, R. Moradian, S. Zinadini, B. Astinchap, Fabrication and characterization of novel antifouling nanofiltration membrane prepared from oxidized

multiwalled carbon nanotube/polyethersulfone nanocomposite, J. Memb. Sci. 375 (2011) 284–293. doi:10.1016/j.memsci.2011.03.055.

[26] R. Sathish Kumar, G. Arthanareeswaran, Y. Lukka Thuyavan, I. A.F., Enhancement of permeability and antibiofouling properties of polyethersulfone (PES) membrane through incorporation of quorum sensing inhibition (QSI) compound, J. Taiwan Inst. Chem. Eng. 72 (2017) 200–212. doi:10.1016/j.jtice.2017.01.012.

[27] H.P. Srivastava, G. Arthanareeswaran, N. Anantharaman, V.M. Starov, Performance of modified poly(vinylidene fluoride) membrane for textile wastewater ultrafiltration, Desalination. 282 (2011) 87–93. doi:10.1016/j.desal.2011.05.053.

[28] R. Sathish Kumar, G. Arthanareeswaran, D. Paul, J.H. Kweon, Effective removal of humic acid using xanthan gum incorporated polyethersulfone membranes, Ecotoxicol. Environ. Saf. 121 (2015) 223–228. doi:10.1016/j.ecoenv.2015.03.036.

[29] R. Zhang, S. Ji, N. Wang, L. Wang, G. Zhang, J.R. Li, Coordination-driven in situ self-assembly strategy for the preparation of metal-organic framework hybrid membranes, Angew. Chemie - Int. Ed. 53 (2014) 9775–9779. doi:10.1002/anie.201403978.

[30] J. Babu, Z.V.P. Murthy, Treatment of textile dyes containing wastewaters with PES/PVA thin film composite nanofiltration membranes, Sep. Purif. Technol. 183 (2017) 66–72. doi:10.1016/j.seppur.2017.03.002.

[31] J. Gao, Z. Thong, K. Yu Wang, T.S. Chung, Fabrication of loose inner-selective polyethersulfone (PES) hollow fibers by one-step spinning process for nanofiltration (NF) of textile dyes, J. Memb. Sci. 541 (2017) 413–423. doi:10.1016/j.memsci.2017.07.016.

[32] L. Zheng, Y. Su, L. Wang, Z. Jiang, Adsorption and recovery of methylene blue from aqueous solution through ultrafiltration technique, 68 (2009) 244–249. doi:10.1016/j.seppur.2009.05.010.

CHAPTER 4 EFFICIENT REMOVAL OF ANIONIC, CATIONIC TEXTILE DYES AND SALT MIXTURE USING A NOVEL CHITOSAN/MIL-100 (FE) BASED NANOFILTRATION MEMBRANE

4.1 Introduction

At present, water shortage and water pollution are severe problems in the world [1]. Especially wastewater from the textile industry processes (dyeing, bleaching, printing, and finishing) creates a massive impact on the environment due to enormous hazardous effluents. Additionally, they are a harmful threat to our lives, causing groundwater pollution, suppressing the human immune system, causing carcinogenic diseases, blockage of sunlight penetration, and adverse effects on aquatic life [2,3]. The fixation of dyes on fabric requires dyestuff, including water, salts (retarding and exhausting agents), and additives (surfactants and dispersing agents). 1 kg of cotton requires 30-60 g of dyestuff, 0.6–0.8 kg of NaCl, and 70-150 L of water in the dyeing process. Salts in the textile effluents add to the pollutants load and increase decoloration time, making more trouble for wastewater treatment [4]. However, almost 700,000 tons/year of dyes are produced worldwide, and the textile dyeing industry contributes to an enormous amount of dyeing effluent discharge [5]. Moreover, the generated effluent may be in acidic or alkaline conditions based on the dyeing procedure, adding more challenges for handling the textile wastewater [6]. The textile effluents are possibly causing carcinogenic and mutagenic diseases in humans. [7]. Therefore, we highly needed an effective treatment method to separate dye and salts from textile wastewater.

In NF technologies, water purification by membrane separation is the most hopeful and powerful tool for separating organic dye molecules and inorganic salts [8]. Recently, biopolymers are more attracted to membrane application due to their excellent sustainability, low cost, toxic-free, superior film-forming ability, easy availability [9,10]. Biopolymers such as chitosan [11,12], alginate [13], and cellulose [14] are mainly used as water treatment membranes. Chitosan (CS) is a promising polymeric membrane for textile wastewater treatment due to its strong hydrophilicity, toxic-free, outstanding film-forming ability, excellent anti-bacterial activity and, distinctive biomedical possessions. Reactive amino and hydroxyl groups on the chitosan offer multifunctional activity [15–17]. In addition, those functional groups make hydrophilic CS, which favors high water diffusion and superior sorption [18]. However, it has drawbacks, such as less mechanical strength, less stability, and low porosity. Modification of the CS membrane by incorporating specific fillers such as SiO_2 [19], TiO_2 [20], Graphene oxide [21], and polyethylene glycol [22] enhances the properties of water treatment [23].

However, inadequate usage in numerous applications has raised the trade-off issue between permeability and selectivity. Incorporating inorganic fillers enhances the membrane properties for effective water treatment, but there have been other issues, including accumulation, aggregation, less dispersibility, and poor compatibility [24–27]. In addition, inorganic particle agglomeration can cause pore blockage, flux reduction, structural defect, and diminish fouling resistance [25,28]. Introducing the metal-organic framework (MOFs) as a novel filler for the polymeric membrane is more efficient than inorganic fillers. MOFs are constructed by the coordination bond and the combination of inorganic nodes and organic ligands. The synergistic properties of inorganic metal clusters and organic ligands in MOFs proposal excellent properties to the membranes. In general, high water stability MOFs possess robust kinetic stability or a strong coordination bond to survive damages of ligand-metal bonds during the reaction of hydrolysis [29]. Highly water-stable MOFs were recently used as a filler for the membrane due to their unique properties, including the high surface area, adjustable pore size, extreme porosity, versatile structure, superior adsorption capacity, and flexibility/rigidity. In addition, it offers excellent permeability and selectivity and better compatibility with polymer.

Furthermore, organic ligands in the MOFs provide a higher affinity toward polymer chains [29–31]. Primarily, MIL-100 (Fe) is synthesized at high temperatures (150ºC for six days) with the presence of environmentally dangerous and corrosive acids, including hydrofluoric acid (HF) and nitric acid (HNO_3), followed by the products are washed at 80 ºC for three hours. [32,33]. Nevertheless, sustainable MIL-100 (Fe) was synthesized without hazardous, corrosive acids under room temperature conditions and shorter duration [34]. The environmentally sustainable synthesis paves the way to fabricate biodegradable MOF membranes for water treatment.

Cu-BTC (MOF) anchored on CS coated polyethersulfone membrane fabricated for the removal of manganese. The positive charge membrane was prepared by the incorporation of MOF (NH2-MIL-101(Cr) and NH2-MIL-101(Al)) into the chitosan matrix for multivalent cations removal and observed 93% rejection of MgCl2 with higher flux [31]. The Cu-BTC/CS membrane enhanced hydrophilicity and surface roughness with a manganese removal efficiency of 86% [35]. The hydrophilic, porous, and high-water adsorption MOF-801 incorporated into the CS matrix provides additional water molecule transport pathways and enables a tortuous path for ethanol. The MOF-801/CS membrane achieves superior water/ethanol separation [36]. However, many research works extensively studied based on CS/MOF membranes for wastewater treatment [37–39].

This research prepares CS/MIL-100 (Fe) composite membranes by film casting to remove the hazardous textile dye/salt mixture. The MIL-100 (Fe) selected as a nanofiller for the CS matrix to enhance water permeability and active in the removal of anionic methyl orange (MO) and cationic methylene blue (MB) dyes, salts (NaCl, Na_2SO_4, $CaCl_2$, and $MgSO_4$), and dye/salt mixture with high antifouling performances and recycling stability. In addition, the composite CS/MIL-100 (Fe) membrane performed remarkably in severe conditions such as various pH (acidic, neutral, and alkaline), concentrations (20-100 ppm), different salts, dye/salts mixture solutions. Thus, our CS/MIL-100 (Fe) membrane is a promising candidate for textile wastewater treatments in real-time applications.

4.2 Preparation of MIL-100 (Fe)

The MIL-100 (Fe) was synthesized by following the reported literature [34]. MIL-100 (Fe) synthesis is a combination of 2 different solutions. Solution 1 comprises dissolved trimesic acid (1.67 g) in 1 M NaOH aqueous solution (23.72 g), which was added dropwise to solution 2 (prepared by iron (II) chloride tetrahydrate (2.26 g) dissolved in deionized water (97.20 g)). The mixed solutions were continuously stirred for 24 h at room temperature. The final product was recovered by washed with ethanol and deionized water using centrifugation at 4000 rpm and dried at room temperature for two days. Figure 4.1(a) shows the schematic representation of the MIL-100 (Fe) synthesis.

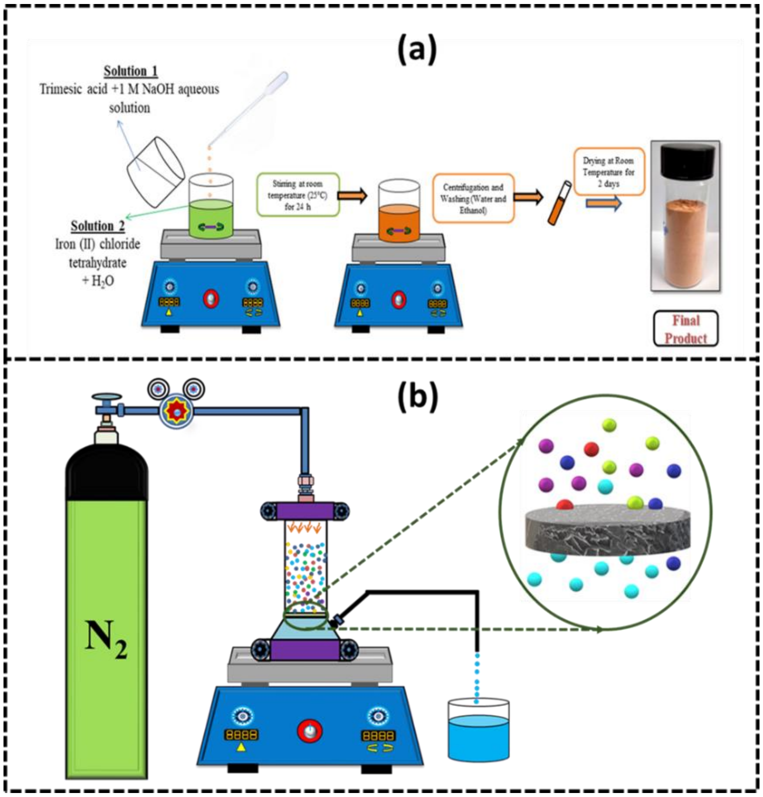
(a)
Solution 1
Trimesic acid +1 M NaOH aqueous solution
Solution 2
Iron (II) chloride tetrahydrate + H_2O
Stirring at room temperature (25°C) for 24 h
Centrifugation and Washing (Water and Ethanol)
Drying at Room Temperature for 2 days
Final Product
(b)
N_2

Figure 4.1 The schematic representation. MIL-100 Fe synthesis (a); nanofiltration setup (b).

4.3 Preparation of CS/MIL-100 (Fe) membranes

Composite NF membranes were fabricated by the film casting technique (Figure 4.2) [17,22]. Initially, MIL-100 (Fe) added (0, 0.1, 0.2, and 0.3 (wt.%), which described as C0, C1, C2, and C3) into 2% acetic acid solution and placed at ultrasonication for 30 min for the uniform dispersion. 4 (wt.%) of chitosan and 1 (wt.%) of PEG added to the above homogeneous solution and placed in the thermally insulated shaker at 55 ºC for 12 h at 160 rpm.

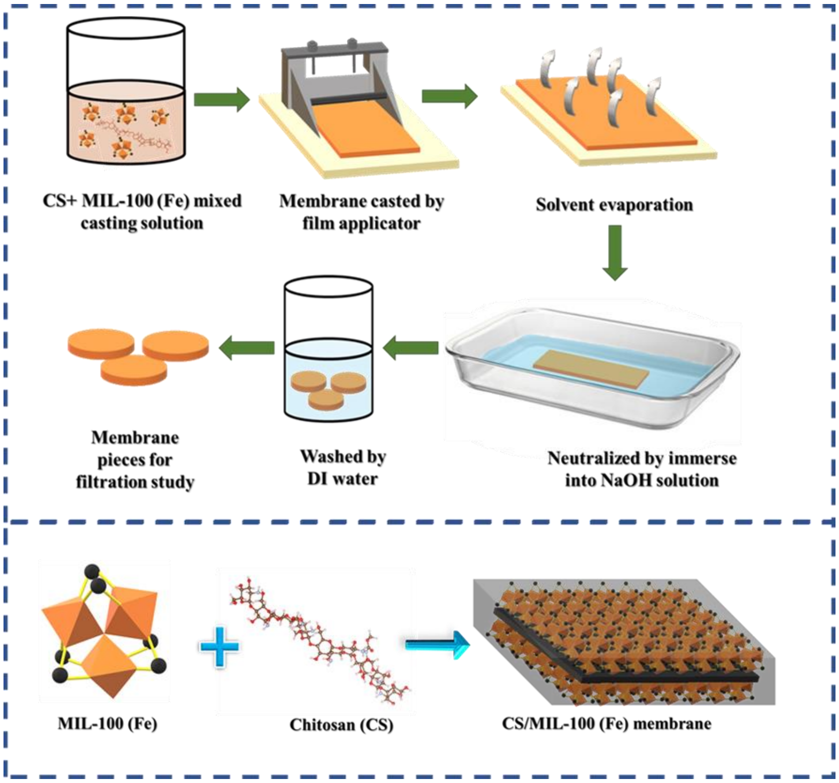
CS+ MIL-100 (Fe) mixed casting solution
Membrane casted by film applicator
Solvent evaporation
Neutralized by immerse into NaOH solution
Washed by DI water
Membrane pieces for filtration study
MIL-100 (Fe)
Chitosan (CS)
CS/MIL-100 (Fe) membrane

Figure 4.2 Schematic diagram of CS/MIL-100 (Fe) membrane fabrication by the film casting method.

Nanofiltration membranes were fabricated by casting on a glass plate using a film applicator with a thickness of 1200 µm and dried at 25 ºC for partial solvent evaporation. Subsequently, the dried membrane was neutralized by immersed in 1 M NaOH solution at 24 h, and excess of NaOH eliminated by washed with DI water. All membranes are preserved in DI water before use.

4.4 Nanofiltration

The filtration study was carried out in dead-end nanofiltration (Sterlitech HP4750 stirred cell) with an active membrane area of 14.6 cm^2 (Figure 4.1(b)). The pre-compaction of membranes was employed by using pure DI water at 0.4 MPa for 60 min. The separation performances of the CS/MIL-100 (Fe) membranes were examined by the filtration experiments using simulated wastewater, with the various concentration and pH of cationic MB and anionic MO dyes and 1000 ppm concentration of NaCl, Na_2SO_4, $CaCl_2$, and $MgSO_4$ salts solutions. The dye concentration was measured by an Ultraviolet-visible (UV-vis) spectrophotometer (MEGA-2100- SCINCO Company–Korea) at a wavelength of 460 nm for MO and 665 nm for MB. The salt concentration is determined by a conductivity meter (DiST 3 by Hanna instruments, South Korea). The pH of the dye solutions was adjusted by 0.1 M NaOH and 0.1 M HCl. The ion existence in the feed and permeate solution was characterized by ion chromatography (Model: ICS-1600, Thermo Scientific. (Dionex Corp.)).

4.5 Result and discussion

4.5.1 MIL-100 (Fe) characterizations

Figure 4.3(a) displays the XRD pattern of MIL-100 (Fe). The attained XRD pattern evidence excellent crystallinity [34,40]. FTIR spectrum shows the presence of symmetric and asymmetric vibrational bonds, which represent the –O–C–O– group at 1442 and 1371 cm^{-1}, respectively (Figure 4.3(b)). The peak at 1624 cm^{-1} indicates the carboxylate groups (C=O), while the other two peaks (760 and 707 cm^{-1}) are owed to C-H bonding [41]. Figure 4.3(c) illustrates N_2 adsorption-desorption isotherms and confirms the high surface area, large pore volume, mean pore diameter, mesoporous cage, and microporous windows of MIL-100 (Fe). The values are 1863 m^2 g^{-1}, 0.8374 cm^3 g^{-1}, 1.8 nm, P/P_0= 0.01 and P/P_0= 0.13, respectively [34,42]. The inset of Figure 4.3(c) represents the pore volume distribution. Figure 4.3(d) shows the FESEM image of the octahedral-shaped morphology of MIL-100 (Fe). The FETEM images display the MIL-100 (Fe) nanoparticles with a 200-260 nm (Figure 4.3(e)-(f)) [40,43]. XPS examined the chemical state and elemental composition of MIL-100 (Fe). Figure 4.3(g) indicates the elements (C, O, and Fe) in MIL-100 (Fe). Figure 4.3(h)-(j) represent the MIL-100 (Fe) XPS spectrum of Fe 2p, C 1s, and O 1s [44]. FESEM-EDS analysis identified the element presence (carbon (79.6%), oxygen (19.3%), and iron (1.1%)) in MIL-100 (Fe), which represents in Figure 4.5. The above results imply that synthesized MIL-100 (Fe) could be a potential nanofiller for composite NF membrane to selectively separate dyes and salts from the textile wastewater.

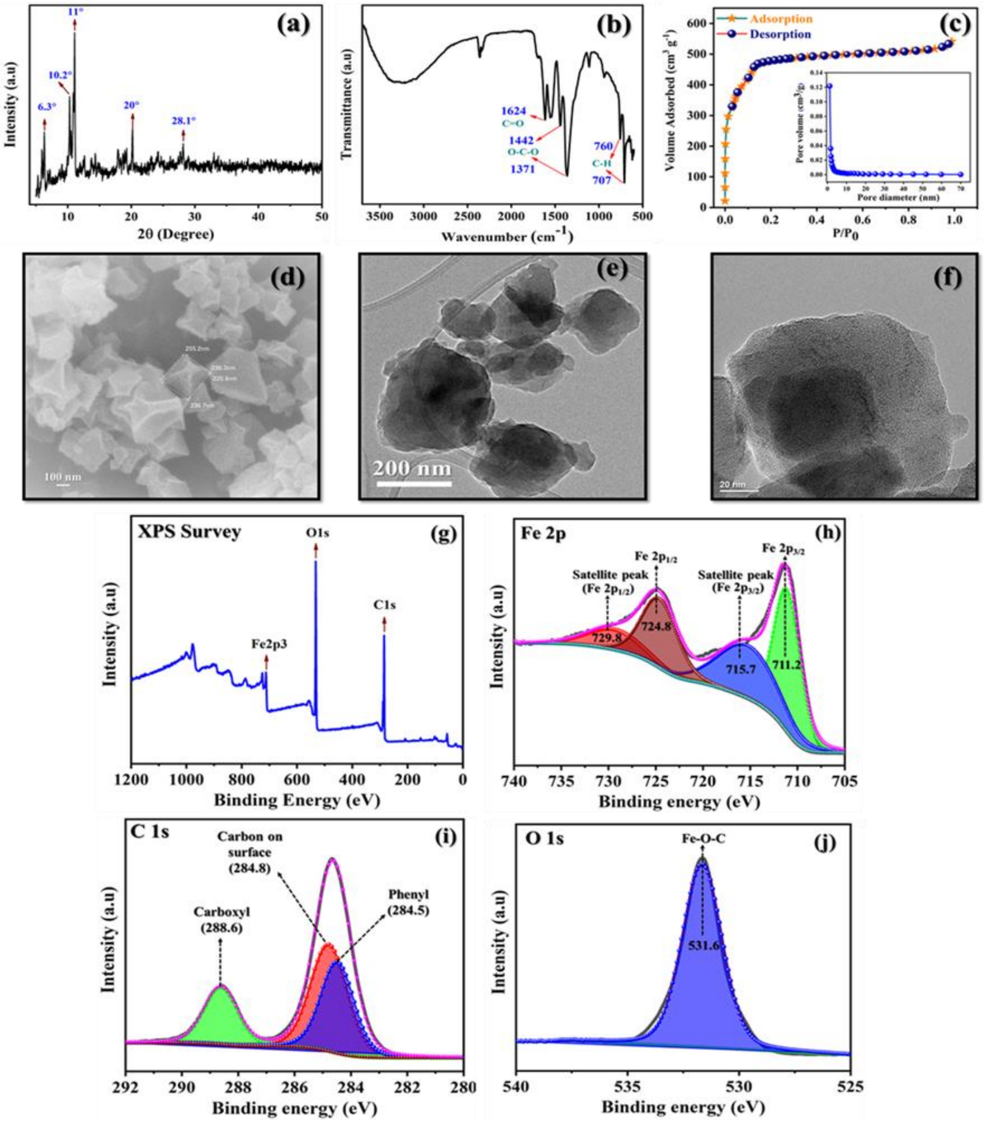

Figure 4.3 Characterization of as-synthesized MIL-100 (Fe). XRD pattern (a); FTIR spectrum (b); N_2 adsorption-desorption isotherms with inset image of pore size distributions (c); FESEM image (d); FETEM images (e)-(f); XPS survey spectrum (g); Fe 2p (h); C 1s (i); O 1s spectrums (j).

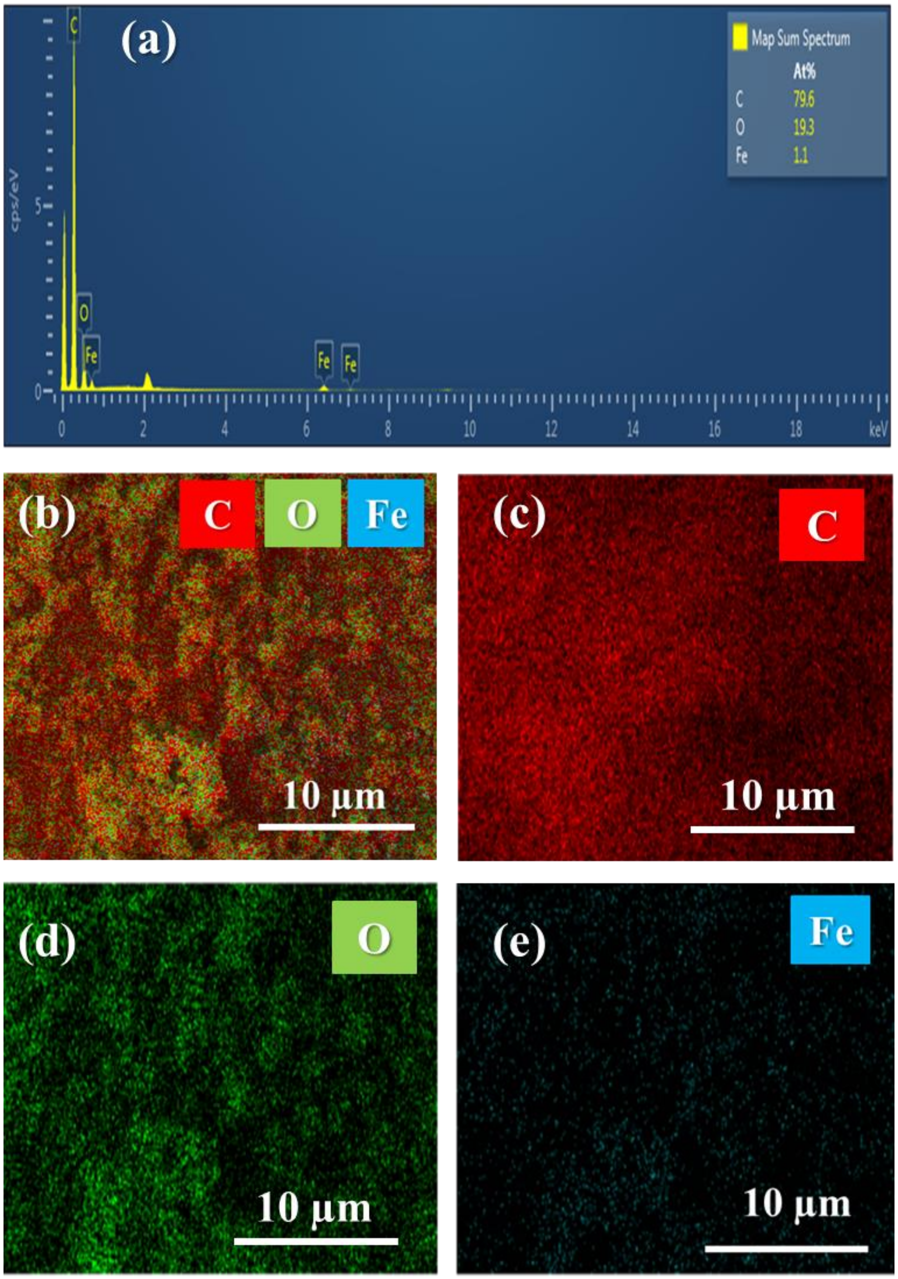

Figure 4.4 EDS Spectra of MIL-100 (Fe) (a); EDS mapping of MIL-100 (Fe) (b)-(e).

4.5.2 Membrane characterization

4.5.2.1 XRD and FTIR analysis of membranes

Figure 4.5(a) shows that the sharp characteristic peaks at 2θ = 20.1° exist in all the membranes, representing the semi-crystalline characteristic of CS and indicates the crystalline structure was unaffected after the MIL-100 (Fe) addition. In enlarged Figure 4.5(a), the growth of sharp peaks at 2θ = 10.5° and 29.2° with the increasing MIL-100 (Fe) loading in the CS matrix. It confirms the stable crystalline structure and strong interaction of chitosan and MIL-100 (Fe) [36]. The peaks observed at 3100-3400 cm^{-1} and 2875 cm^{-1} assigned to the presence of hydrogen bond of the hydroxyl group (O-H) stretching and asymmetric stretching of the C-H group, respectively (Figure 4.5(b)). The peak at 1651 cm^{-1} assigned to the vibration of C-N stretching and C=O stretching in the primary amide (amino group) and secondary amide group (–NHCO–) of the chitosan membrane. The peak at 1581 cm^{-1} assigned to N-H bending vibration [35]. In enlarged Figure 4.5(b), the transmittance (%) intensity of primary and secondary amide groups at 1651 cm^{-1} and the hydroxyl group at 3100-3400 cm^{-1} lowered with increasing loading (0-0.3%) of MIL-100 (Fe) incorporation in the CS matrix. The result proposed a stable attachment between Fe atoms and -NH$_2$ groups with the impeccable MIL-100 (Fe) bonding to the chitosan polymer chain [45].

4.5.2.2 Morphological analyses of membranes

Figure 4.6(a)-(d) represents the surface morphology of pure CS (C0) and CS/MIL-100 (Fe) (C1-C3) membranes. A defect-free and smooth flat surface appeared on the C0 membrane (Figure 4.6(a)). Figure 4.6(b)-(d) shows the roughness increments and MIL-

100 (Fe) distribution on the membrane surface. The observed surface morphology of CS/MIL-100 (Fe) membranes ascribed due to the impact of hydrophilic functional groups of MIL-100 (Fe), which enable the excellent miscibility with the chitosan matrix. These actions are highly recommended and contributing to the formation of the pores and favor for dye and salt separation and antifouling performances of the membrane [11,46].

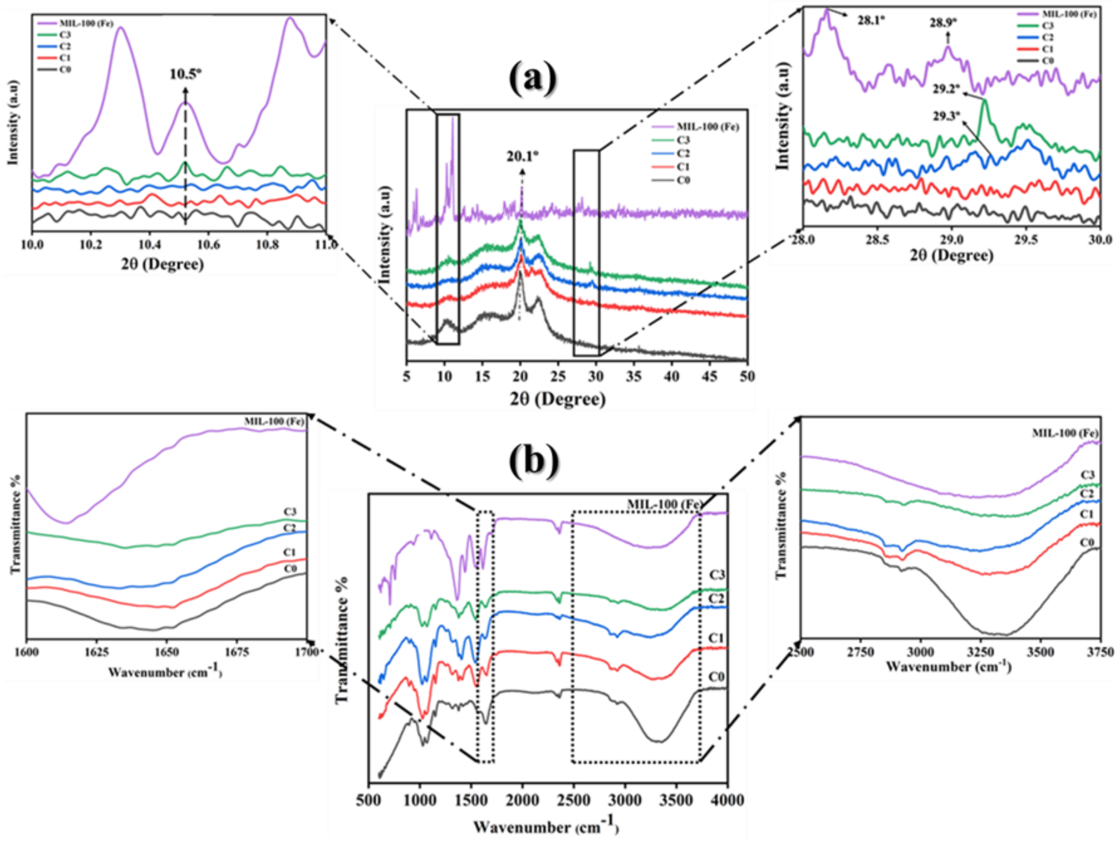

Figure 4.5 XRD (a) and FTIR (b) spectra of C0-C1 membranes and MIL-100 (Fe).

Figure 4.6(e)-(h) represents the cross-sectional images of membranes. The membrane preparation methods influenced the observed cross-sectional morphology [17]. The dense morphology appeared in the C0 membrane (Figure 4.6(e)). In Figure 4.6(f)-(h), the CS/MIL-100 (Fe) composite membranes (C1-C3) displays the improved porous structure and enhanced the membrane thickness with the MIL-100 (Fe) addition into the CS matrix, which favors the improvement of an internal macro void, dense top and bottom layers with a porous interlayer [47]. The C3 membrane displays dense (top and bottom layer) and porous (loose interlayer) compare to other membranes. The thick skin top layer act as a barricade for rejecting the dye and salts. The flexible inner layer creates a path to water molecule transportation. The penetration and intercalation of hydrophilic MIL-100 (Fe) particles into the chitosan matrix create porous structure formation. The combined effect of enhanced hydrophilicity and morphology supports high permeability, excellent separation, and antifouling performances for textile wastewater treatment [17].

4.5.2.3 Surface roughness of membranes

The membrane roughness was examined by a 3D nanoprofiller. Figure 4.6(i)-(l) shows the 2D images with contact angle, average roughness (R_a), and root means squared roughness (R_q) of the membrane surface. Figure 4.6(m)-(p) displays the 3D images of the membrane surface. The smooth surface with lower roughness (R_a=10.93 nm, R_q= 13.75 nm) existed on the C0 membrane. The C1-C3 membranes displayed improved surface roughness (R_a values from 76.57 to 187.42 nm and R_q values from 94.47 to 222.12 nm) with heightened rigid-valley structure (Figure 4.6(m)-(p)). The roughness increments indicate the existence of MIL-100 (Fe) clusters (carboxylic groups) pillaring on the CS active sites (hydroxyl and amine groups), which tuning the membrane surface charge [35,48]. The charged membrane surface is recommended to separate the charged ions and dye molecules from the wastewater by electrostatic interaction and electrostatic repulsion and intrinsically achieve high water permeation [49]. It evidences that improved surface roughness by MIL-100 (Fe) incorporation lowered the membrane contact angles from 67.8 to 41.2° (Figure 4.6(i)-(l)), which favors hydrophilicity enhancements. The improved membrane hydrophilicity is supported for higher flux and diminishes foulant adherence by the protective hydration layer formation. The enhanced pore size, porosity, and surface area of the CS/MIL-100 (Fe) membrane were listed in Table. 4.1. The hydrophilic MIL-100 (Fe) incorporation improves the pore size and surface properties of the CS/MIL-100 (Fe) membrane, which impacts the high permeability with the selective separation of charged hydrated ions and dye molecules from the wastewater by sieve mechanism [50,51].

Table 4.1 The membrane surface properties.

Parameters	CS (C0)	CS/MIL-100 (Fe) (C3)
Surface area (m^2/g)	0.0463	0.2133
Pore size (nm)	1.6	4.6
Porosity (%)	80.0	89.1

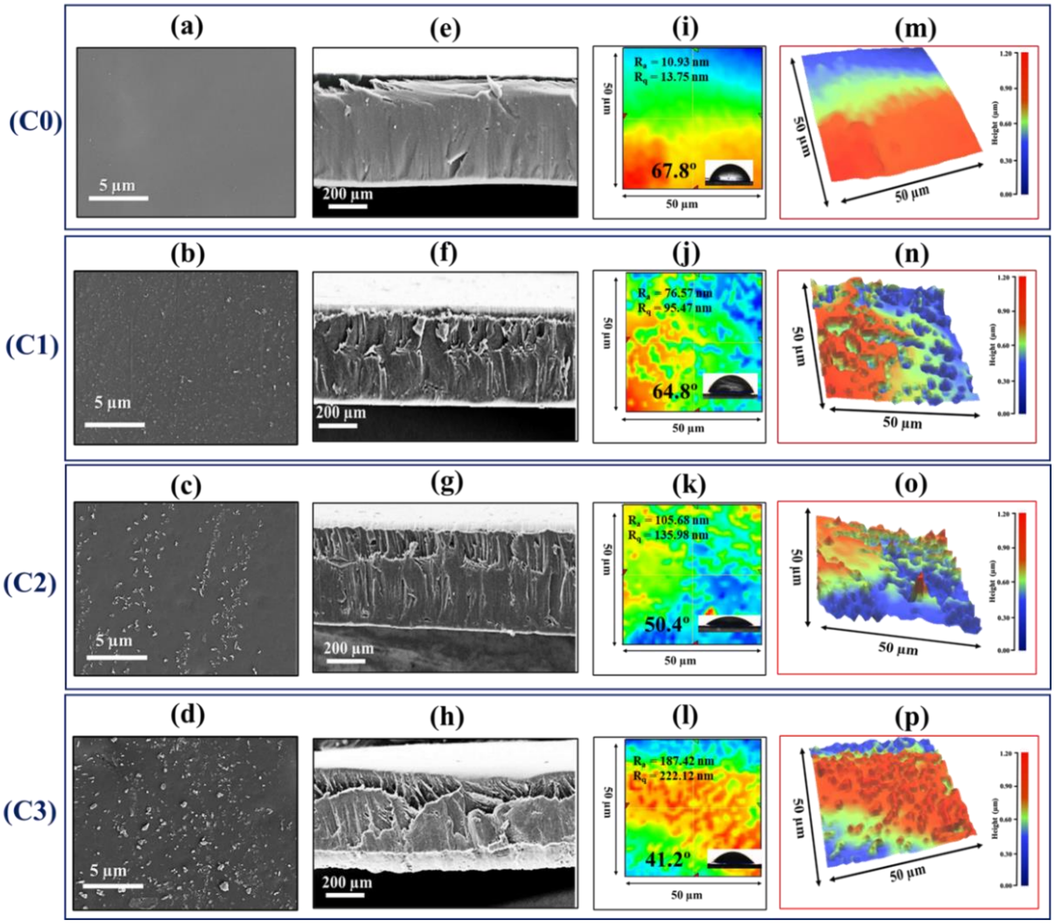
(a)
(e)
(i)
(m)
(C0)
5 µm
200 µm
Ra = 10.93 nm
Rq = 13.75 nm
67.8°
50 µm
50 µm
50 µm
50 µm
(b)
(f)
(j)
(n)
(C1)
5 µm
200 µm
Ra = 76.57 nm
Rq = 95.47 nm
64.8°
50 µm
50 µm
50 µm
50 µm
(c)
(g)
(k)
(o)
(C2)
5 µm
200 µm
Ra = 105.68 nm
Rq = 135.98 nm
50.4°
50 µm
50 µm
50 µm
50 µm
(d)
(h)
(l)
(p)
(C3)
5 µm
200 µm
Ra = 187.42 nm
Rq = 222.12 nm
41.2°
50 µm
50 µm
50 µm
50 µm
Height (µm)
1.20
0.90
0.60
0.30
0.00

Figure 4.6 Membrane morphology and surface roughness. FESEM images of top surface (a)-(d); cross-sectional view (e)-(h); 2D and contact angle images (i)-(l); 3D images (m)-(p).

4.5.2.4 Elemental analysis of membranes

XPS and EDS analyses were performed to understand the chemical structure and elemental compositions of pure CS and CS/MIL-100 (Fe) membranes. Figure 4.7 shows the elemental composition and spectra of pure CS and CS/MIL-100 (Fe) membranes. The Fe element peak in EDS spectra (Figure 4.7) and the appearance of Fe 2p3 peak at 710 eV

(Figure 4.8(a)) indicates the MIL-100 (Fe) functional groups strongly bond with the CS functional groups. Figure 4.9 and Figure 4.10 represent the elemental mapping of pure CS and CS/MIL-100 (Fe) membranes, respectively. Elemental composition and O/N ratio of membranes obtained from XPS analysis listed in Table. 4.2. The attributed higher O/N ratio of CS/MIL-100 (Fe) membranes compared to pure CS due to MIL-100 (Fe) occurrence with large oxygen-contain functional groups. Its evidence that MIL-100 (Fe) is prosperously anchored into the CS matrix [35]. Additionally, in Figure 4.11, the presence of Fe 2p peak at 711.2 and 724.8 eV with two satellite peaks, 719.3 and 731.8 eV, confirms the divalent nature of Fe in the MIL-100 (Fe). Figure 4.8(b) and Figure 4.8(c) shows the XPS C 1s deconvoluted spectra of membranes with the three major peaks, which are positioned at 284.5 (C−C/C=C), 286.1 (C−N), and 287.8 eV (O=C−N and O=C−O) of CS and CS/MIL-100 (Fe) membrane, respectively. The enlarged elevation appeared at 287 eV for the CS/MIL-100 (Fe) membrane. It specifies the impact of oxygen-contain functional groups stimulus for the robust anchoring of MIL-100 (Fe) into the CS matrix, which favors improving the membrane surface charge, water permeance, and separation of charged ions and dyes.

Table 4.2 **Elemental compositions of membranes.**

Membrane	Atomic concentration (%)				O/N ratio
	C (1s)	O (1s)	N (1s)	Fe (2p3)	
Pure CS	73.62	22.06	4.32	-	4.11
CS/MIL-100 (Fe)	74.47	21.42	4.03	0.08	4.32

4.5.2.5 Surface charge of membranes

The surface charge of the membrane was observed in terms of various parameters such as zeta potential, mobility, and isoelectric point of the CS and CS/MIL-100 (Fe) membranes at different pH conditions (Figure 4.8(d)-(i)). In Figure 4.8(d), the isoelectric point of pure CS and CS/MIL-100 (Fe) membrane occurred at 3.9 and 4.2, respectively. The observed positive charge in the acidic medium due to the protonation of the -NH_2 group on the chitosan [52]. CS/MIL-100 (Fe) membrane shows enhanced surface charge as zeta potential (higher positive potential at acidic and higher negative potential at alkaline) than CS membrane due to increasing the ionic strength, which favors higher mobility. Figure 4.8(e) shows the CS/MIL-100 (Fe) membrane holds higher mobility than the CS membrane at acidic and alkaline pH.

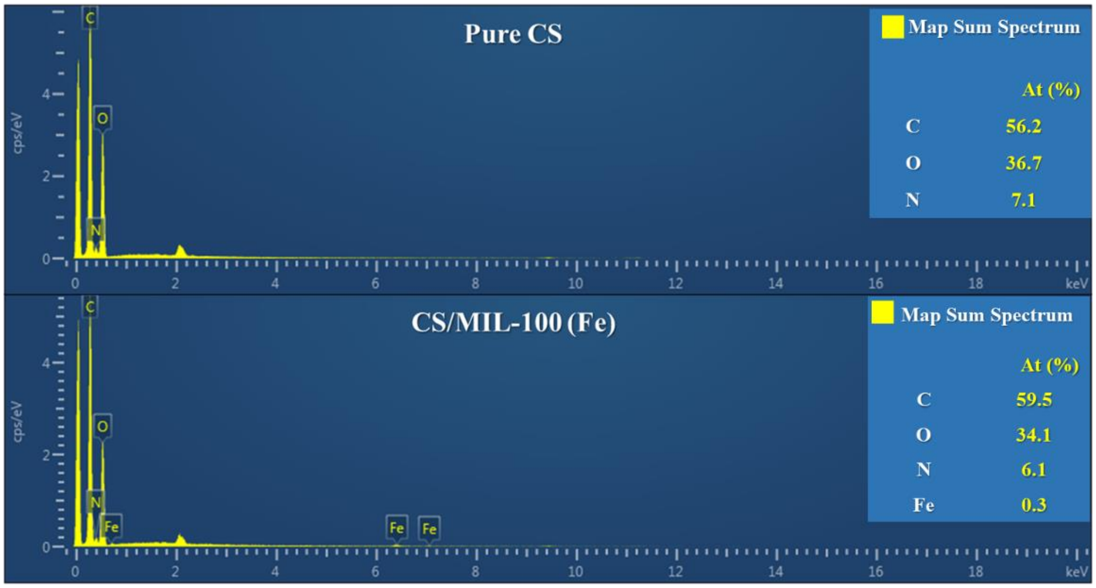

Figure 4.7 EDS Spectra of pure CS and CS/MIL-100 (Fe) membranes.

Figure 4.8((f)-(g)) and Figure 4.8((h)-(i)) represent the zeta potential and mobility of CS and CS/MIL-100 (Fe) membrane across the various distance (sample position) at different pH, respectively. The zeta potential and mobility show an increasing trend towards decreasing the measurement of the sample position at positive and negative direction due to enhancement of ionic strength [53]. The CS/MIL-100 (Fe) membrane owns dissociable amine and carboxylic groups, which exhibit a positive and negative charge. An extensive carboxylic group in the CS/MIL-100 (Fe) membrane possesses a higher negative charge than pure CS membranes.

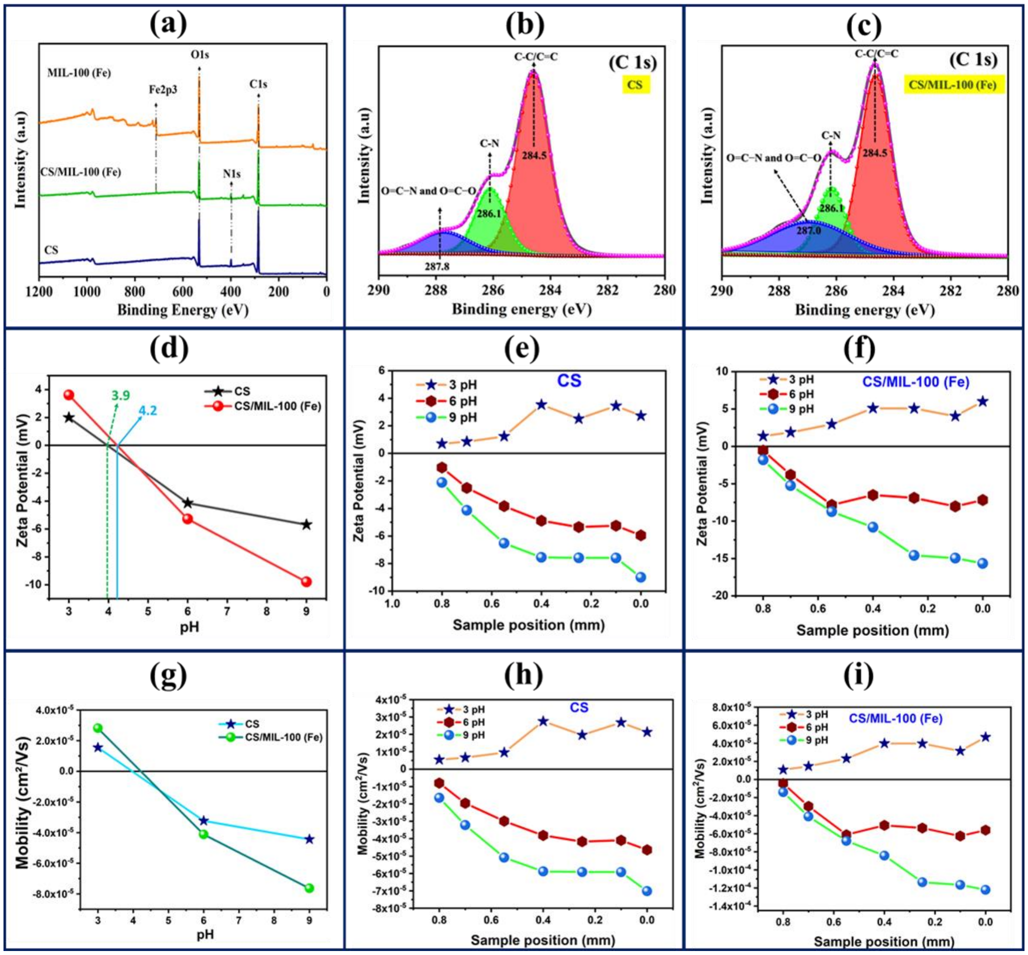

Figure 4.8 Elemental and surface charge characterization. Survey spectra (a); C 1s of CS (b) and CS/MIL-100 (Fe) (c); zeta potential (d) and mobility (e); Effect of sample position at various pH for zeta potential (f)-(g) and mobility (h)-(i).

The FTIR and XPS analysis also support the enriched carboxylic groups present on the CS/MIL-100 (Fe) membrane due to the incorporation of MIL-100 (Fe). In addition, the dually charged CS/MIL-100 (Fe) membrane enables the high rejection rate of positively and negatively charged ions/dye molecules and significantly improves the water permeability [35,48,54].

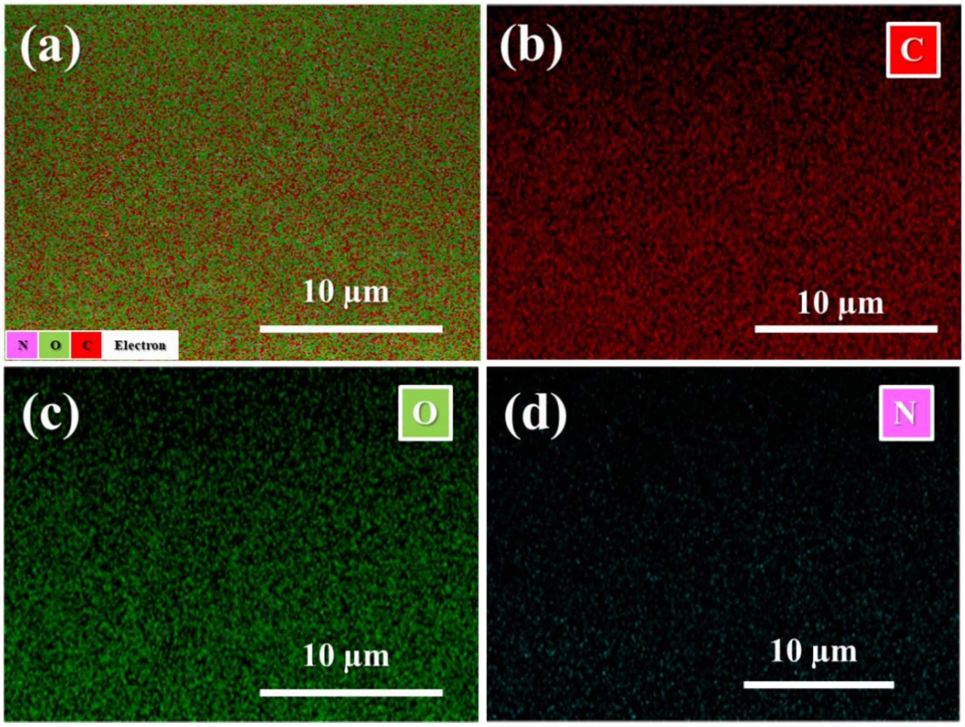
(a)
10 µm
N
O
C
Electron
(b)
C
10 µm
(c)
O
10 µm
(d)
N
10 µm

Figure 4.9 EDS mapping of pure CS membrane.

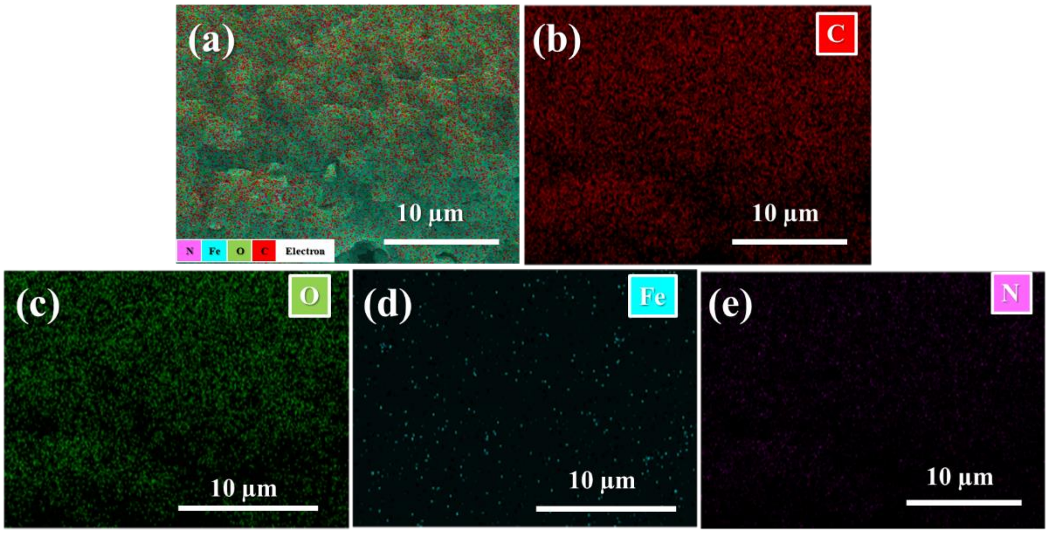
(a)
10 µm
N
Fe
O
C
Electron
(b)
C
10 µm
(c)
O
10 µm
(d)
Fe
10 µm
(e)
N
10 µm

Figure 4.10 EDS mapping of CS/MIL-100 (Fe) membrane.

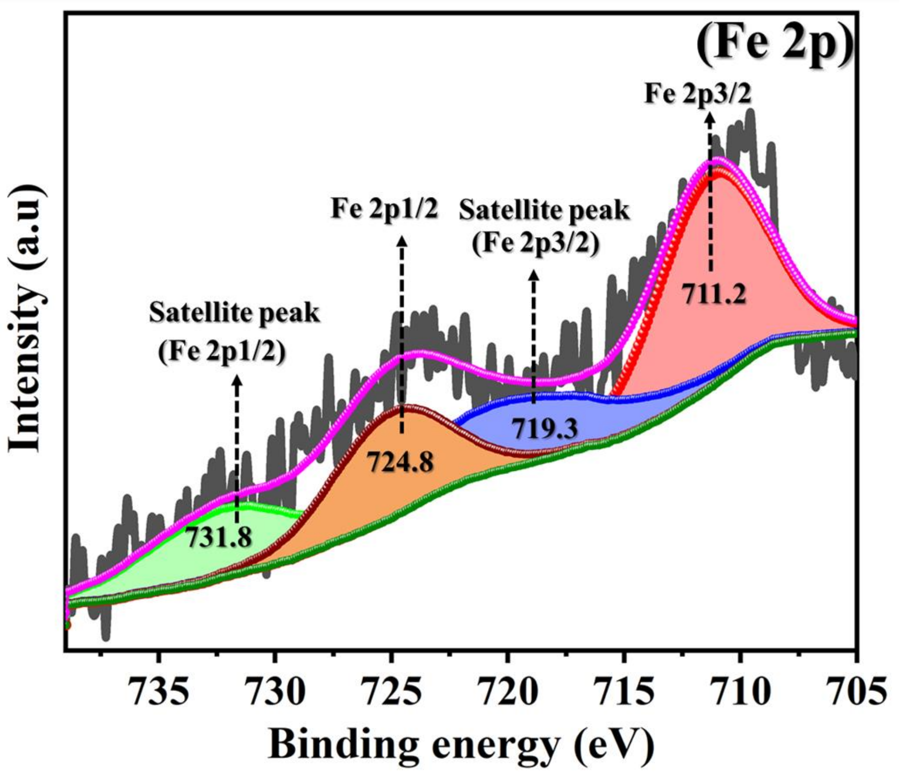

Figure 4.11 XPS spectrum of Fe 2p of the CS/MIL-100 (Fe) membrane.

4.5.3 Membrane performances

The membrane performances were evaluated by pure water flux (PWF), rejection percentage, antifouling performances, and reusability experiments.

4.5.3.1 Permeability of membranes

The incorporation of MIL-100 (Fe) in the CS matrix significantly influenced permeability improvement from 4.2 (C0) to 52.5 L/m^2 h (C3) with the addition of 0-0.3 wt.%. The results suggest that less MIL-100 (Fe) was sufficient to persuade a substantial CS structure change. The observed higher permeability is associated with facilitating the water transport channel to the membranes due to the intrinsic nanopore of hydrophilic

MIL-100 (Fe) incorporation [55]. The CS/MIL-100 (Fe) membrane stability was inspected by applied various pressures (0.2, 0.4, and 0.6 MPa). Figure 4.12(a) shows the pure water flux linearly increased with applied pressure, evidencing the CS/MIL-100 (Fe) membrane appropriate for textile wastewater treatment.

4.5.3.2 Dye rejection of membranes

In Figure 4.12(b), the CS/MIL-100 (Fe) membranes showed higher rejection (%) of MB and MO compare to pure CS (C0) at 0.4 MPa. The incorporated MIL-100 (Fe) activated to form a dense active layer with the porous interlayer on the CS/MIL-(Fe) membrane surface, which improves the water permeation path with the higher rejection of dyes. The increasing amount of MIL-100 (Fe) incorporation (C0 to C3) increases the rejection (%) of MB and MO. However, the C3 membrane performed with outstanding dye rejection of 99% of MB and 99% of MO without compromising the high-water permeability compared to other membranes. Excessive addition of MIL-100 (Fe) may lead to interfacial defect formation and porous structure altered because of MIL-100 (Fe) accumulation [56]. Compared to other membranes, the C3 membrane exhibited the highest dye rejection with high permeability. Accordingly, the C3 membrane was selected as the representative for the following experiments.

The surface charge and pH significantly impact separation performances, which are observed by feed the MB and MO dye solution at different pH conditions (3-11 pH) to the C3 membrane (Figure 4.12(c)). The higher rejection (%) of MB and MO was obtained at high alkaline (pH 11) and acid (pH 3) conditions, respectively. The incorporated MIL-100 (Fe) altered the membrane surface into a negative and positive charge at alkaline and acidic conditions, respectively, as expected from zeta potential measurement results. In Figure 4.12(c), the C3 membrane achieved a high rejection percentage of MB (99%) at > 9 pH due to the strong electrostatic interaction between positive charge MB dye and negative charge CS/MIL-100 (Fe) membrane [57,58].

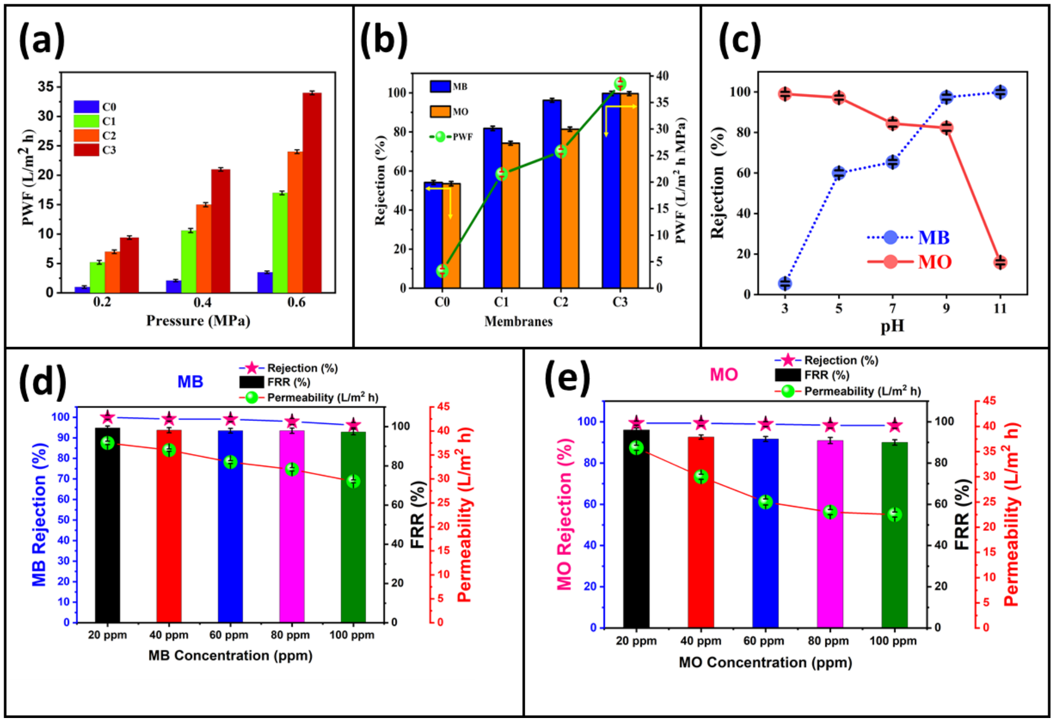

Figure 4.12 The rejection performances of dyes through the membranes. The effect of TMP on PWF (a); effect of MB and MO rejection, PWF at 0.4 MPa (b); effect of pH (c); effect of dye concentration on MB (d); MO (e).

MIL-100 (Fe) incorporated C3 membrane is a positive charge (enhanced cationic NH_3^+ groups) at acidic conditions (3 pH), which enhances the higher rejection percentage of negatively charged methyl orange dye (99%) by increasing the coulombic interaction force. On the other hand, at> 9 pH, the MO rejection (%) was low due to the deprotonation of NH_3^+, which improving the repulsive force between dye molecules and membrane surface [59]. Figure 4.13(a)-(b) represents the UV-vis absorbance spectra of MB and MO at different pH (3 to11).

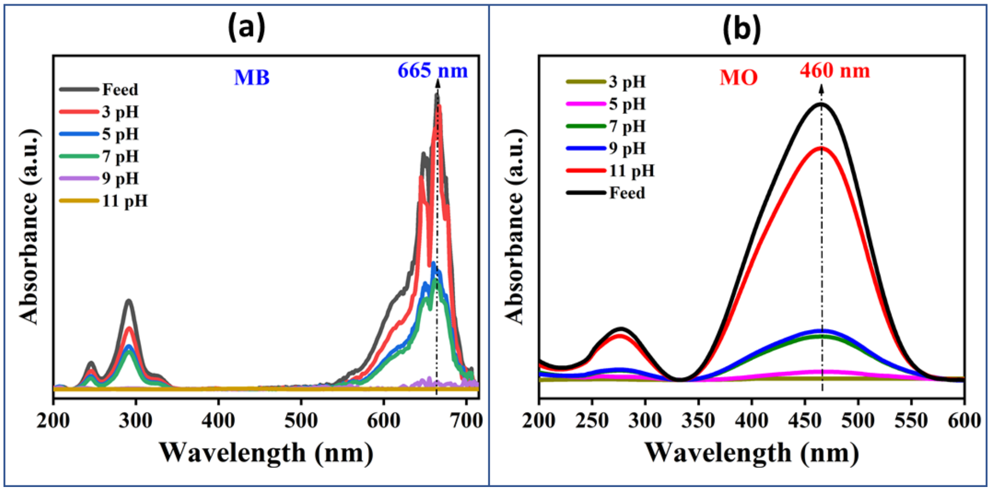

Figure 4.13 UV-vis absorption spectra of feed and permeate of MB at various pH (a); UV-vis absorption spectra of feed and permeate of MO at different pH (b).

Figure 4.14 illustrates the dye molecule separation mechanism by CS/MIL-100 (Fe) membrane in the acidic and alkaline environment. The stability of the C3 membrane was investigated with various feed concentrations (20-100 ppm) of MB and MO at 11 and 3 pH, respectively (Figure 4.12(d)-(e)). Increasing the dye concentration of MB and MO feed solution causes permeability decline (37.5 to 29.5 L/m^2 h for MB and 34.7 to 22.5 L/m^2 h for MO). At various feed concentrations of MB and MO dye, the C3 membrane was stable to maintain more than 95% rejection. They attained higher rejection and complete color removal due to the MIL-100 (Fe) incorporation into the CS matrix. The high specific affinity toward dye molecules by hydrophilic MIL-100 (Fe) incorporation facilitates high water purification and complete color removal [32]. Figure 4.15(a)-(b) represents the UV-vis absorbance of MB and MO with the images of feed and permeate solutions.

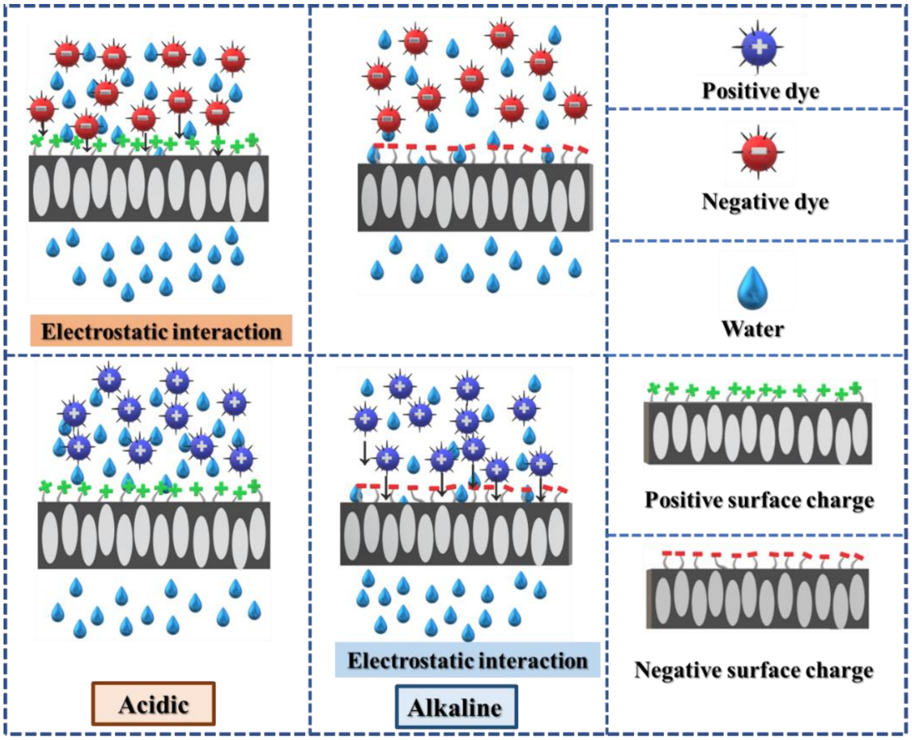
Positive dye
Negative dye
Water
Electrostatic interaction
Positive surface charge
Negative surface charge
Electrostatic interaction
Acidic
Alkaline

Figure 4.14 Schematic representation of the dye molecule separation mechanism by CS/MIL-100 (Fe) membrane at the acidic and alkaline environment.

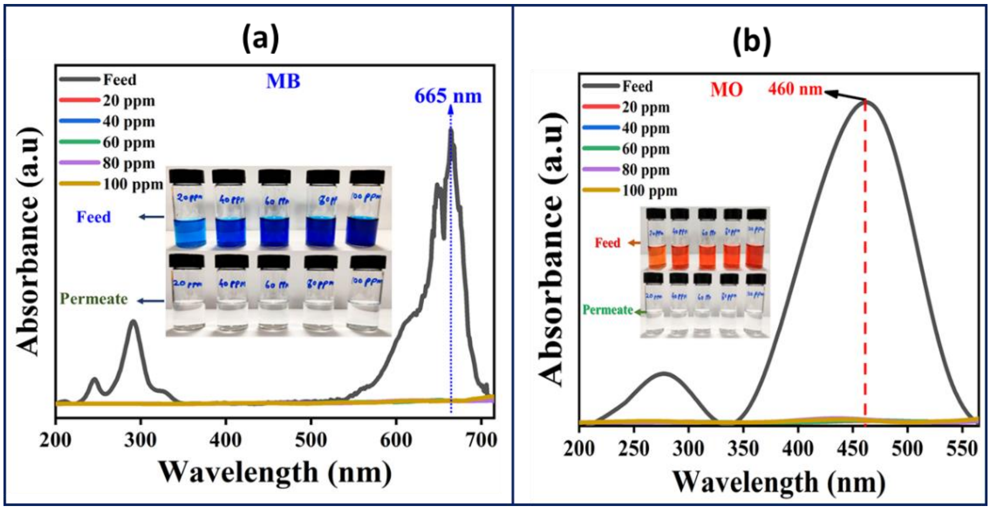

Figure 4.15 UV-vis absorption spectra with the inset images of feed and permeate solution (a) MB and (b) MO.

4.5.3.3 Antifouling performance of membranes

Fouling formation is a severe issue in real textile wastewater treatment applications due to permeability reduction, high energy consumption, degrading the life span of membranes, productivity loss, etc. The FRR evaluated the antifouling performance of the C3 membrane. Figure 4.12(d)-(e) shows the C3 membrane FRR decreases with increasing the feed concentration but maintaining more than 90% of FRR. Besides, the FRR of MB higher than MO. The presence of vibrant hydrophilic functional groups of MIL-100 (Fe) and high water adsorption contributed to the robust hydration layer development, enhanced structural stability, and diminished fouling formation [60,61].

4.5.3.4 Salt rejection of membranes

In order to improve the exhaustion and fixation of dyes on fabric, a large quantity of salt is required. NaCl and Na_2SO_4 salts are primary utilized as exhausting and retarding agents in the dyeing process. The salt content in the textile effluent creates additional pollutants and increases the decoloration time [4]. Extreme salt concentration (0-100 g/L) is desirable for the reactive dyeing process [62]. The C3 membrane desalination performance was studied by filtrating 1000 ppm concentration of salt solutions (NaCl, Na_2SO_4, $CaCl_2$, and $MgSO_4$) at neutral pH (Figure 4.16(a)) . The salt rejection evaluated by choosing the mono (Na^+ and Cl^-) and divalent ions (SO_4^{2-}, Mg^{2+} and Ca^{2+}). The C3 membrane obtained higher water permeability (37 L/m^2 h MPa) for NaCl than other salts. Significantly, higher divalent ions rejection achieved than monovalent ions due to the size exclusion (NaCl (R_{actual} - 11.1% and R_{real} - 11.5%) < $CaCl_2$ (R_{actual} – 12.5% and R_{real} – 13.4%) < Na_2SO_4 (R_{actual} - 43% and R_{real} - 44%) < $MgSO_4$ (R_{actual} – 50% and R_{real} - 52.5%). Figure 4.16(b) displays the ions (cations and anions) separation performances. The ions rejection (%) of each salts following the trend of $MgSO_4$ (Mg^{2+} - 41.6%, SO_4^{2-} - 44.7%) > Na_2SO_4 (Na^+ - 37.4%, SO_4^{2-} - 41.5%) > $CaCl_2$ (Ca^{2+} - 15%, Cl^- - 14.8%) > NaCl (Na^+ - 6.2%, Cl^- - 4.7%). Mechanism of molecular sieving root for the rejection of large hydrated ions (SO_4^{2-} (0.379 nm) > Cl^- (0.332 nm)). $-COO^-$ group occurrence creates a high negative surface charge of the membrane, which favors high rejection of SO_4^{2-} compare to Cl^- because of the higher negative charge [17].

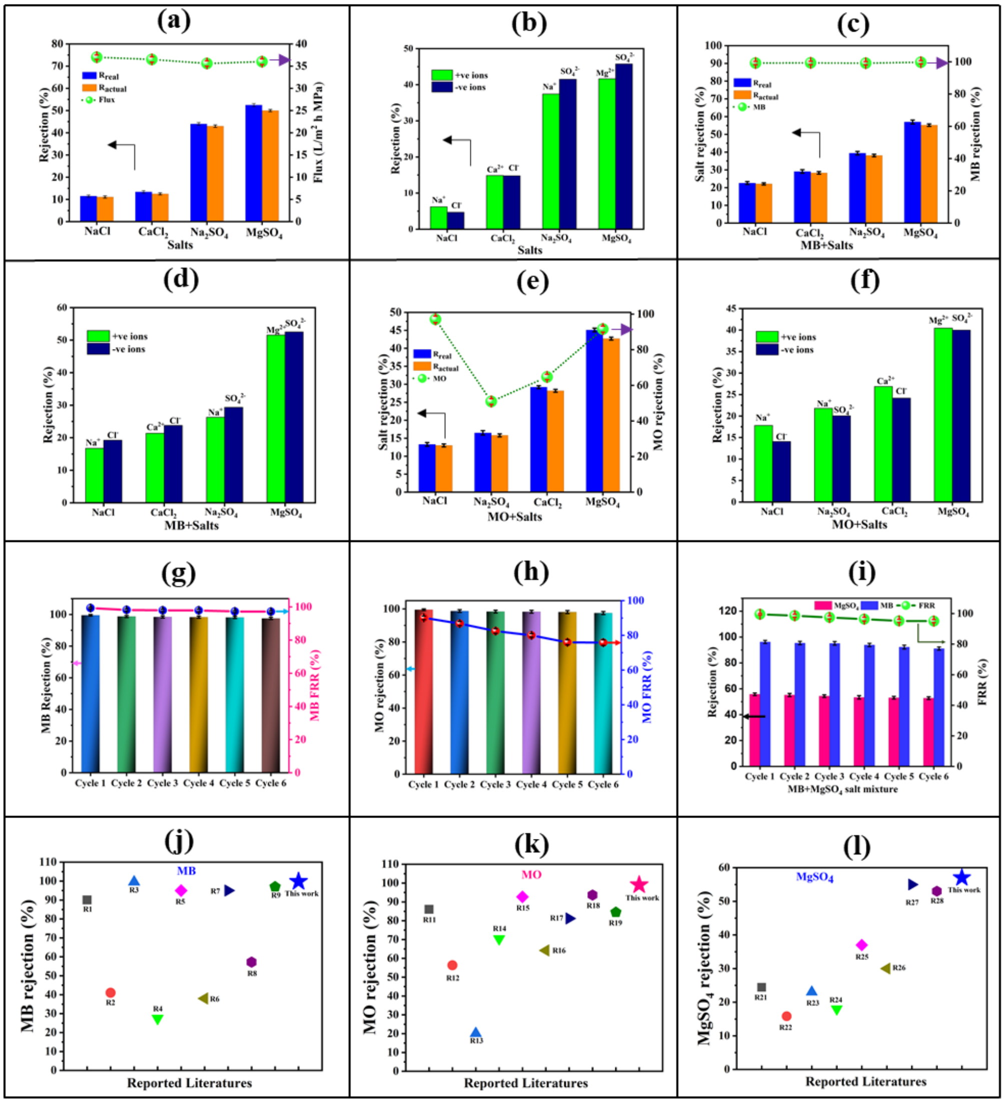

Figure 4.16 The rejection performances of dye/salt mixture through membranes. Salts (a); ions in salts (b); MB+salts (c); ions in MB+salts (d); MO+salts (e); ions in MO+salts (f). Cyclic stability of MB (g); MO (h); MB+$MgSO_4$ (i). CS/MIL-100 (Fe) rejection (%) comparison with reported membranes. MB (j); MO (k); $MgSO_4$ (l).

4.5.3.5 Dye/salt mixture rejection of membrane

As stated in the introduction section, the textile wastewater consists of a certain quantity of salts; therefore, it is essential to investigate the impact of salts on dye/salt mixture separation. The C3 membrane was examined with a various feed solution of 1000 ppm of 4 different salts (NaCl, Na_2SO_4, $CaCl_2$, and $MgSO_4$) mixed with MB and MO dyes (20 ppm) at alkaline (pH 11) and acidic (pH 3) conditions, respectively. Figure 4.16(c) shows the higher MB rejection (> 98%) and moderate salt rejection. Strong electrostatic interaction between negatively charged CS/MIL-100 (Fe) membrane and positive charge dye molecule (MB) explains the superior rejection (%) of MB. Electrostatic repulsion and size exclusion mechanism causes higher rejection (%) of $MgSO_4$. Figure 4.16(c) displays the strong repulsive force between salt ions and CS/MIL-100 (Fe) membrane surface results in higher R_{real} (%) compared to R_{actual} (%) such as $MgSO_4$ (R_{real} - 57.0% and R_{actual} - 54.2%) > Na_2SO_4 (R_{real} - 39.2% and R_{actual} - 38.0%) > $CaCl_2$ (R_{real} - 29.1% and R_{actual} - 28.2%) > NaCl (R_{real} - 22.4% and R_{actual} - 22.0%). Figure 4.16(d) displays the cations and anions rejection (%) of MB+salts mixed solution. The MB mixed salts rejection trend based on the cations and anions rejection (%) was in the order of $MgSO_4$ (Mg^{2+} - 51.6%, SO_4^{2-} - 52.5%) > Na_2SO_4 (Na^+ - 26.3%, SO_4^{2-} - 29.3%) > $CaCl_2$ (Ca^{2+} - 21.4%, Cl^- - 23.8%) > NaCl (Na^+ - 16.8%, Cl^- - 19.2%). The strong electrostatic repulsion between membrane surface and salt ions influenced the higher rejection of divalent anions (SO_4^{2-}) than monovalent anions (Cl^-). $MgSO_4$ rejection higher than Na_2SO_4 due to the effect of the dominant sieve mechanism. Moreover, hydrated radius of Mg^{2+} (0.428 nm) ion is larger than Na^+ (0.358 nm) ion [63]. Figure 4.17(a) and Figure 4.17(b) illustrate the complete color removal and diminished UV-vis absorbance peak of the permeate solution of the MB dye/salt mixture, respectively. It also evidenced the effective membrane separation performances of the C3 membrane. Figure 4.16(e) represents the MO rejection with salt rejection (R_{real} and R_{actual}) of MO dye/salt mixture solutions at the acidic condition. In Figure 4.16(e), the R_{real} (%) is higher than R_{actual} (%) due to the higher repulsive force effect between the salt ions and the C3 membrane surface. The salt rejection trend was followed by $MgSO_4$ (R_{real} - 44.1% and R_{actual} - 42.7%) > $CaCl_2$ (R_{real} -29.1% and R_{actual} - 28.1%) > Na_2SO_4 (R_{real} - 16.5% and R_{actual} - 14.8%) > NaCl (R_{real} - 13.3% and R_{actual} -13%). The MO mixed salts rejection trend based on the cations and anions rejection (%) followed the order: $MgSO_4$ (Mg^{2+} - 40.5%, SO_4^{2-} - 40%) > $CaCl_2$ (Ca^{2+} - 27.0%, Cl^- - 24.2%) > Na_2SO_4 (Na^+ - 21.8%, SO_4^{2-} - 20.1%) > NaCl (Na^+ - 17.8%, Cl^- - 14.1%) (Figure 4.16(f)). The positive charge C3 membrane at acidic pH highly rejects the cations (Mg^{2+}, Ca^{2+}, and Na^+) than anions (Cl^- and SO_4^{2-}) due to the existence of enhanced positive charge amine groups in CS/MIL-100 (Fe) membrane. Moreover, the superior hydrated radius of Mg^{2+} leads to a higher rejection % of $MgSO_4$ than other salts [17]. The moderate MO rejection was achieved by the electrostatic interaction between the negative charge dye molecule and the positive charge membrane surface.

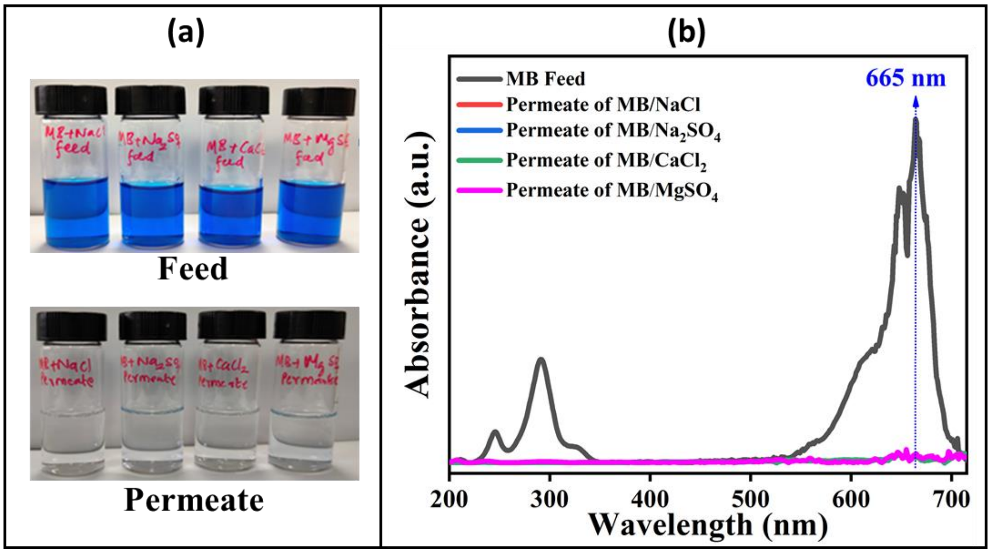

Figure 4.17 The images of feed, permeate, and retentate of MB dye/salt mixture (a); UV-vis absorbance spectrum of MB dye/salt mixture at 665 nm for permeate and feed solution (b).

Mg^{2+} and Ca^{2+} have a higher charge density than Na^+, which favors the higher rejection of $MgSO_4$ and $CaCl_2$ than sodium salts (NaCl and Na_2SO_4) [17]. The C3 membrane observed a higher rejection percentage of dye and salt for MB/salt’s solution mixtures when compared to MO/salt’s mixtures. The C3 membrane treated with mixed feed solution consists of 20 ppm of MB and MO and 1000 ppm of NaCl, Na_2SO_4, $CaCl_2$, and $MgSO_4$ at neutral pH (pH 7) to evaluate the performances of real textile dyeing wastewater treatment. Table. 4.3 shows the rejection efficiency, hydrated radius, and stoke radius of cations and anions in the mixed solution. Due to electrostatic repulsive force influences, the divalent anions (SO42–) possess higher rejection efficiency than other ions. In addition, 42.3% of salt rejection and 90% dye rejection were achieved for this mixed solution calculated from salt and dyes concentration. Figure 4.18 shows the schematic representation separation performances of CS/MIL-100 (Fe) membrane.

Table 4.3 Hydrated radius, Stokes radius, and rejection % of ions.

Ion	Hydrated radius (nm) [4]	Stokes radius (nm) [4]	Rejection % of mixed solution
Chloride (Cl^-)	0.332	0.121	14.0
Sodium (Na^+)	0.358	0.184	14.2
Sulphate (SO_4^{2-})	0.379	0.230	20.7
Calcium (Ca^{2+})	0.412	0.310	16.6
Magnesium (Mg^{2+})	0.428	0.347	17.0

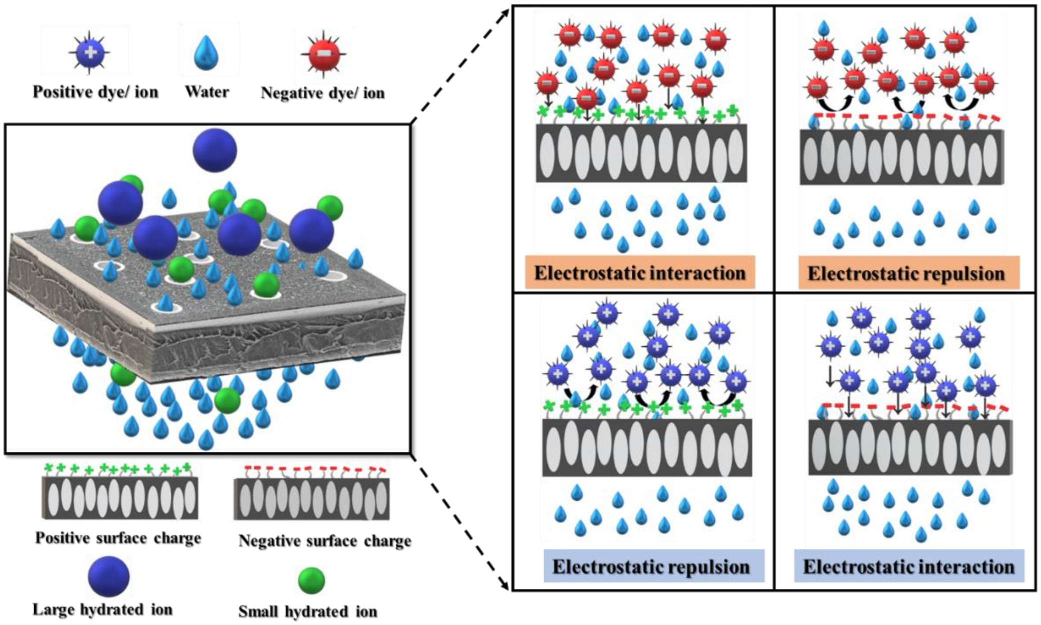
Positive dye/ ion
Water
Negative dye/ ion
Positive surface charge
Negative surface charge
Large hydrated ion
Small hydrated ion
Electrostatic interaction
Electrostatic repulsion
Electrostatic repulsion
Electrostatic interaction

Figure 4.18 Schematic representation separation performances of CS/MIL-100 (Fe) membrane.

4.5.3.6 Reusability of membranes

The reusable stability of CS/MIL-100 (Fe) membranes is an essential factor in the actual textile wastewater treatment application. The C3 membrane used here to treat MB (20 ppm), MO (20 ppm), and MB (20 ppm) + $MgSO_4$ (1000 ppm) solution continuously run for six cycles. Figure 4.16(g) shows the reusability of the C3 membrane by representing the rejection (%) and FRR (%) of MB. The rejection % and FRR% upheld 99% and 95% respectively for six cycles due to the incorporated excellent hydrolytic MIL-100 (Fe), which constructs a solid and stable CS/MIL-100 (Fe) composite membrane. The complete color removal validates the excellent MB removal properties of the C3 membrane, which is displayed in Figure 4.19. The permeate intensity of the UV-vis absorbance spectra ultimately decreased for the six cycles than feed intensity, which confirms MB's high rejection by the C3 membrane.

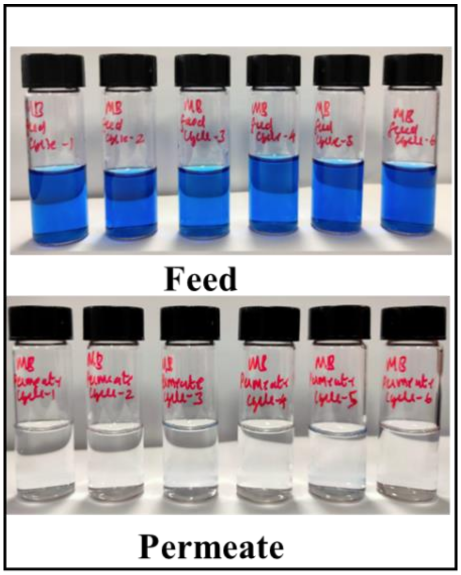

Figure 4.19 The feed and permeate images of MB solutions for six cycles.

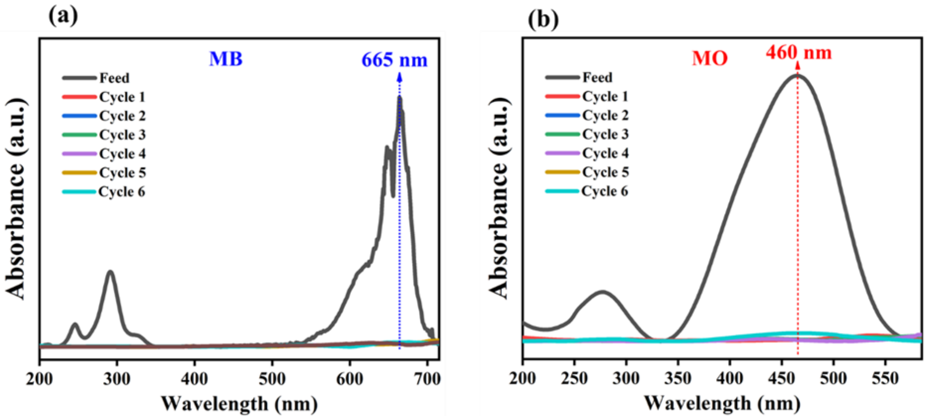

Figure 4.20 UV-vis absorbance spectrum of feed and permeate for six cycles MB (a); MO (b).

Figure 4.20(a) demonstrates the UV-vis absorbance spectra of feed and permeate of MB at 665 nm for six cycles [51]. Figure 4.16(h) shows the MO (20 ppm) rejection for the reusability of the C3 membrane for six cycles. The C3 membrane maintains a higher rejection (> 90%) and FRR (> 75%). The complete MO dye removal evidence with six cycles UV-vis absorbance spectra (460 nm) (Figure 4.20(b)). Figure 4.16(i) displays the C3 membranes for the removal of the MB/MgSO4 salt mixture and antifouling performance for six continuous cycles. The rejection (%) was maintained over MB (95%) and $MgSO_4$ salt (55%) for MB/$MgSO_4$ mixture feed solution. The reduced permeate solution intensity of UV-vis absorbance of MB/$MgSO_4$ mixture and nearly 100% of color removal achieved for the complete six cycles (Figure 4.21(a)). Figure 4.16(j)-(l) shows the CS/MIL-100 (Fe) rejection (%) comparison with reported membranes. MB (j); MO (k); MB+$MgSO_4$ (l).

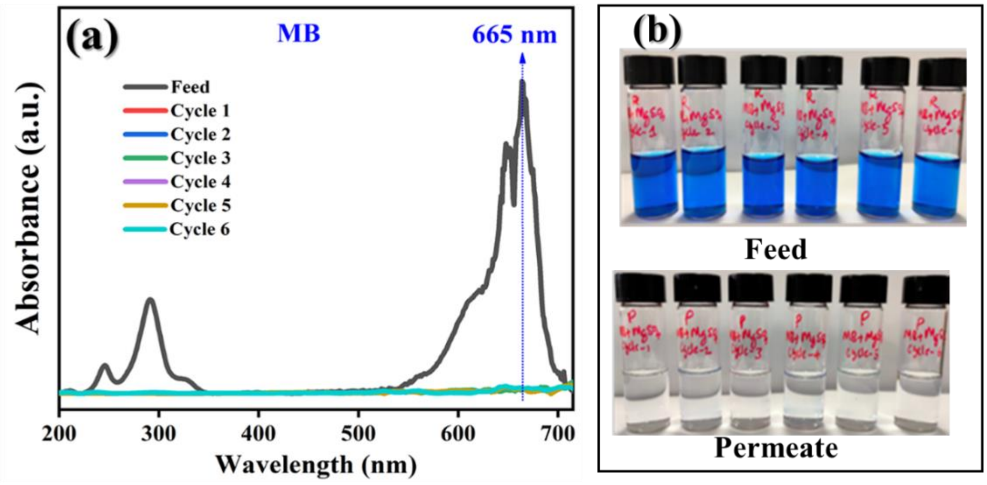

Figure 4.21 Reusability of C3 membrane for MB/$MgSO_4$ mixture. (a) UV-vis absorbance spectrum of feed and permeate of MB/$MgSO_4$ salt mixer solutions at 665 nm for six cycles; (b) The images of permeate and feed solutions of MB/$MgSO_4$ salt for six cycles.

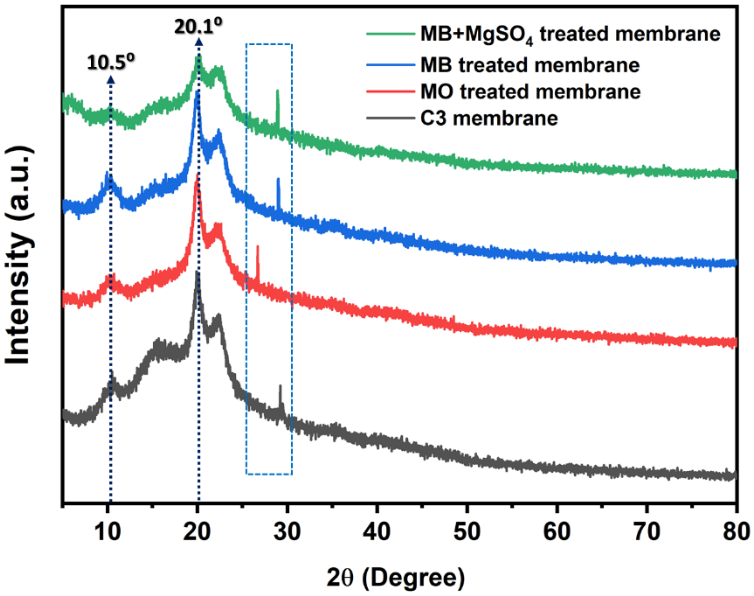

Figure 4.22 XRD peaks of membrane for before and after cyclic filtration.

It is evidenced by the high stability in harsh conditions and excellent MB/$MgSO_4$ mixture separation performance of C3 membrane. The FRR (%) decreases toward increasing the number cycle due to fouling formation with a higher MB/$MgSO_4$ rejection percentage due to the strong electrostatic interaction between MB and C3 membrane surface. The C3 membrane achieved more than 90% of FRR for MB/$MgSO_4$ mixture for six cycles. They diminished fouling formation by the enhanced hydrophilicity of the C3 membrane is offered by the MIL-100 (Fe) addition [64,65]. The existence of productive carboxylic groups on the CS/MIL-100 (Fe) membrane improves the hydrophilicity and hydration layer formation by hydrogen bonds, which support the high reusable stability of the C3 membrane. Figure 4.22 shows the characteristic XRD spectra of the C3 membrane before and after the cyclic filtration study. The crystalline peaks of $2\theta = 10.5°$ and $21°$ present at all the membranes confirm the high degree of crystallinity maintenance of the C3 membrane after the cyclic filtration study. It was gained due to the strong inter and intramolecular hydrogen bonding between the $-NH_2$ and -OH groups in the CS/MIL-100 (Fe) membrane [66]. The peaks present between $2\theta = 26°$ and $29°$ at all the membranes assigned to the MIL-100 (Fe) presence in the CS matrix. The XRD peaks exist after MB, MO, and MB+$MgSO_4$ treated membranes, evidence the CS/MIL-100 (Fe) membrane structure could not affect after the long-term cyclic filtration study and shows the strong membrane stability. All evidence proves the CS/MIL-100 (Fe) membrane is a potential candidate for eliminating the hazardous pollutants from the textile dyeing wastewater [51,60,67].

4.6 Conclusion

This study reported a modest but significant approach to fabricate CS/MIL-100 (Fe) membrane with high permeability and outstanding separation performance for hazardous anionic and cationic dye and dye/salts mixtures from the textile dyeing wastewater. Here, the hydrophilic MIL-100 (Fe) incorporation improves the membrane properties toward the excellent textile dyeing wastewater treatment. The prepared CS/MIL-100 (Fe) composite membrane improved water permeability from 4.2 to 52.5 L/m^2 h with a 99% rejection of both MB and MO dyes. Besides, the CS/MIL-100 (Fe) membrane also displays a higher rejection of more than 98% of MB dye and 51.6% of Mg2+ and 52.5% of SO42- ions from the feed solution MB+$MgSO_4$ mixtures. Furthermore, the CS/MIL-100 (Fe) membranes show excellent rejection and antifouling performances with high recycling stability of 6 cycles at a feed solution of MB, MO, and MB/$MgSO_4$ mixture. The novel of this work is to emphasize that the incorporation of MIL-100 (Fe) nanofiller into the CS matrix (CS/MIL-100 (Fe) membrane) is an effective strategy to develops a potential candidate for the treatment of textile dyeing wastewater.

4.7 References

[1] J. Jin, X. Du, J. Yu, S. Qin, M. He, K. Zhang, G. Chen, High performance nanofiltration membrane based on SMA-PEI cross-linked coating for dye/salt separation, J. Memb. Sci. 611 (2020) 118307. https://doi.org/10.1016/j.memsci.2020.118307.

[2] A. Malik, R. Akhtar, E. Grohmann, Environmental Deterioration and Human Health, Springer Netherlands, Dordrecht, 2014. https://doi.org/10.1007/978-94-007-7890-0.

[3] J. Huang, K. Zhang, The high flux poly (m-phenylene isophthalamide) nanofiltration membrane for dye purification and desalination, Desalination. 282 (2011) 19–26. https://doi.org/10.1016/j.desal.2011.09.044.

[4] M. Muthukumar, Studies on the effect of inorganic salts on decolouration of acid dye effluents by ozonation, Dye. Pigment. 62 (2004) 221–228. https://doi.org/10.1016/j.dyepig.2003.11.002.

[5] S. Ma, S. Lee, K. Kim, J. Im, H. Jeon, Purification of organic pollutants in cationic thiazine and azo dye solutions using plasma-based advanced oxidation process via submerged multi-hole dielectric barrier discharge, Sep. Purif. Technol. 255 (2021) 117714. https://doi.org/10.1016/j.seppur.2020.117714.

[6] S. Leaper, A. Abdel-Karim, T.A. Gad-Allah, P. Gorgojo, Air-gap membrane distillation as a one-step process for textile wastewater treatment, Chem. Eng. J. 360 (2019) 1330–1340. https://doi.org/10.1016/j.cej.2018.10.209.

[7] I. Mantasha, S. Hussain, M. Ahmad, M. Shahid, Two dimensional (2D) molecular frameworks for rapid and selective adsorption of hazardous aromatic dyes from aqueous phase, Sep. Purif. Technol. 238 (2020) 116413. https://doi.org/10.1016/j.seppur.2019.116413.

[8] B. Van der Bruggen, C. Vandecasteele, Removal of pollutants from surface water and groundwater by nanofiltration: overview of possible applications in the drinking water industry, Environ. Pollut. 122 (2003) 435–444. https://doi.org/10.1016/S0269-7491(02)00308-1.

[9] F. Russo, F. Galiano, A. Iulianelli, A. Basile, A. Figoli, Biopolymers for sustainable membranes in CO2 separation: a review, Fuel Process. Technol. (2020) 106643. https://doi.org/10.1016/j.fuproc.2020.106643.

[10] Sapna, R. Sharma, D. Kumar, Chitosan-Based Membranes for Wastewater Desalination and Heavy Metal Detoxification, in: Nanoscale Mater. Water Purif., Elsevier, 2019: pp. 799–814. https://doi.org/10.1016/B978-0-12-813926-4.00037-9.

[11] S.K. Ramachandran, A. Gangasalam, Reduction of chemical oxygen demand and color from the rice mill wastewater by chitosan/2(5 H)-furanone-incorporated ultrafiltration membrane system, Sep. Sci. Technol. 54 (2019) 409–424. https://doi.org/10.1080/01496394.2018.1505914.

[12] X. Tao, K. Li, H. Yan, H. Yang, A. Li, Simultaneous removal of acid green 25 and mercury ions from aqueous solutions using glutamine modified chitosan

magnetic composite microspheres, Environ. Pollut. 209 (2016) 21–29. https://doi.org/10.1016/j.envpol.2014.11.020.

[13] Q. Li, Y. Li, X. Ma, Q. Du, K. Sui, D. Wang, C. Wang, H. Li, Y. Xia, Filtration and adsorption properties of porous calcium alginate membrane for methylene blue removal from water, Chem. Eng. J. 316 (2017) 623–630. https://doi.org/10.1016/j.cej.2017.01.098.

[14] G. Gnanasekaran, S. Balaguru, G. Arthanareeswaran, D.B. Das, Removal of hazardous material from wastewater by using metal organic framework (MOF) embedded polymeric membranes, Sep. Sci. Technol. 54 (2019) 434–446. https://doi.org/10.1080/01496394.2018.1508232.

[15] A. Kovtun, E. Campodoni, L. Favaretto, M. Zambianchi, A. Salatino, S. Amalfitano, M.L. Navacchia, B. Casentini, V. Palermo, M. Sandri, M. Melucci, Multifunctional graphene oxide/biopolymer composite aerogels for microcontaminants removal from drinking water, Chemosphere. 259 (2020) 127501. https://doi.org/10.1016/j.chemosphere.2020.127501.

[16] Z. Jiang, Y. Yu, H. Wu, Preparation of CS/GPTMS hybrid molecularly imprinted membrane for efficient chiral resolution of phenylalanine isomers, J. Memb. Sci. 280 (2006) 876–882. https://doi.org/10.1016/j.memsci.2006.03.006.

[17] Q. Long, Z. Zhang, G. Qi, Z. Wang, Y. Chen, Z.-Q. Liu, Fabrication of Chitosan Nanofiltration Membranes by the Film Casting Strategy for Effective Removal of Dyes/Salts in Textile Wastewater, ACS Sustain. Chem. Eng. 8 (2020) 2512–2522.

https://doi.org/10.1021/acssuschemeng.9b07026.

[18] A.M. Sajjan, H.G. Premakshi, M.Y. Kariduraganavar, Synthesis and characterization of GTMAC grafted chitosan membranes for the dehydration of low water content isopropanol by pervaporation, J. Ind. Eng. Chem. 25 (2015) 151–161. https://doi.org/10.1016/j.jiec.2014.10.027.

[19] M.M.A. Nikje, Z.M. Tehrani, Novel Hybrid Membranes Based on Chitosan and Organically-Modified Nano-SiO2, Des. Monomers Polym. 12 (2009) 315–322. https://doi.org/10.1163/156855509X448280.

[20] D. Yang, J. Li, Z. Jiang, L. Lu, X. Chen, Chitosan/TiO2 nanocomposite pervaporation membranes for ethanol dehydration, Chem. Eng. Sci. 64 (2009) 3130–3137. https://doi.org/10.1016/j.ces.2009.03.042.

[21] X. Qian, N. Li, Q. Wang, S. Ji, Chitosan/graphene oxide mixed matrix membrane with enhanced water permeability for high-salinity water desalination by pervaporation, Desalination. 438 (2018) 83–96. https://doi.org/10.1016/j.desal.2018.03.031.

[22] S.B. Rekik, S. Gassara, J. Bouaziz, A. Deratani, S. Baklouti, Enhancing hydrophilicity and permeation flux of chitosan/kaolin composite membranes by using polyethylene glycol as porogen, Appl. Clay Sci. 168 (2019) 312–323. https://doi.org/10.1016/j.clay.2018.11.029.

[23] F. Khoerunnisa, W. Rahmah, B. Seng Ooi, E. Dwihermiati, N. Nashrah, S. Fatimah, Y.G. Ko, E.-P. Ng, Chitosan/PEG/MWCNT/Iodine composite

membrane with enhanced antibacterial properties for dye wastewater treatment, J. Environ. Chem. Eng. 8 (2020) 103686. https://doi.org/10.1016/j.jece.2020.103686.

[24] S.-L. Wu, F. Liu, H.-C. Yang, S.B. Darling, Recent progress in molecular engineering to tailor organic–inorganic interfaces in composite membranes, Mol. Syst. Des. Eng. 5 (2020) 433–444. https://doi.org/10.1039/C9ME00154A.

[25] M. Baghbanzadeh, D. Rana, C.Q. Lan, T. Matsuura, Effects of Inorganic Nano-Additives on Properties and Performance of Polymeric Membranes in Water Treatment, Sep. Purif. Rev. 45 (2016) 141–167. https://doi.org/10.1080/15422119.2014.1068806.

[26] D. Qadir, H. Mukhtar, L.K. Keong, Mixed Matrix Membranes for Water Purification Applications, Sep. Purif. Rev. 46 (2017) 62–80. https://doi.org/10.1080/15422119.2016.1196460.

[27] P.S. Goh, B.C. Ng, W.J. Lau, A.F. Ismail, Inorganic nanomaterials in polymeric ultrafiltration membranes for water treatment, Sep. Purif. Rev. 44 (2015) 216–249. https://doi.org/10.1080/15422119.2014.926274.

[28] R.Y. Hong, Q. Chen, Dispersion of Inorganic Nanoparticles in Polymer Matrices: Challenges and Solutions, in: Adv. Polym. Sci., 2014: pp. 1–38. https://doi.org/10.1007/12_2014_286.

[29] A. Elrasheedy, N. Nady, M. Bassyouni, A. El-Shazly, Metal organic framework based polymer mixed matrix membranes: Review on applications in water

purification, Membranes (Basel). 9 (2019). https://doi.org/10.3390/membranes9070088.

[30] J. Li, H. Wang, X. Yuan, J. Zhang, J.W. Chew, Metal-organic framework membranes for wastewater treatment and water regeneration, Coord. Chem. Rev. 404 (2020) 213116. https://doi.org/10.1016/j.ccr.2019.213116.

[31] X.H. Ma, Z. Yang, Z.K. Yao, Z.L. Xu, C.Y. Tang, A facile preparation of novel positively charged MOF/chitosan nanofiltration membranes, J. Memb. Sci. 525 (2017) 269–276. https://doi.org/10.1016/j.memsci.2016.11.014.

[32] Y. Jia, Q. Jin, Y. Li, Y. Sun, J. Huo, X. Zhao, Investigation of the adsorption behaviour of different types of dyes on MIL-100(Fe) and their removal from natural water, Anal. Methods. 7 (2015) 1463–1470. https://doi.org/10.1039/C4AY02726D.

[33] Y. Fang, Z. Yang, H. Li, X. Liu, MIL-100(Fe) and its derivatives: from synthesis to application for wastewater decontamination, Environ. Sci. Pollut. Res. 27 (2020) 4703–4724. https://doi.org/10.1007/s11356-019-07318-w.

[34] K. Guesh, C.A.D. Caiuby, Á. Mayoral, M. Díaz-García, I. Díaz, M. Sanchez-Sanchez, Sustainable Preparation of MIL-100(Fe) and Its Photocatalytic Behavior in the Degradation of Methyl Orange in Water, Cryst. Growth Des. 17 (2017) 1806–1813. https://doi.org/10.1021/acs.cgd.6b01776.

[35] M. Mozafari, S.F. Seyedpour, S.K. Salestan, A. Rahimpour, A.A. Shamsabadi, M.D. Firouzjaei, M.R. Esfahani, A. Tiraferri, H. Mohsenian, M. Sangermano, M.

Soroush, Facile Cu-BTC surface modification of thin chitosan film coated polyethersulfone membranes with improved antifouling properties for sustainable removal of manganese, J. Memb. Sci. 588 (2019) 117200. https://doi.org/10.1016/j.memsci.2019.117200.

[36] Q. Li, Q. Liu, J. Zhao, Y. Hua, J. Sun, J. Duan, W. Jin, High efficient water/ethanol separation by a mixed matrix membrane incorporating MOF filler with high water adsorption capacity, J. Memb. Sci. 544 (2017) 68–78. https://doi.org/10.1016/j.memsci.2017.09.021.

[37] M. El-Shahat, A.E. Abdelhamid, R.M. Abdelhameed, Capture of iodide from wastewater by effective adsorptive membrane synthesized from MIL-125-NH2 and cross-linked chitosan, Carbohydr. Polym. 231 (2020) 115742. https://doi.org/10.1016/j.carbpol.2019.115742.

[38] S. Jamshidifard, S. Koushkbaghi, S. Hosseini, S. Rezaei, A. Karamipour, A. Jafari rad, M. Irani, Incorporation of UiO-66-NH2 MOF into the PAN/chitosan nanofibers for adsorption and membrane filtration of Pb(II), Cd(II) and Cr(VI) ions from aqueous solutions, J. Hazard. Mater. 368 (2019) 10–20. https://doi.org/10.1016/j.jhazmat.2019.01.024.

[39] M. Vinu, S. Pal, J.D. Chen, Y.F. Lin, Y.L. Lai, C.S. Lee, C.H. Lin, Microporous 3D aluminum MOF doped into chitosan-based mixed matrix membranes for ethanol/water separation, in: J. Chinese Chem. Soc., Chinese Chemical Society Taiwan, 2019: pp. 1165–1171. https://doi.org/10.1002/jccs.201900172.

[40] S. Huang, K.-L. Yang, X.-F. Liu, H. Pan, H. Zhang, S. Yang, MIL-100(Fe)-catalyzed efficient conversion of hexoses to lactic acid, RSC Adv. 7 (2017) 5621–5627. https://doi.org/10.1039/C6RA26469G.

[41] H. Lv, H. Zhao, T. Cao, L. Qian, Y. Wang, G. Zhao, Efficient degradation of high concentration azo-dye wastewater by heterogeneous Fenton process with iron-based metal-organic framework, J. Mol. Catal. A Chem. 400 (2015) 81–89. https://doi.org/10.1016/j.molcata.2014.02.007.

[42] P.J. Kim, Y.W. You, H. Park, J.S. Chang, Y.S. Bae, C.H. Lee, J.K. Suh, Separation of SF6 from SF6/N2 mixture using metal-organic framework MIL-100(Fe) granule, Chem. Eng. J. 262 (2015) 683–690. https://doi.org/10.1016/j.cej.2014.09.123.

[43] N.U. Qadir, S.A.M. Said, R.B. Mansour, K. Mezghani, A. Ul-Hamid, Synthesis, characterization, and water adsorption properties of a novel multi-walled carbon nanotube/MIL-100(Fe) composite, Dalt. Trans. 45 (2016) 15621–15633. https://doi.org/10.1039/c6dt02640k.

[44] F. Zhang, J. Shi, Y. Jin, Y. Fu, Y. Zhong, W. Zhu, Facile synthesis of MIL-100(Fe) under HF-free conditions and its application in the acetalization of aldehydes with diols, Chem. Eng. J. 259 (2015) 183–190. https://doi.org/10.1016/j.cej.2014.07.119.

[45] M. Kumar, B.P. Tripathi, V.K. Shahi, Crosslinked chitosan/polyvinyl alcohol blend beads for removal and recovery of Cd(II) from wastewater, J. Hazard.

Mater. 172 (2009) 1041–1048. https://doi.org/10.1016/j.jhazmat.2009.07.108.

[46] E. Salehi, P. Daraei, A. Arabi Shamsabadi, A review on chitosan-based adsorptive membranes, Carbohydr. Polym. 152 (2016) 419–432. https://doi.org/10.1016/j.carbpol.2016.07.033.

[47] S.S. Madaeni, A.H. Taheri, Effect of Casting Solution on Morphology and Performance of PVDF Microfiltration Membranes, Chem. Eng. Technol. 34 (2011) 1328–1334. https://doi.org/10.1002/ceat.201000177.

[48] R. Dai, X. Wang, C.Y. Tang, Z. Wang, Dually Charged MOF-Based Thin-Film Nanocomposite Nanofiltration Membrane for Enhanced Removal of Charged Pharmaceutically Active Compounds, Environ. Sci. Technol. 54 (2020) 7619–7628. https://doi.org/10.1021/acs.est.0c00832.

[49] M. Zhang, K. Guan, Y. Ji, G. Liu, W. Jin, N. Xu, Controllable ion transport by surface-charged graphene oxide membrane, Nat. Commun. 10 (2019) 1253. https://doi.org/10.1038/s41467-019-09286-8.

[50] Q. Gu, T.C. Albert Ng, Q. Sun, A.M. Kotb Elshahawy, Z. Lyu, Z. He, L. Zhang, H.Y. Ng, K. Zeng, J. Wang, Heterogeneous ZIF-L membranes with improved hydrophilicity and anti-bacterial adhesion for potential application in water treatment, RSC Adv. 9 (2019) 1591–1601. https://doi.org/10.1039/C8RA08758J.

[51] J. Ma, X. Tang, Y. He, Y. Fan, J. Chen, HaoYu, Robust stable MoS2/GO filtration membrane for effective removal of dyes and salts from water with enhanced permeability, Desalination. 480 (2020) 114328.

https://doi.org/10.1016/j.desal.2020.114328.

[52] A. Refaat Alawady, A. Ali Alshahrani, T. Ali Aouak, N. Mohamed Alandis, Polysulfone membranes with CNTs/Chitosan biopolymer nanocomposite as selective layer for remarkable heavy metal ions rejection capacity, Chem. Eng. J. 388 (2020) 124267. https://doi.org/10.1016/j.cej.2020.124267.

[53] Y. Shim, H.-J. Lee, S. Lee, S.-H. Moon, J. Cho, Effects of Natural Organic Matter and Ionic Species on Membrane Surface Charge, Environ. Sci. Technol. 36 (2002) 3864–3871. https://doi.org/10.1021/es015880b.

[54] M. Mänttäri, A. Pihlajamäki, M. Nyström, Effect of pH on hydrophilicity and charge and their effect on the filtration efficiency of NF membranes at different pH, J. Memb. Sci. 280 (2006) 311–320. https://doi.org/10.1016/j.memsci.2006.01.034.

[55] H. Liu, M. Zhang, H. Zhao, Y. Jiang, G. Liu, J. Gao, Enhanced dispersibility of metal–organic frameworks (MOFs) in the organic phase via surface modification for TFN nanofiltration membrane preparation, RSC Adv. 10 (2020) 4045–4057. https://doi.org/10.1039/C9RA09672H.

[56] S. Zhou, J. Gao, J. Zhu, D. Peng, Y. Zhang, Y. Zhang, Self-cleaning, antibacterial mixed matrix membranes enabled by photocatalyst Ti-MOFs for efficient dye removal, J. Memb. Sci. 610 (2020) 118219. https://doi.org/10.1016/j.memsci.2020.118219.

[57] F. Tan, M. Liu, K. Li, Y. Wang, J. Wang, X. Guo, G. Zhang, C. Song, Facile

synthesis of size-controlled MIL-100(Fe) with excellent adsorption capacity for methylene blue, Chem. Eng. J. 281 (2015) 360–367. https://doi.org/10.1016/j.cej.2014.06.044.

[58] P. Zhang, J.L. Gong, G.M. Zeng, B. Song, H.Y. Liu, S.Y. Huan, J. Li, Ultrathin reduced graphene oxide/MOF nanofiltration membrane with improved purification performance at low pressure, Chemosphere. 204 (2018) 378–389. https://doi.org/10.1016/j.chemosphere.2018.04.064.

[59] F. Marrakchi, W.A. Khanday, M. Asif, B.H. Hameed, Cross-linked chitosan/sepiolite composite for the adsorption of methylene blue and reactive orange 16, Int. J. Biol. Macromol. 93 (2016) 1231–1239. https://doi.org/10.1016/j.ijbiomac.2016.09.069.

[60] J. Cao, Y. Su, Y. Liu, J. Guan, M. He, R. Zhang, Z. Jiang, Self-assembled MOF membranes with underwater superoleophobicity for oil/water separation, J. Memb. Sci. 566 (2018) 268–277. https://doi.org/10.1016/j.memsci.2018.08.068.

[61] Y. Wu, M. Gao, W. Chen, Z. Lü, S. Yu, M. Liu, Efficient removal of anionic dye by constructing thin-film composite membrane with high perm-selectivity and improved anti-dye-deposition property, Desalination. 476 (2020) 114228. https://doi.org/10.1016/j.desal.2019.114228.

[62] B. Van der Bruggen, E. Curcio, E. Drioli, Process intensification in the textile industry: the role of membrane technology, J. Environ. Manage. 73 (2004) 267–274. https://doi.org/10.1016/j.jenvman.2004.07.007.

[63] Y.-F. Mi, G. Xu, Y.-S. Guo, B. Wu, Q.-F. An, Development of antifouling nanofiltration membrane with zwitterionic functionalized monomer for efficient dye/salt selective separation, J. Memb. Sci. 601 (2020) 117794. https://doi.org/10.1016/j.memsci.2019.117794.

[64] F. Mohammadnezhad, M. Feyzi, S. Zinadini, A novel Ce-MOF/PES mixed matrix membrane; synthesis, characterization and antifouling evaluation, J. Ind. Eng. Chem. 71 (2019) 99–111. https://doi.org/10.1016/j.jiec.2018.09.032.

[65] F. Gholami, S. Zinadini, A.A. Zinatizadeh, A.R. Abbasi, TMU-5 metal-organic frameworks (MOFs) as a novel nanofiller for flux increment and fouling mitigation in PES ultrafiltration membrane, Sep. Purif. Technol. 194 (2018) 272–280. https://doi.org/10.1016/j.seppur.2017.11.054.

[66] B.S. Rathore, N.P.S. Chauhan, M.K. Rawal, S.C. Ameta, R. Ameta, Chitosan–polyaniline–copper(II) oxide hybrid composite for the removal of methyl orange dye, Polym. Bull. 77 (2020) 4833–4850. https://doi.org/10.1007/s00289-019-02994-7.

[67] H. Ruan, C. Guo, H. Yu, J. Shen, C. Gao, A. Sotto, B. Van der Bruggen, Fabrication of a MIL-53(Al) Nanocomposite Membrane and Potential Application in Desalination of Dye Solutions, Ind. Eng. Chem. Res. 55 (2016) 12099–12110. https://doi.org/10.1021/acs.iecr.6b03201.

CHAPTER 5 NOVEL MIL-100 (FE) INCORPORATED HIGH-FLUX POLYSULFONE NANOFILTRATION MEMBRANE AND ITS EXCELLENT REMOVAL PERFORMANCE OF MICROPLASTIC ADSORBED DYE CONTAMINANT FROM TEXTILE WASTEWATER

5.1 Introduction

Rapid industrialization, urbanization, and population growth have given rise to an immense responsibility to address the problems of increasing water shortage and environmental pollution [1]. At present, the volume of textile wastewater being discharged into the aquatic environment is rising enormously, and these large quantities of colored chemicals are non-biodegradable and highly hazardous. The manufacture and trading events of textile industries contribute towards the majority of microplastics (MPs) pollution. More than 5.4 million tons of synthetic textile fibers were manufactured worldwide in 2016, which can contact the aquatic environment and contribute 90% of microplastic pollution [2]. MPs are highly moveable and omnipresent in the discharged wastewaters owing to the characteristics of insolubility and lightweight. Based on the physical structures, MPs are characterized as fibers, microbeads, sheets, and fragments. In chemically, MPs are polymers, which include polyvinyl chloride (PVC), polypropylene (PP), polyethylene (PE), polyethylene terephthalate (PET), polystyrene (PS), and polyamide (PA) [3]. Numerous dye molecules, salts, and additives have been intensively utilized in the textile dyeing process in textile industries. The precarious dyestuff in the wastewater from the dyeing process would harm humans and creatures living in aqueous environments. Therefore, it is essential to remove the dye contaminants from textile wastewater [4–6]. To date, many conventional techniques, such as adsorption, advanced oxidation processing, distillation, flocculation, and membrane separation, have been widely used for dye wastewater treatment [7,8].

In recent years, membrane separation has attracted extensive interest for wastewater treatment owing to its excellent benefits of low energy consumption yet higher separation efficiency combined with a convenient operating procedure [9]. In addition, various membrane-separation techniques based on different separation strategies and membrane properties have been developed, such as microfiltration, ultrafiltration, nanofiltration, and reverse osmosis [10]. Specifically, nanofiltration (NF) technologies offer the highest potential as the most powerful tool for separating organic molecules and inorganic salts, including the effect of Donnan, steric, and dielectric exclusion [11,12]. However, developing an innovative NF membrane can reject almost 100 % of dye and salt with high water flux. Therefore, numerous studies have focused on fabricating novel composite NF membranes composed of nanofillers and a polymer matrix for selective contaminant removal from wastewater [13–15]. More recently, polysulfone (PSF) [16], polyamide (PA) [17], poly(vinylidene fluoride) (PVDF) [18], and polyethersulfone (PES) [6] were used as the leading raw materials for the fabrication of membranes. However, the disadvantages of polymeric membranes are their lack of hydrophilicity, low anti-fouling ability, limited mechanical stability, and insufficient chemical stability, and they significantly restrict their use in wide-reaching applications [19,20]. Membrane modification is a superior technique to overcome these obstacles. Incorporating novel nanomaterials into polymers has impressively contributed to developing renewable composite membranes for wastewater treatment [21]. Carbon nanomaterials, metal oxides, and metal-organic frameworks (MOFs) are significantly utilized among these materials.

MOFs have been broadly active as novel candidates for fabricating futuristic composite membranes due to their high porosity, superior surface area, tunable pore structure, a good affinity for polymers, an abundance of functional groups, and high adsorption capacity [8,22]. The incorporation of MOFs (BUT-8(A)) into a polyethyleneimine (PEI) matrix exhibited higher water permeability of 396–683 Lm^{-2} h^{-1} MPa^{-1} with an unprecedented rejection rate of aqueous dye solutions. The introduction of hydrophilic BUT-8(A) nanoparticles is the main reason for the high permeability of the BUT-8(A)/PEI-HPAN-50 composite membrane. The sulfonic groups of BUT-8(A) boost the water affinity and engage in solid interaction with the amine groups of the PEI chains, promoting rejection [23]. Likewise, mixed matrix membranes were fabricated using P84 polyimide and a cadmium-based metal-organic framework (MOF-2(Cd)). The dye removal rate of the membrane increased to 99.9%, 81.2%, and 68.4% for MB, EY, and SY, respectively, with high water permeability of 117.8–171.4 L/m^2 h bar [24]. Cu-MOF incorporated polydopamine NF membrane shows the improved hydrophilicity and permeability of the membrane. Furthermore, the porous structure of Cu-MOF provides additional pathways for water. The embedded Cu-MOF membrane was initiate to reject anionic and cationic dyes based on an electrostatic repulsive mechanism [25].

MPs' toxicity primarily originates from its absorption or adsorption ability of contaminants from the environment. PVC MPs were adsorbing organic contaminants (MB dye) with the influences of surfactants [26]. MPs with adsorbed pollutants from the wastewater were treated with membrane filtration is an effective technique for treating textile wastewater. However, the MPs' pore size is much larger than membrane pores, impacting the higher rejection of MPs adsorbed contaminants by size exclusion mechanism [27].

The potential treatment of MPs and other emerging contaminants removal from the textile wastewater is rarely found. In this work, a high flux charged nanofiltration membrane was fabricated via the phase inversion technique to remove the contaminants from textile wastewater. The hydrophilic MIL-100 (Fe) nanoparticles were incorporated into a polysulfone matrix to enhance the performance of the membrane. MIL-100 (Fe) incorporation on the hydrophilicity, porosity, pore size, morphology, permeability, separation, and anti-fouling performance of PSF membranes was studied. The fabricated PSF/MIL-100 (Fe) composite membrane displayed excellent rejection of MB, MPs (PVC and PE) +MB, and salts ($MgSO_4$, Na_2SO_4, $CaCl_2$, and NaCl) with high permeability. Owing to these properties, the incorporation of hydrophilic MIL-100 (Fe) nanoparticles in the PSF matrix proved to be a promising candidate for textile wastewater treatment.

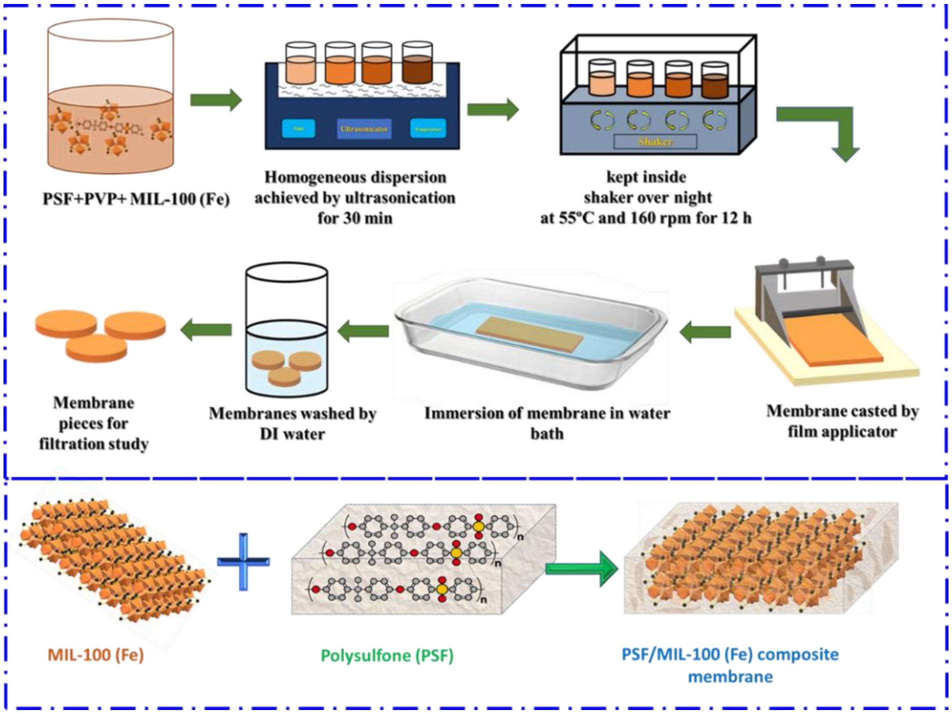
PSF+PVP+ MIL-100 (Fe)
Homogeneous dispersion achieved by ultrasonication for 30 min
Ultrasonicator
kept inside shaker over night at 55°C and 160 rpm for 12 h
Shaker
Membrane casted by film applicator
Immersion of membrane in water bath
Membranes washed by DI water
Membrane pieces for filtration study
MIL-100 (Fe)
Polysulfone (PSF)
PSF/MIL-100 (Fe) composite membrane

Figure 5.1 Schematic representation of the fabrication process of PSF/MIL-100 (Fe) membranes.

5.2 Preparation of PSF/MIL-100 (Fe) membranes

The phase inversion technique was followed to prepare the pristine PSF and PSF/MIL-100 (Fe) membranes. Figure 5.1 shows a schematic representation of the membrane preparation. Initially, 17.5 wt% of PSF and 2 wt% of PVP in NMP were used as the casting solution. Initially, 0, 0.25, 0.5, and 1 % of MIL-100 (Fe) was dispersed into NMP and subjected to ultrasonication for 30 min. Then, the PSF and PVP were added slowly to this solution. The resulting mixtures were kept in a thermally insulated shaker at 55 ºC for 12 h. Next, the well-mixed solutions were cast on a clean glass plate using a film applicator to obtain a film with a thickness of 200 μm and immediately immersed in a bath of DI water maintained at 4 ºC. The membrane was washed several times with DI water before use. Based on the amount of MIL-100 (Fe) incorporated into the PSF matrix, the membranes were named M0, M0.25, M0.5, M0.75, and M1.

5.3 Characterization of PSF/MIL-100 (Fe) membranes

The crystalline structures of the PSF/MIL-100 (Fe) membranes were characterized by X-ray diffraction (XRD, PANanalytical's Empyrean) in the scan range of 5–80°. The cross-sectional morphology of the membranes was characterized by field-emission scanning electron microscopy (FESEM, TESCAN, MIRA3, Center for Research Facilities (CRF), Jeju National University, Jeju, Republic of Korea) at 15 kV. All the membrane samples were fractured in liquid nitrogen and sputter coated with Pt to obtain a clear cross-sectional view. The elemental distribution was observed by energy-dispersive spectroscopy (EDS, TESCAN, MIRA3, Center for Research Facilities (CRF), Jeju National University, Jeju, Republic of Korea) with element mapping measurements conducted at 15 kV. A filtration study of PSF/MIL-100 (Fe) membranes was carried out to remove MB dye, salts, and microplastics. The hydrophilicity of the membranes was characterized by water contact angle measurements (Goniometer, Phonix 300, Surface & Electro-Optics Co., Ltd., Korea) under atmospheric conditions. Specifically, 5 µL of DI water was dropped onto the membrane surface to measure the water contact angle.

5.4 Nanofiltration

The filtration study was performed using dead-end nanofiltration (Sterlitech HP4750 stirred cell) with an active membrane area of 14.6 cm^2. The pre-compaction of membranes was affected by using pure DI water at 3 bar for 60 min, and the effect of TMP on the membrane performance was studied by varying the pressure in the range of 2–10 bar. The separation performance of the PSF/MIL-100 (Fe) membranes was examined by using various concentrations of MB (10–100 ppm), PVC and PE MPs (0.5, 1, 1.25, and 1.5 g/L) + MB feed solutions and by varying the pH of the MB dye and PVC and PE MPs + MB solutions, the TMP from 2 to 10 bar, the addition of NaCl, Na_2SO_4, $CaCl_2$, and $MgSO_4$ (1000 ppm solutions), and the reusability of MB dye rejections for 1–6 cycles. All the experiments were operated under continuous stirring at 350 rpm using a magnetic stirrer to minimize the concentration polarization. The dye concentration was measured by ultraviolet-visible (UV-vis) spectrophotometry (MEGA-2100- SCINCO Company–Korea) at a wavelength of 665 nm for MB. The salt concentration was determined by a conductivity meter (DiST 3 by Hanna instruments, South Korea). The pH of the dye solutions was adjusted with 0.1 M NaOH and 0.1 M HCl.

5.5 Result and discussion

5.5.1 XRD analysis of membranes

The XRD patterns of the prepared MIL-100 (Fe) incorporated in the PSF membrane are shown in Figure 5.2. The XRD results of the prepared MIL-100 (Fe), pristine PSF, and PSF/PVP membranes were analyzed and displayed in the exact Figure The broad peaks at $2\theta=17^{o}$ for the pristine PSF, PSF/PVP, and PSF/PVP/MIL-100 (Fe) membrane correspond to the amorphous structure of polysulfone [30]. The diffraction peaks of MIL-100 (Fe) appear at $2\theta=5.5$, 10.2, and 11^{o} and are consistent with the simulated XRD pattern of MIL-100 (Fe) [28]. In the case of the PSF/PVP/MIL-100 (Fe) membranes, the appearance of the sharp peaks at $2\theta=5.5$, 10.2, and 11^{o} provide evidence for the existence of MIL-100 (Fe) in the PSF composite membranes. The peak at 2θ=22º corresponds to the amorphous structure of PSF and PVP in the PSF/PVP membrane.

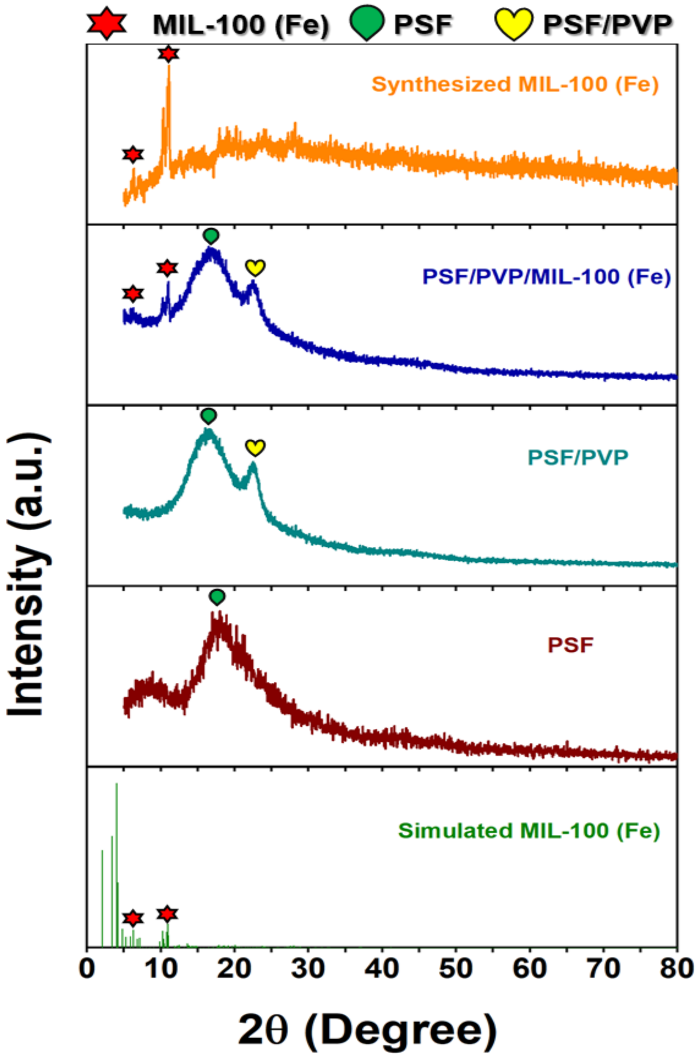

Figure 5.2 XRD patterns of membranes and MIL-100 (Fe)

5.5.2 Cross-sectional view of the membrane

The cross-sectional morphology of the membranes was characterized by FESEM analysis. Figure 5.3 presents the cross-sectional FESEM images of the pristine PSF membranes and those incorporating MIL-100 (Fe) at different magnifications. All the membranes have an asymmetric structure consisting of a dense top skin layer and sub-layers. Changes in the internal structural morphology of the PSF membrane after MIL-100 (Fe) inclusion are visualized in the form of the pore size abundance. PSF membranes incorporating MIL-100 (Fe) are more porous than pristine PSF membranes, especially the M0.5 membrane. A membrane with a larger pore size allows higher flux. [31]. The composite membranes displayed longer and wider finger-like structures than the pristine PSF membrane.

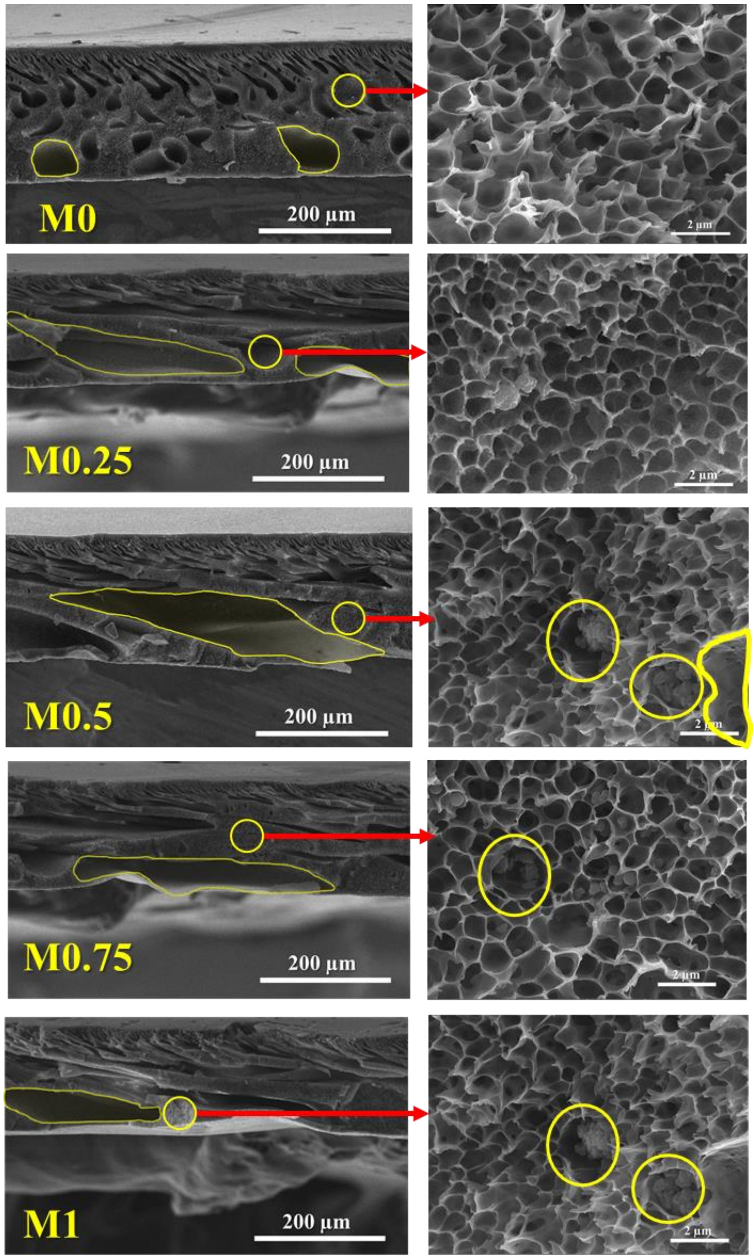
M0
200 µm
2 µm
M0.25
200 µm
2 µm
M0.5
200 µm
2 µm
M0.75
200 µm
2 µm
M1
200 µm
2 µm

Figure 5.3 Cross-sectional view of the membranes

Interestingly, the M0.5 membrane had larger pores. These modifications, which are the result of the hydrophilic functional groups of MIL-100 (Fe), can accelerate the demixing rate of the non-solvent (water) and solvent (NMP) during the process of phase inversion. The effect thereof is to enlarge the pore channels. Nevertheless, a higher loading (M0.75 and M1) of MIL-100 (Fe) decreases the pore structure [32,33]. Visualization at higher magnification revealed a sponge-like structure, which illustrates the interconnecting pore structure of membranes. The pore structure of the composite membrane fabricated using MOFs as an additive could be enhanced significantly compared to the pristine PSF membrane.

5.5.3 EDS analysis of membrane

The existence of MIL-100 (Fe) nanoparticles in the composite membrane was confirmed by using elemental mapping for the pristine PSF and PSF/MIL-100 (Fe) membranes, as shown in Figure 5.4 and Figure 5.5, respectively. EDS mapping is a valuable technique with which to visualize the distribution of elements on the membrane. The corresponding elements of the PSF membrane, including carbon (C), oxygen (O), sulfur (s), and fluorine (F), have existed in both the pristine and composite PSF/MIL-100 (Fe) membranes. Thus, the existence of Fe in the PSF/MIL-100 (Fe) membrane corresponds to the incorporation of MIL-100 (Fe) nanoparticles [34].

5.5.4 Pure water flux of membranes

The results of the membranes' pure water flux (PWF) analyses are presented in Figure 5.6(a). Incorporating MIL-100 (Fe) nanoparticles in the PSF matrix induces a much higher PWF than pristine PSF. This is rationalized by considering that the addition of hydrophilic and porous MIL-100 (Fe) provides new pathways for water transport, i.e., decreased tortuosity, to penetrate water molecules into the composite membranes.

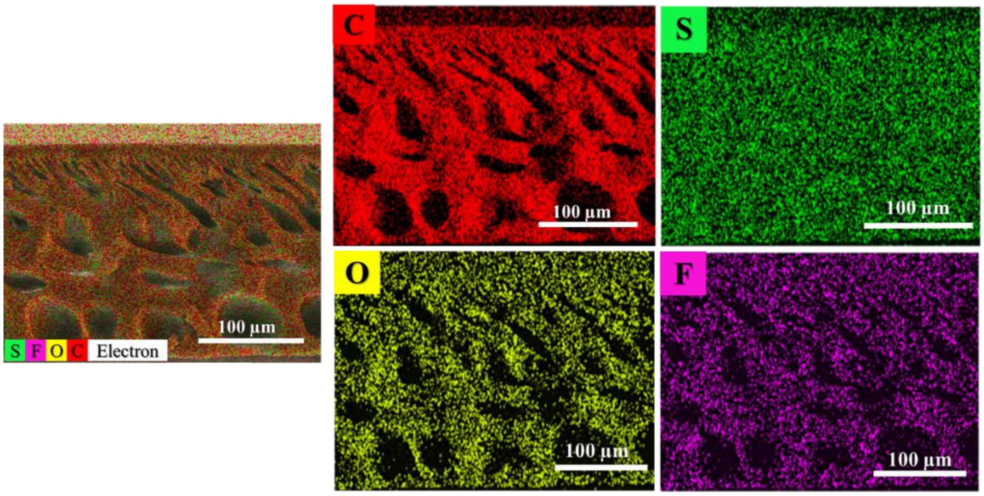
C
S
100 µm
100 µm
100 µm
S F O C Electron
O
F
100 µm
100 µm

Figure 5.4 EDS mapping of pristine PSF membrane

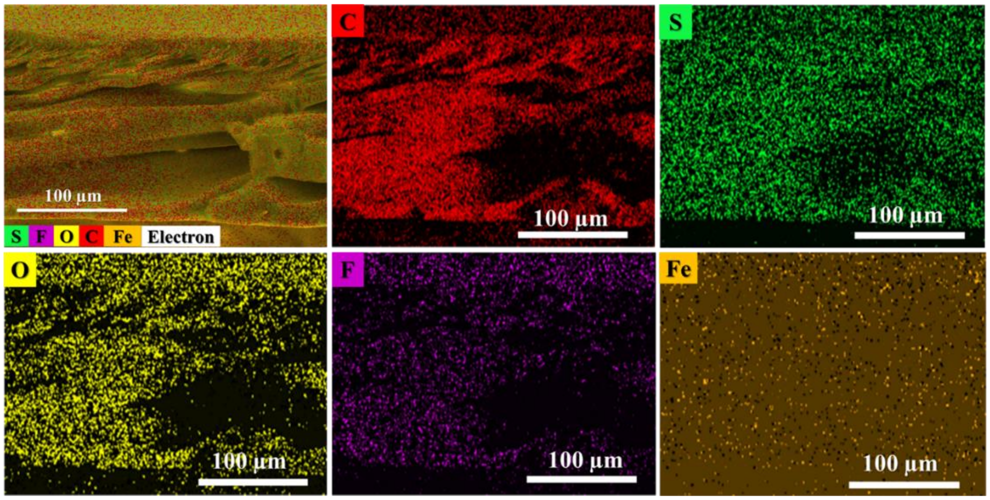
C
S
100 µm
S F O C Fe Electron
100 µm
100 µm
O
F
Fe
100 µm
100 µm
100 µm

Figure 5.5 EDS mapping of PSF/MIL-100 (Fe) membrane.

The incorporation of MIL-100 (Fe) in the PSF casting solution could significantly influence two aspects of membrane development: (i) enhancement of the hydrophilicity of the PSF membrane, (ii) modification of the structure, and pore size of the membranes. First, the composite membrane surface's enhanced hydrophilicity attracts water molecules to facilitate the transport of water molecules in the membranes. Second, the small channels and the broader internal pores on the PSF/MIL-100 (Fe) membranes were observed in the cross-sectional view of the membranes (Figure 5.5) can diminish the barrier to water molecules and offer additional pathways for water molecules [35]. The PWF was enhanced to as much as M0.5 before decreasing, owing to increasing MIL-100 (Fe) concentration into the PSF matrix. The M0.5 membrane attained a higher PWF of 72 L/m^2 h bar, which is significantly higher (10.3 times) than that of the pristine PSF (M0) membrane. The hydrophilic functional groups of MIL-100 (Fe) promote a high degree of water permeation by forming a hydration layer on the membrane surface. Contrary to the hydrophilicity enhancement of M0.75 and M1 membranes, the PWF was lower due to the blocking of membrane pores. Apart from this, the modified membrane has a higher rejection rate (%) [36].

5.5.5 Porosity and mean pore size of membranes

The effect of MIL-100 (Fe) on the membrane porosity and pore size is presented in Figure 5.6(a). The porosity and pore size of the membrane was elevated as MIL-100 (Fe) concentration increased up to 0.5 wt.% (M0.5). The maximum obtained porosity and mean pore size values of the M0.5 membrane were 91% and 8 nm, respectively. The results were consistent with the cross-sectional view and PWF of the membranes. Incorporating the hydrophilic MIL-100 (Fe) nanoparticles enhances the pore size and porosity by accelerating the exchange of the non-solvent and solvent during the phase inversion process. However, further increases in MIL-100 (Fe) in the membrane cause the pore size and porosity to decrease due to the viscosity of the solution increases, which slows down the liquid-liquid exchange process. Moreover, a more considerable amount of MIL-100 (Fe) promotes the accumulation process, which harms the membranes by blocking the pores [33,36].

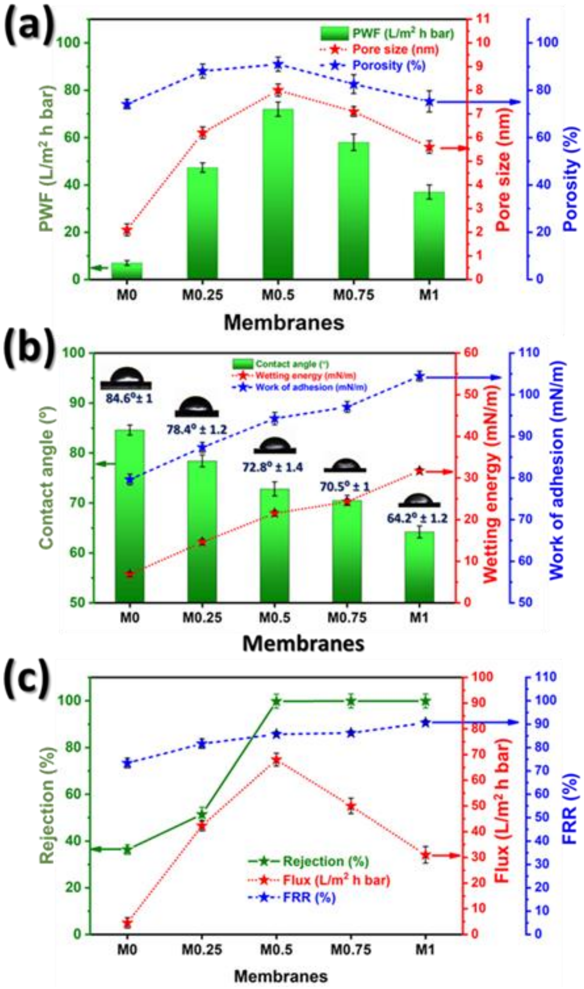

Figure 5.6 (a) PWF, porosity, and pore size; (b) contact angle, wetting energy, and work of adhesion; (c) rejection (%), flux, and FRR (%).

5.5.6 Contact angle of membranes

The surface hydrophilicity is one of the key features of the membrane, which mainly impacts the membrane permeability and anti-fouling properties. On the other hand, superior membrane hydrophilicity attracted more water molecules and reduced the deposition of contaminants on the membranes, resulting in higher permeability with enhanced anti-fouling ability. A water contact angle test was conducted to determine membrane hydrophilicity. Figure 5.6(b) shows the results of this test with the membranes shown in the inset images. The MIL-100 (Fe) incorporated membrane (M1) has a reduced contact angle of 64.2º ±1.2 compared with the pristine PSF membrane (84.6º ±1). The addition of 0.25, 0.5, 0.75, and 1 wt.% of MIL-100 (Fe) lowers the contact angle from 78.4º±1.2 to 72.8º±1.4, 70.5º±1, and 64.2º ±1.2, respectively. The mitigated contact angle of the PSF/MIL-100 (Fe) membrane indicates the enhancement of the hydrophilicity, resulting from the inherently rich hydrophilic MIL-100 (Fe) nanoparticles incorporated in the PSF matrix. The formation of the hydration layer on the membrane surface favorably improves hydrophilicity. The existence of hydroxyl (–OH) and acidic (–COOH) functional groups on the MIL-100 (Fe) gives rise to a strong interaction with the PSF matrix, which induces the hydrophilicity and formation of the hydration layer. The enhanced hydrophilicity results in outstanding anti-fouling properties with high flux [36,37].

5.5.7 Work of adhesion and wetting energy

The work of adhesion (WA) and wetting energy (WE) of the membrane were measured to investigate the wetting properties of the membranes after MIL-100 (Fe) incorporation. The WA explains the interaction between the wetting liquid and the membrane surface. Figure 5.6(b) presents the WA and WE result of the membranes. The WA and WE values for the composite PSF/MIL-100 (Fe) membranes were higher than those of the pristine PSF membranes. Interestingly, the M1 membrane had superior WA and WE of 104.5 mN/M and 31.7 mN/M, respectively, because of the stronger adhesive force, which provides the ultimate evidence of the improvement of the wetting nature of the composite PSF/MIL-100 (Fe) membranes [38].

5.5.8 Filtration performance of membranes

The prepared membranes' separation performances were investigated with various feed of MB, MB+MPs, and salts solutions. Initially, all membranes were treated with MB solution. Figure 5.6(c) shows the rejection (%), MB flux, and FRR (%) of the membranes. The MB rejection (%) of the PSF/MIL-100 (Fe) composite membrane was higher than that of the pristine PSF membrane. Interestingly, the MB rejection rate for M0.5, M0.75, and M1 remained more than 99%. This result is attributed to the increasing number of MIL-100 (Fe) functional groups, which enhances the membrane's rejection properties. Hydrophilic MIL-100 (Fe) in the PSF matrix provides additional pathways for water molecule permeation. Moreover, the hydrophilic MIL-100 (Fe) forms the hydration layers on the membrane surface, enhancing the anti-fouling properties [36]. Therefore, the effect prevents the dye molecules and other contaminants from being adsorbed within a specific range on the membrane surface. Therefore, it favors a higher rejection (%) of the MB dye molecules ([9]. As shown in Figure 5.7(a), the UV-vis absorbance permeate intensity decreased and completely diminished for the M0.5 to M1 membranes, indicating high MB rejection performances. Figure 5.7(b) shows that M0.5, M0.75, and M1 membranes achieved complete color removal, supporting the higher rejection performance of the PSF/MIL-100 (Fe) membranes. The PSF/MIL-100 (Fe) composite membrane's antifouling properties were enhanced before decreasing again, as observed from the calculated FRR (%). Interestingly, the M0.5 membrane achieved permeability, rejection, and anti-fouling (FRR%) properties superior to those of the other membranes, with an obtained maximum of 68 L/m^2 h bar values, > 99 % 85.7%, respectively. Based on the above results, the M0.5 membrane outperformed the other membranes, and it was used as the active membrane in subsequent studies.

5.5.8.1 Effect of pH on the membrane performances

5.5.8.1.1 MB rejection

The pH can influence the membrane rejection performance because it modifies the membrane surface's ability to undergo interaction due to the dissociation of functional groups [24]. The M0.5 membrane was exposed to MB (20 ppm) in the pH range of 3–11. Figure 5.8(a) presents the rejection % of MB at different pH levels. The surface charge of the membrane consistently responds to the pH of the feed solution, which affects the rejection % of MB at different pH levels. The M0.5 membrane achieved higher rejection at alkaline pH levels by incorporating MIL-100 (Fe), tuning the membrane surface charge with positively charged functional groups and hydration layer formation towards rejecting the cationic MB dye [39]. Figure 5.9 presents the UV-vis absorption spectra and images of the feed and permeate MB solution at different pH levels.

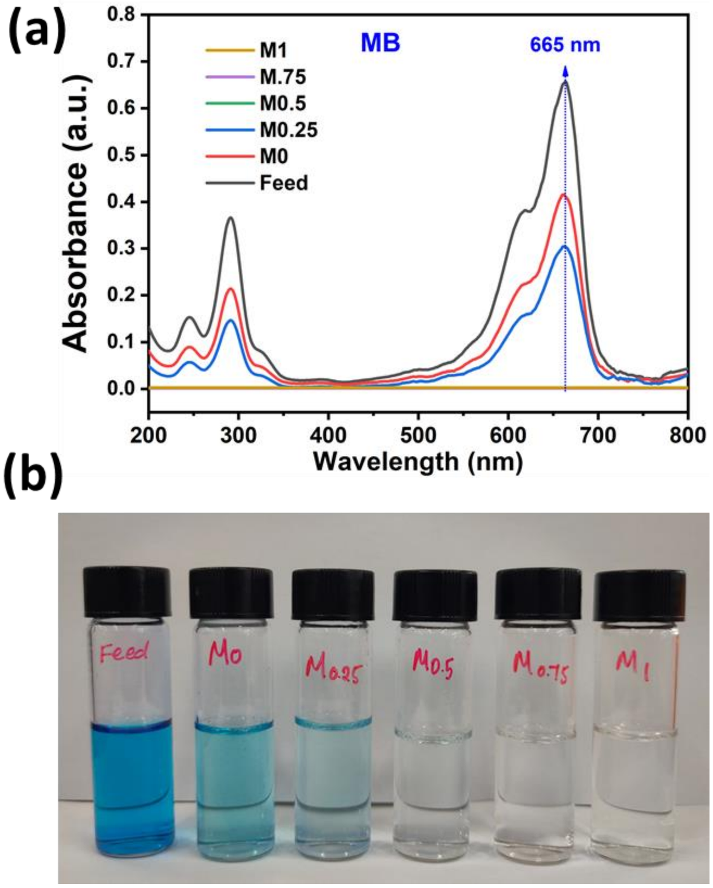

Figure 5.7 UV-vis absorption spectra (a), visual images of feed, and permeate MB solutions (b).

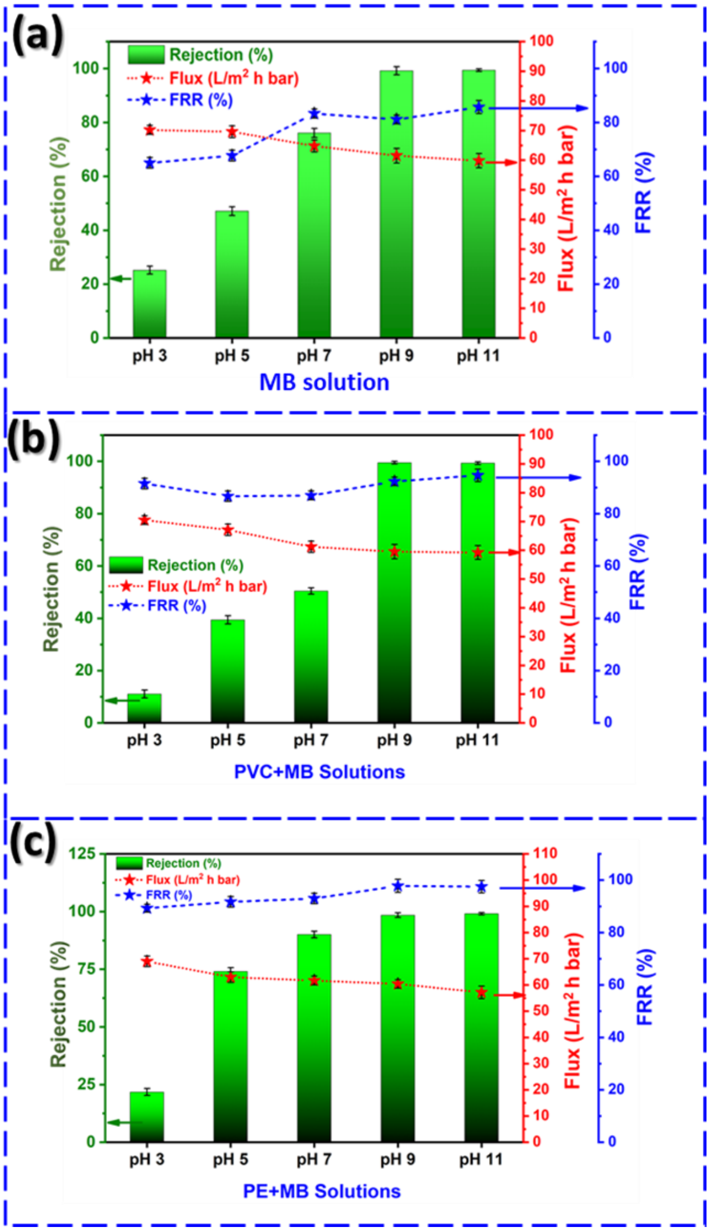

Figure 5.8 Rejection performance at various pH: (a) rejection (%), flux and FRR % of MB solution; (b) MB rejection (%), flux, and FRR % of PVC+MB solution; (c) MB rejection (%), flux, and FRR % of PE+MB solution.

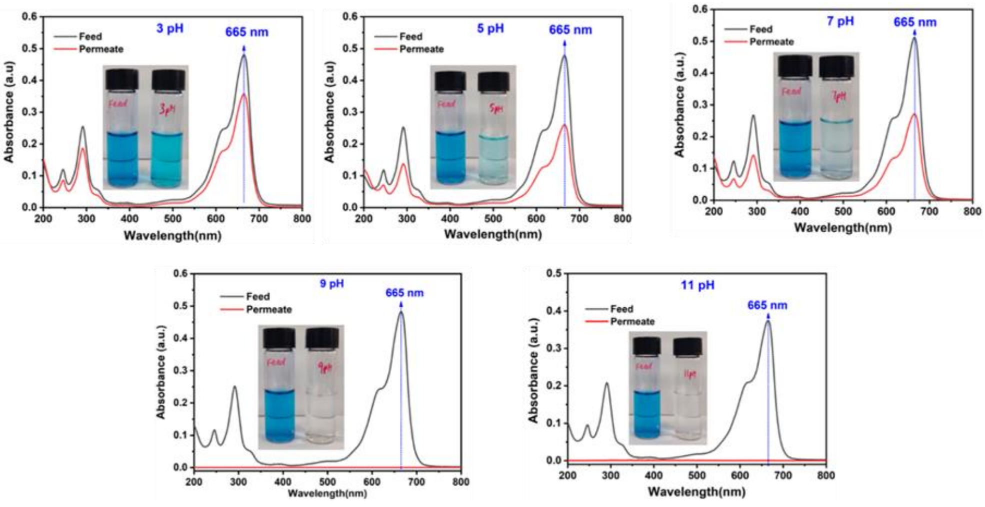

Figure 5.9 UV-vis absorption spectra and images of feed and permeate solutions of MB at various pH.

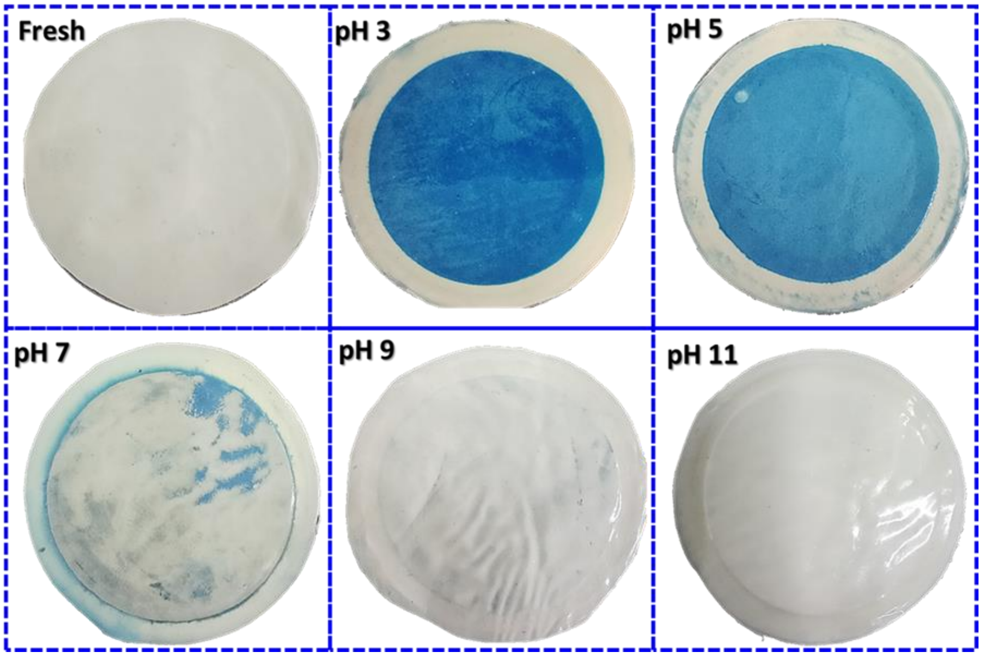
Fresh
pH 3
pH 5
pH 7
pH 9
pH 11

Figure 5.10 Image of untreated and treated membranes at various pH.

Figure 5.10 shows the fresh and treated membrane images with various pH of feed solution. The UV-vis spectra revealed that the permeate intensity decreased and that the extent to which the color disappeared from the permeate solution changed as the pH varies. At higher pH (> pH 9), MB rejection was higher, as confirmed by the diminishing intensity of the peak on the UV-vis spectra and the complete disappearance of color (i.e., the complete removal of MB) from the permeate solutions at pH 9 and 11. At alkaline pH (9 and 11), the MB adsorbed on the membrane surface entirely diminished due to the hydration layer formation on the membrane surface by hydrophilic MIL-100 (Fe) incorporation inhibits the complete interaction between MB dye and the PSF/MIL-100 (Fe) membrane surface [37].

5.5.8.1.2 Rejection of MPs adsorbing MB

To investigate the PSF/MIL-100 (Fe) membrane separation performance of mixed feed solutions of dye and microplastics at different pH. First, the feed solution, including various pH of MB (20 ppm) and MPs (1 g/L), was used for the filtration experiment; pH is an essential parameter for membrane separation. In Figure 5.8(b)-(c), as expected at alkaline pH (> pH 9), the M0.5 membrane attained higher rejection of MB (>99%) than acidic and neutral pH. The incorporation of hydrophilic MIL-100 (Fe) provides additional water molecules pathways and hydration layer formation on the membrane, which offers the higher flux and FRR%. The MIL-100 (Fe) incorporated PSF membrane at alkaline pH highly resists the MB dye and MPs permeation, impacting gradual flux decline than acidic pH. Figure 5.11 displays the feed, permeate, and retentate spectra of MB and MPs solutions at alkaline pH (9 and 11). At alkaline pH, the MB solution retentate intensity increased to 21.1% for 11 pH and 3.7% for 9 pH from feed solution intensity, owing to the higher rejection properties of the M0.5 membrane. However, the retentate intensity decreased (PVC+MB (25.1%) and PE+MB (17.4%)) with a complete decline (nearly zero) of permeate intensity when used mixed MB and MPs solution.

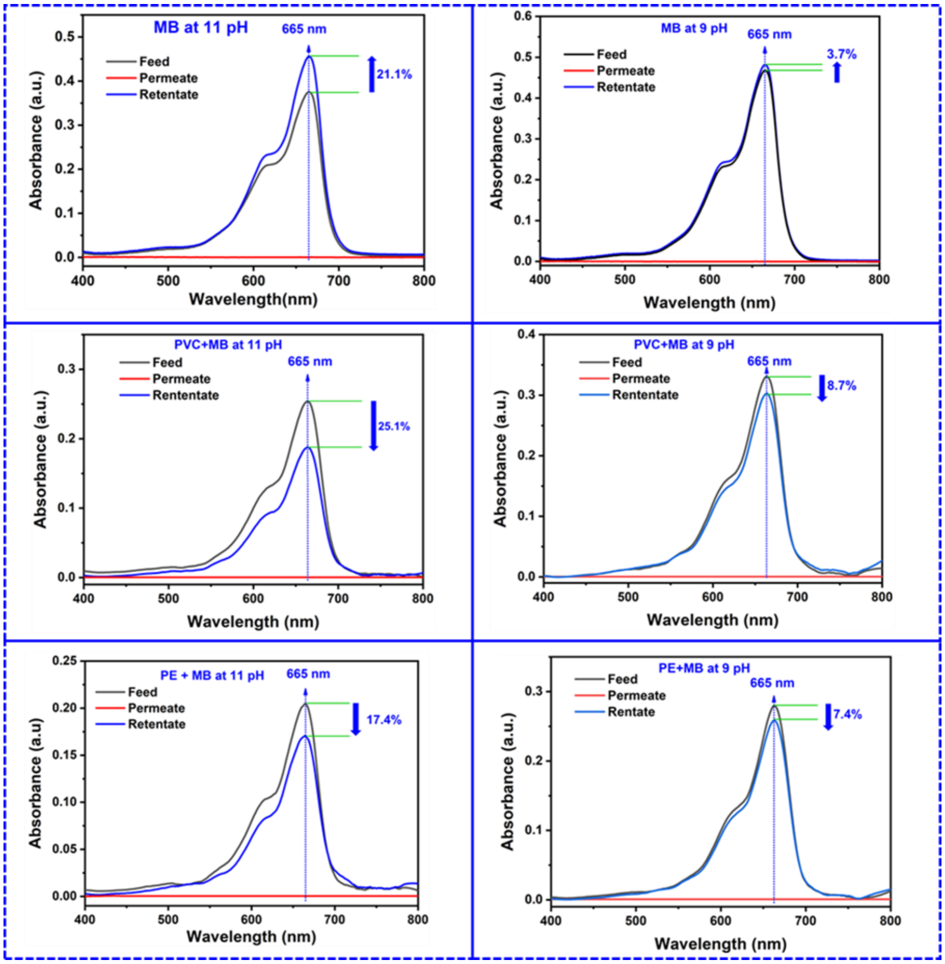

Figure 5.11 UV-vis absorption spectra of feed, permeate, and retentate solutions at alkaline pH (9 and 11).

Its attained due to the strong electrostatic interaction between MB dye and microplastics and the high rejection performance of the M0.5 membrane surface by electrostatic repulsion. The reduced intensity (%) is higher for PVC+MB than PE+MB due to dominant physical adsorption between cationic MB and PVC MPs at alkaline pH [26]. The permeate intensity was almost equivalent to pure water, which indicates the PSF/MIL-100 (Fe) membrane effectively rejects the MPs adsorbed MB dye contaminants. The size of the MPs is larger (length of PVC (110 ± 27 µm and PE (22 ± 30 µm) and width of PVC (88 ± 21 µm and PE (15 ± 11 µm) [27]) than the prepared membrane pore size, which influences the physical sieving and size exclusion mechanism toward the rejection of MPs. Figure 5.12 and Figure 5.13 represent the feed, permeate, and retentate spectra of MB and MPs solutions at neutral and acidic pH.

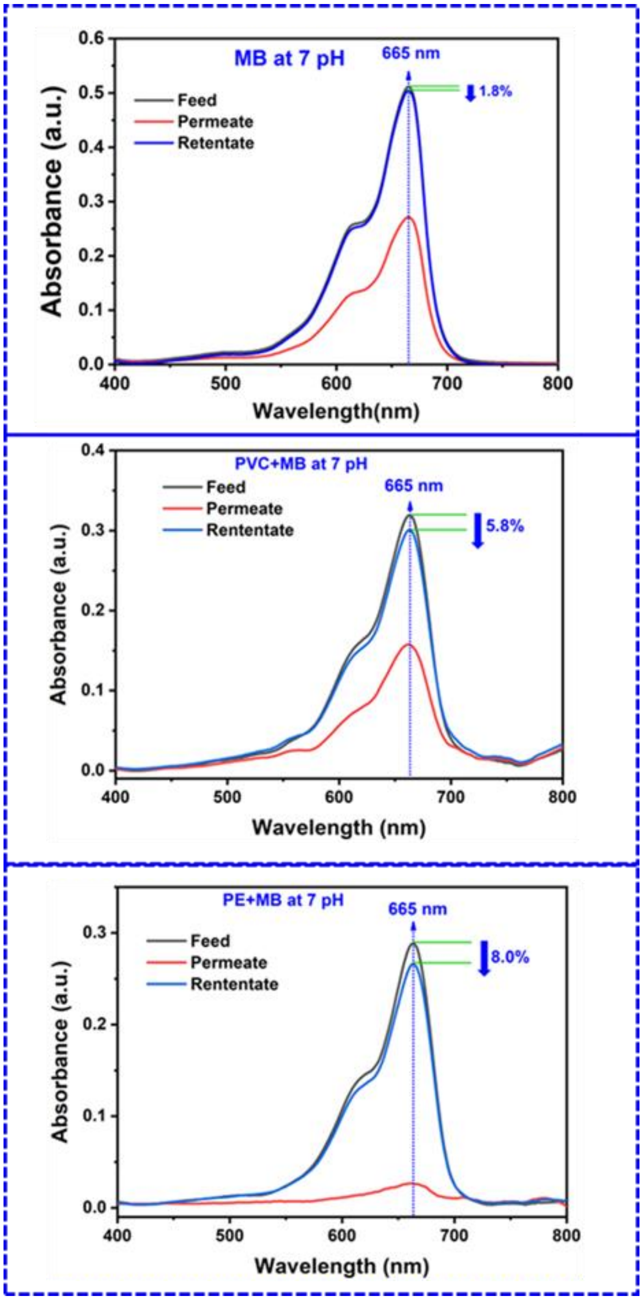

Figure 5.12 UV-vis absorption spectra of feed, permeate, and retentate solutions at neutral pH (7).

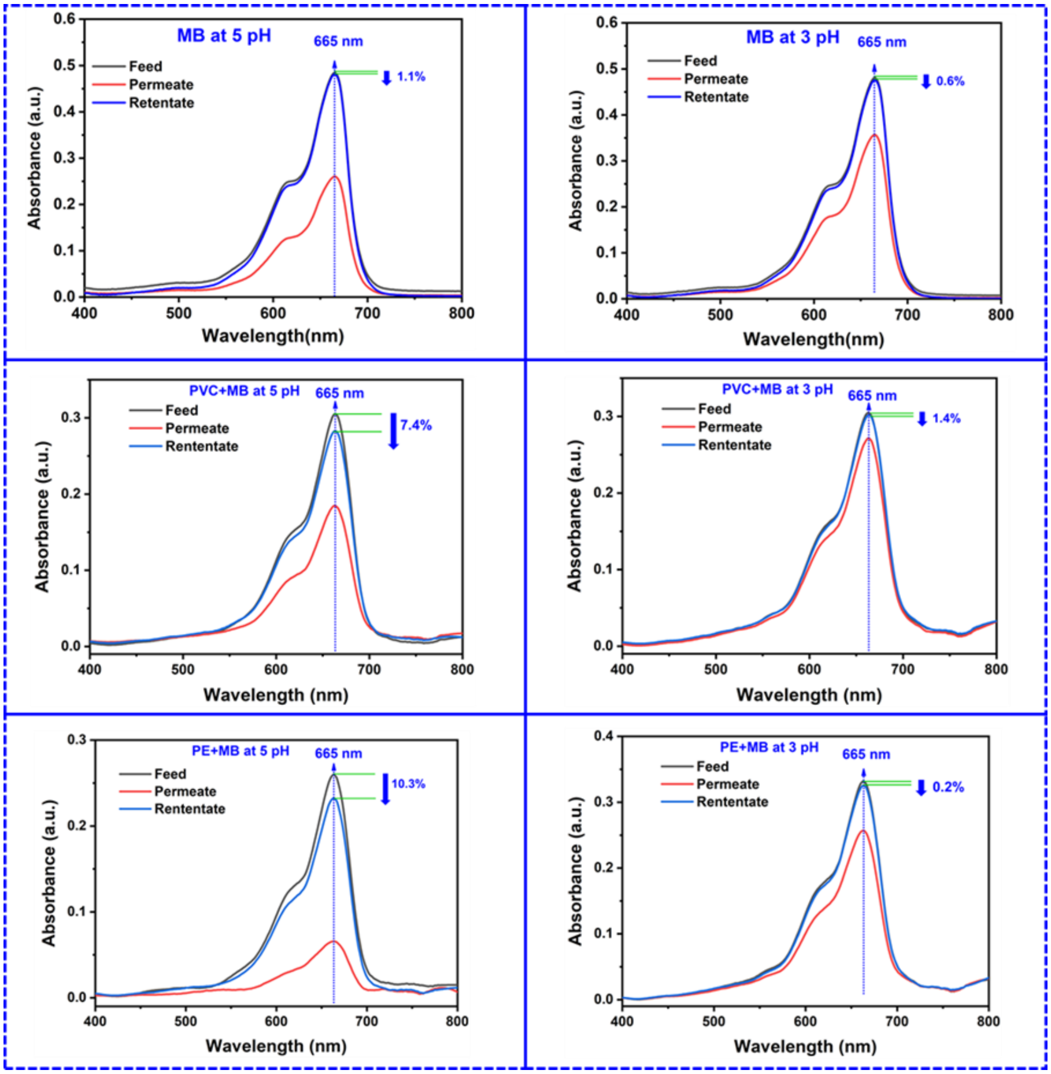

Figure 5.13 UV-vis absorption spectra of feed, permeate, and retentate solutions at acidic pH (3 and 5).

5.5.8.2 Effect of concentration on membrane performances

5.5.8.2.1 MB rejection

The impact of the dye concentration of the MB solution on the M0.5 membrane is shown in Figure 5.14(a). The figure shows that as the feed solution's concentration increased from 10 ppm to 100 ppm, it influences the moderate MB dye's flux decline. However, the rejection % of the M0.5

.

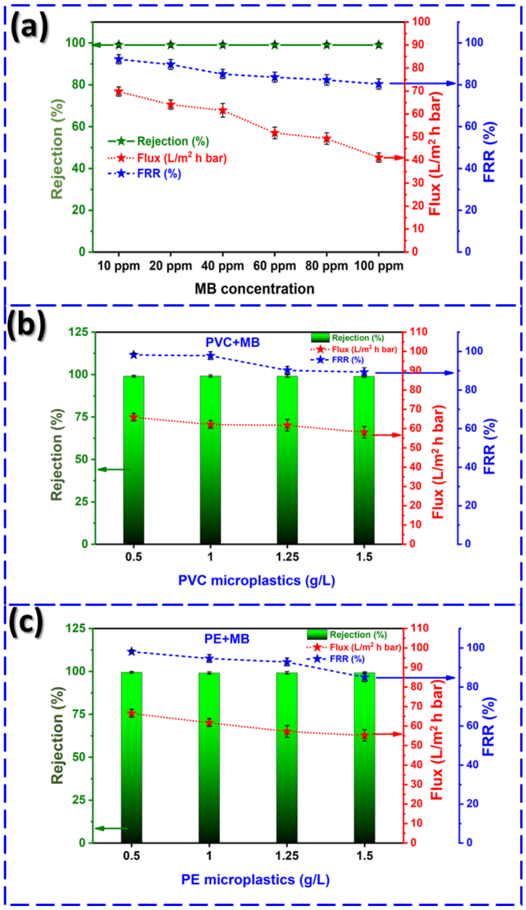

Figure 5.14 Rejection performance at various concentration: (a) rejection (%), flux and FRR % of MB solution; (b) MB rejection (%), flux, and FRR % of PVC+MB solution; (c) MB rejection (%), flux, and FRR % of PE+MB solution.

Membrane was sustained at more than 99.0%. The FRR % was maintained at more than 80%, indicating the enhanced anti-fouling properties of the M0.5 membrane. This outstanding anti-fouling performance of the M0.5 membrane could be credited to enhancing the hydrophilicity and the strong bonding between the organic ligand and the carboxylic groups of MIL-100 (Fe) and the PSF matrix.

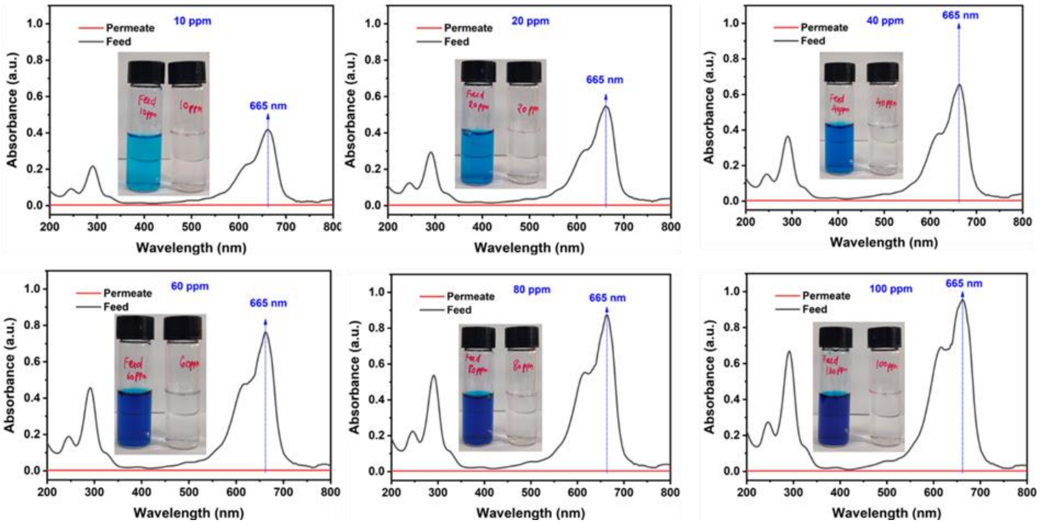

Figure 5.15 UV-vis absorption spectra and visual images of feed and permeate solutions of MB at various concentrations.

As shown in Figure 5.15, the MB feed solutions at various feed concentrations (10–100 ppm) turned clear after permeation through the PSF/MIL-100 (Fe) (M0.5) membrane, demonstrating nearly complete MB rejection. The characteristic peaks associated with the MB dye molecule disappeared and were replaced by peaks similar to those on the UV-vis absorption spectrum of pure water.

5.5.8.2.2 Rejection of MPs adsorbing MB

The separation performance of the M0.5 membrane was examined at various concentrations of MPs (0.5, 1, 1.25, and 1g/L) and MB (20 ppm) solutions at 11 pH. The increasing concentration of MPs from 0.5 to 1 g/L improved the driving force of MB adsorption. Figure 5.16 and 17 display the higher reduction of the retentate intensity of PVC+MB (23.8 to 25.1%) and PE+MB (10.7 to 17.4%). In Figure 5.14((b)-(c)), the experiment results show that the M0.5 membrane exhibits outstanding rejection % of MB (>99%) for all different feed concentrations. Flux decline attained gradually with increasing concentration of feed solution.

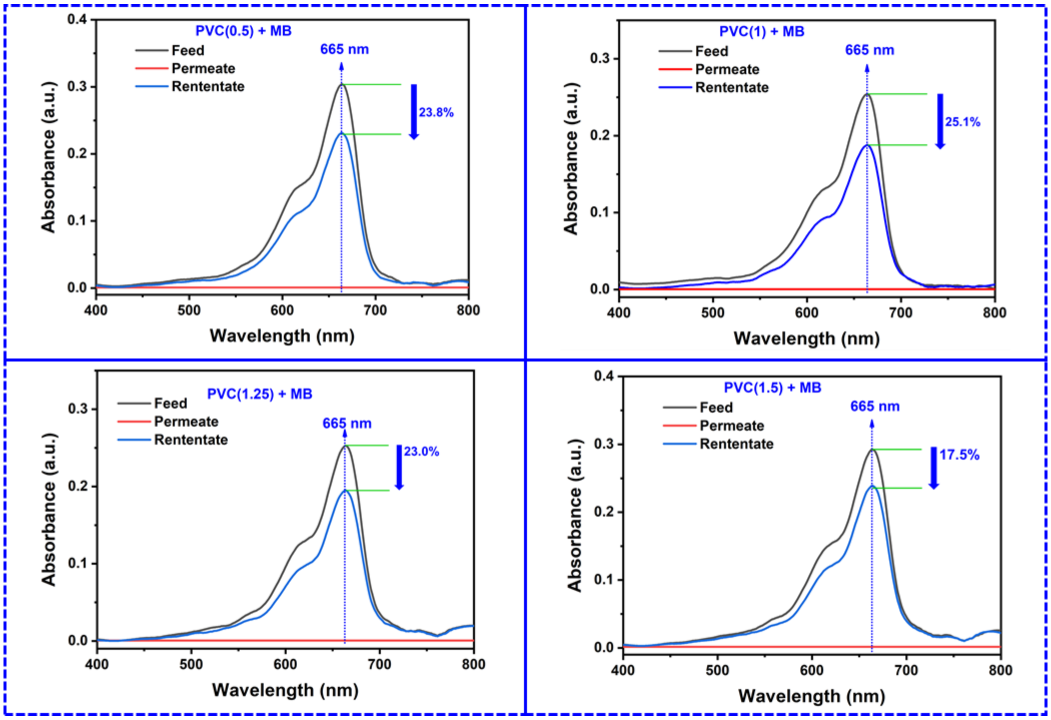

Figure 5.16 UV-vis absorption spectra of feed, permeate, and retentate solutions with MB solution at various PVC concentrations (0.5, 1, 1.25, and 1.5 g/L).

The FRR% was sustained at a higher level for PVC+MB at 0.5 to 1 g/L; then, it decreased for 1.25 to 1.5 g/L of PVC MPs. It was achieved due to the intense physical attraction between PVC MPs and MB and higher rejection properties of the PSF/MIL-100 (Fe) membrane at alkaline pH. The FRR% was gradually decreased for PE+MB but sustained more than 80%. The optimum concentration (1 g/L) of MPs favors high adsorption of MB compare to others. Figure 5.16 and 17 display the lowed reduction of retentate intensity when the feed solution consists of more the 1 g/L of MPs due to MPs' limitation of adsorption capacity. Electrostatic repulsion and size exclusion influence the higher rejection of MB and MPs.

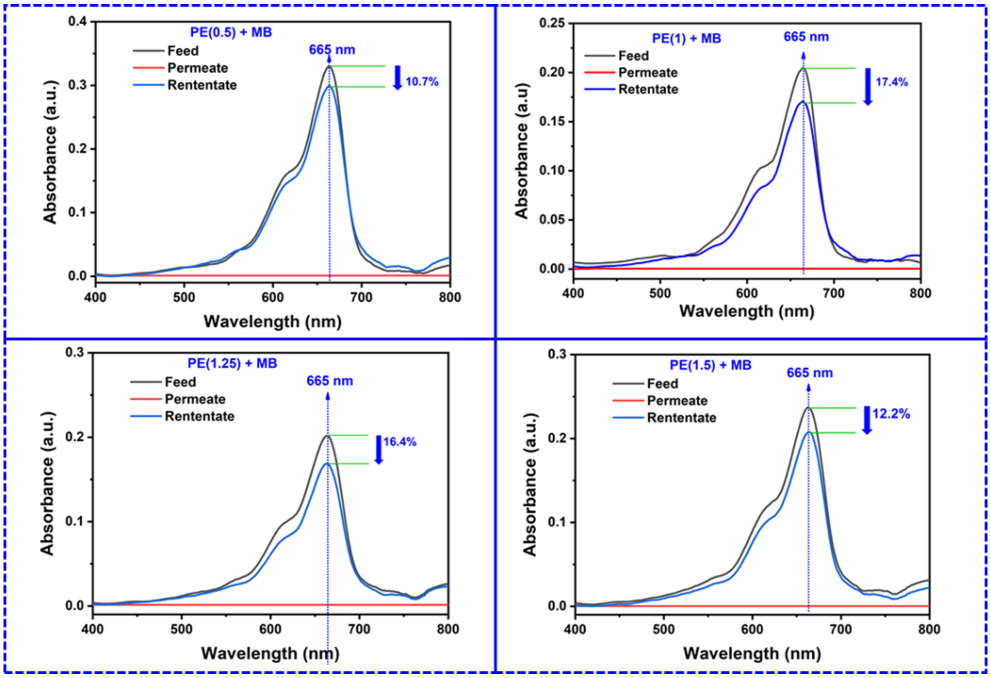

Figure 5.17 UV-vis absorption spectra of feed, permeate, and retentate solutions with MB solution at various PE concentrations (0.5, 1, 1.25, and 1.5 g/L).

5.5.8.3 Effect of pressure on the membrane

Figure 5.18(a) shows the PWF of the M0.5 membrane for various levels of the transmembrane pressure (TMP). As predicted, the PWF of the membranes increased with increasing TMP. The MB rejection performance of the M0.5 membrane was assessed by varying the TMP from 2 to 10 bar, as shown in Figure 5.18(b). The MB dye concentration and pH of the feed solution were fixed at 20 ppm and pH 9, respectively. The changes in the MB rejection % were insignificant. The M0.5 membrane attained a rejection rate of more than 98% at different TMPs. Figure 5.19(a) shows the equivalent UV-vis spectra of the feed and permeate solutions of the MB dye and indicates that dye removal was nearly complete.

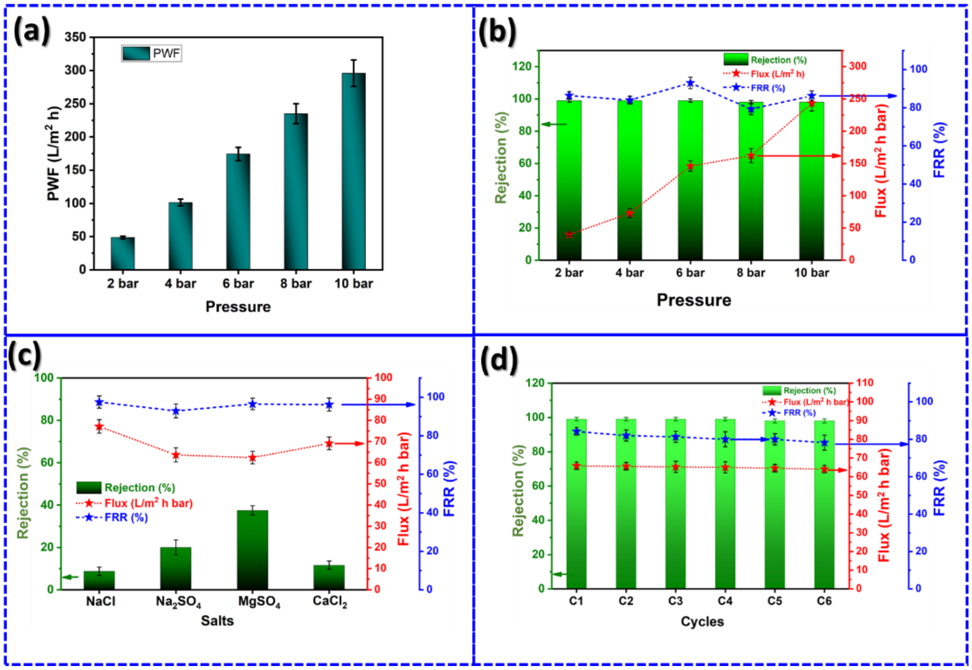

Figure 5.18 Membrane performance: (a) PWF at various TMPs, (b) MB rejection (%), flux, and FRR % at various TMPs, (c) rejection (%), flux, and FRR % of various salts solution, (d) reusability performance of the membrane.

At the same time, the optical images of the MB dye solutions before and after filtration also provided evidence of the effective MB separation efficiency of the PSF/MIL-100 (Fe) membrane (Figure 5.19(b)). The permeate flux increased from 40 to 243.3 L/m^2 h with increasing TMP. The anti-fouling performance of the M0.5 membrane was sustained by achieving an FRR% of more than 80% [24].

5.5.9 Salt rejection of membranes

The MIL-100 (Fe) loading ability to enhance the salt rejection performance was verified by examining the M0.5 membrane performance using solutions of NaCl, Na_2SO_4, $CaCl_2$, and $MgSO_4$ (1000 ppm). Figure 5.18(c) shows the salt separation performance of the membrane. $MgSO_4$ and Na_2SO_4 were rejected to a greater extent than $CaCl_2$ and NaCl, causing the Donnan effect's mechanism of size sieving and the Donnan effect. The repulsion of the divalent ions by the negatively charged PSF/MIL-100 (Fe) membrane is more potent than that of the monovalent ions. The hydrated diameter of SO_4^{2-} (0.76 nm) is more significant than Cl^-(0.66 nm). The rejection rate of $MgSO_4$ was higher than that of Na_2SO_4 because of the dominant impact of the size sieving mechanism. The hydrated diameter of Mg^{2+}(0.86 nm) is more significant than that of Na^+(0.72 nm) [40]. The existence of well-organized sub-nanometer pores in hydrophilic MIL-100 (Fe) may also act as a water transport medium to facilitate high water permeability while restricting the permeation of the charged hydrated salt ions. The permeation of NaCl is higher than that of the other salts because the size exclusion mechanism ensures that hydrated monovalent ions such as Na^+ and Cl^- are more easily transported through the sub-nanometer-sized pores of the MIL-100 (Fe) nanoparticles than divalent ions [41]. The FRR% of all the salts exceeded 97%, which indicates that forming a hydrophilic thin layer by incorporating hydrophilic MIL-100 (Fe) enhances the permeability, fouling resistance, and salt rejection in composite PSF/MIL-100 (Fe) membranes.

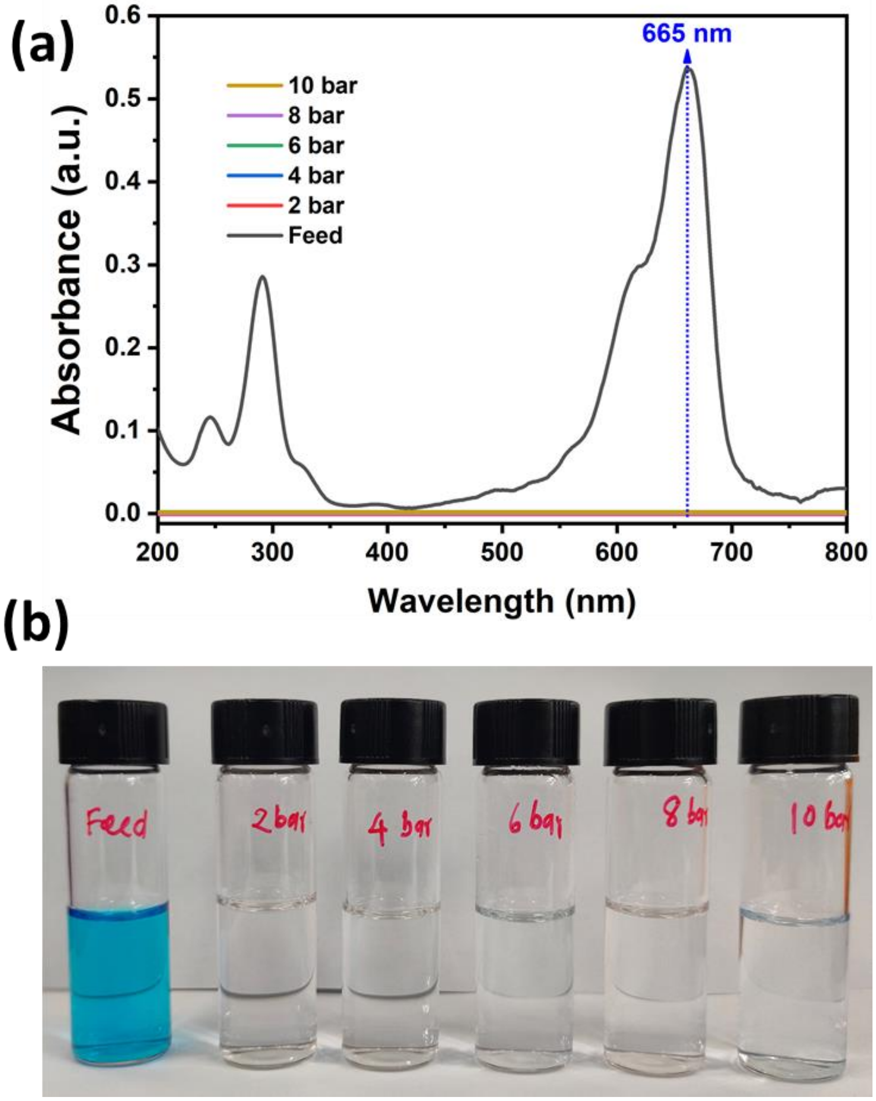

Figure 5.19 UV-vis absorption spectra (a), visual images of feed and permeate of MB solutions for M0.5 membrane at various TMP (b).

5.5.10 Cycling performance

The ability to repeatedly use and reuse the PSF/MIL-100 (Fe) is of the utmost importance to determine the membrane stability for actual wastewater treatment. Figure 5.18(d) represents the MB separation performance of the M0.5 membrane after 1–6 cycles. The MB flux and FRR % were slightly decreased, but the rejection % was sustained at more than 98%. Organic ligands in the MIL-100 (Fe) can strengthen the compatibility between the PSF matrix and MIL-100 (Fe) nanoparticles, enabling highly stable membranes to be developed. The M0.5 membrane rejection performance during continuous cycling was investigated by comparing the UV-vis absorption spectra of the feed and permeate solutions of MB. The absorbance intensity of the permeate solutions completely diminished and resembled the UV-vis absorption spectra of pure water Figure 5.20(a). Furthermore, this result confirms the high separation efficiency of the M0.5 membrane for MB dye rejection. As shown in Figure 5.20(b), the clear permeate solution after six continuous cycles provides evidence for the high MB dye rejection stability of the M0.5 membrane. The obtained outcomes imply that the PSF/MIL-100 (Fe) composite membrane has outstanding cycling ability.

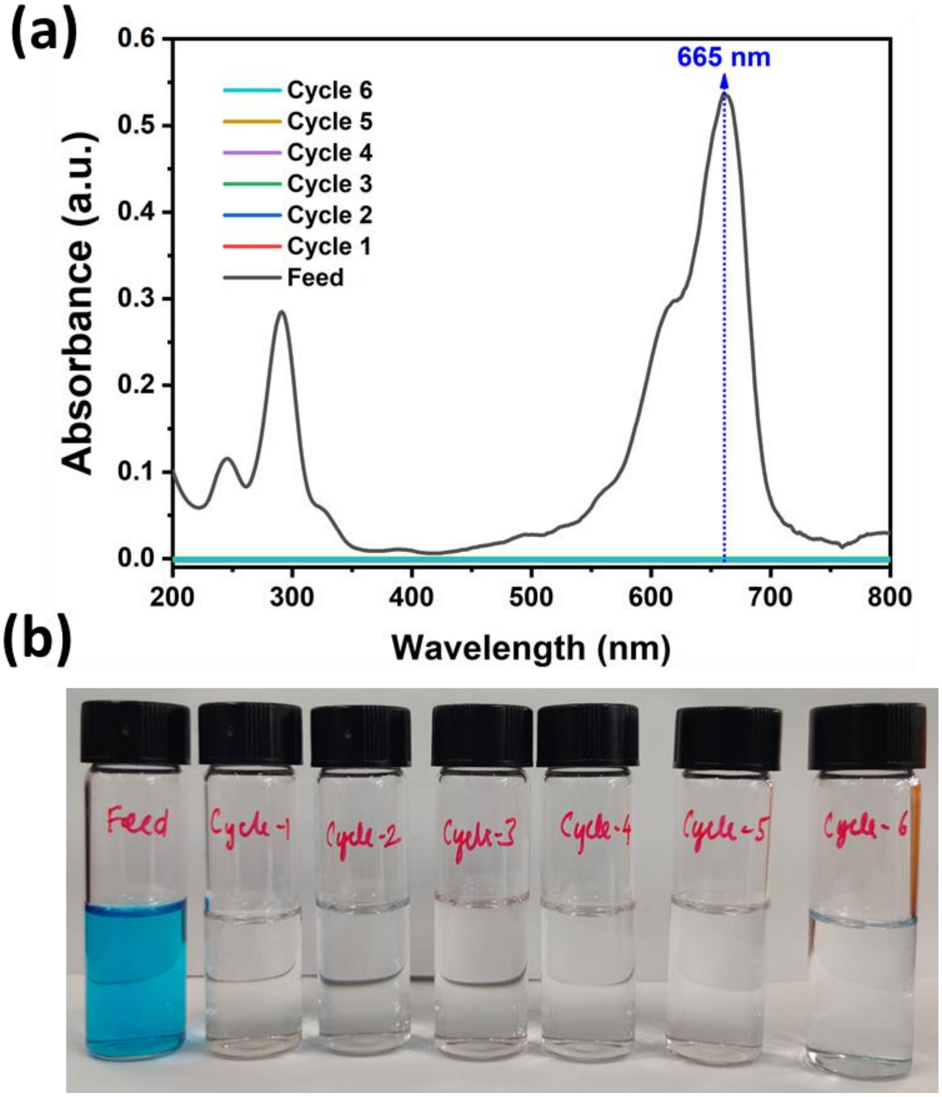

Figure 5.20 UV-vis absorption spectra (a), visual images of feed and permeate of MB solutions for reusability of 1-6 cycles of M0.5 membrane (b).

5.6 Conclusions

In this research work, we fabricated a novel composite membrane composed of hydrophilic MIL-100 (Fe) in a polysulfone matrix for the excellent removal of hazardous MPs adsorbed dye contaminants from textile wastewater. The prepared membranes were characterized by XRD, cross-sectional morphology, contact angle, wettability, work of adhesion, porosity, pore size, and pure water flux measurements. The membrane that contained an optimal amount of hydrophilic MIL-100 (Fe) in the PSF matrix (0.5 wt%, the M0.5 membrane) offered high MB rejection, superior permeability, enhanced pore size, and delivered high anti-fouling performance. Moreover, the performance of the M0.5 membrane was outstanding for various dye and MPs concentrations and TMPs. In addition, the M0.5 membrane delivered good salt rejection performance and could be reused for six cycles of MB dye rejection. Incorporating hydrophilic MIL-100 (Fe) enhanced the PSF matrix's performance towards removing the MB dye, MPs, and salts from the textile wastewater based on size exclusion, the steric and Donnan effect, electrostatic interaction, and repulsion mechanism. These results confirm that the PSF/MIL-100 (Fe) membrane is potentially suitable for treating real textile wastewater.

5.7 References

[1] M.C.M. van Loosdrecht, D. Brdjanovic, Anticipating the next century of wastewater treatment, Science (80-.). 344 (2014) 1452–1453. https://doi.org/10.1126/science.1255183.

[2] H. Deng, R. Wei, W. Luo, L. Hu, B. Li, Y. Di, H. Shi, Microplastic pollution in water and sediment in a textile industrial area, Environ. Pollut. 258 (2020) 113658. https://doi.org/10.1016/j.envpol.2019.113658.

[3] H. Hidayaturrahman, T. Lee, A study on characteristics of microplastic in wastewater of South Korea: Identification, quantification, and fate of microplastics during treatment process, Mar. Pollut. Bull. 146 (2019) 696–702. https://doi.org/10.1016/j.marpolbul.2019.05.071.

[4] X.L. Cao, Y.N. Yan, F.Y. Zhou, S.P. Sun, Tailoring nanofiltration membranes for effective removing dye intermediates in complex dye-wastewater, J. Memb. Sci. 595 (2020) 117475. https://doi.org/10.1016/j.memsci.2019.117475.

[5] Y.-F. Mi, G. Xu, Y.-S. Guo, B. Wu, Q.-F. An, Development of antifouling nanofiltration membrane with zwitterionic functionalized monomer for efficient dye/salt selective separation, J. Memb. Sci. 601 (2020) 117795. https://doi.org/10.1016/j.memsci.2019.117795.

[6] G. Gnanaselvan, B. Sasikumar, G. Arthanareeswaran, Y.S. Mok, Performance of composite PES/MOF-5 membranes for the treatment of textile wastewater, Desalin. WATER Treat. 156 (2019) 220–228.

https://doi.org/10.5004/dwt.2019.23777.

[7] P. Zhao, R. Li, W. Wu, J. Wang, J. Liu, Y. Zhang, In-situ growth of polyvinylpyrrolidone modified Zr-MOFs thin-film nanocomposite (TFN) for efficient dyes removal, Compos. Part B Eng. 176 (2019) 107208. https://doi.org/10.1016/j.compositesb.2019.107208.

[8] S. Zhou, X. Feng, J. Zhu, Q. Song, G. Yang, Y. Zhang, B. Van der Bruggen, Self-cleaning loose nanofiltration membranes enabled by photocatalytic Cu-triazolate MOFs for dye/salt separation, J. Memb. Sci. 623 (2021) 119058. https://doi.org/10.1016/j.memsci.2021.119058.

[9] Y. Liu, M. Zhu, M. Chen, L. Ma, B. Yang, L. Li, W. Tu, A polydopamine-modified reduced graphene oxide (RGO)/MOFs nanocomposite with fast rejection capacity for organic dye, Chem. Eng. J. 359 (2019) 47–57. https://doi.org/10.1016/j.cej.2018.11.105.

[10] Y. Liu, D. Gan, M. Chen, L. Ma, B. Yang, L. Li, M. Zhu, W. Tu, Bioinspired dopamine modulating graphene oxide nanocomposite membrane interposed by super-hydrophilic UiO-66 with enhanced water permeability, Sep. Purif. Technol. 253 (2020) 117552. https://doi.org/10.1016/j.seppur.2020.117552.

[11] Q. Long, Z. Zhang, G. Qi, Z. Wang, Y. Chen, Z.-Q. Liu, Fabrication of Chitosan Nanofiltration Membranes by the Film Casting Strategy for Effective Removal of Dyes/Salts in Textile Wastewater, ACS Sustain. Chem. Eng. 8 (2020) 2512–2522. https://doi.org/10.1021/acssuschemeng.9b07025.

[12] J. Hu, M. Li, L. Wang, X. Zhang, Polymer brush-modified graphene oxide membrane with excellent structural stability for effective fractionation of textile wastewater, J. Memb. Sci. 618 (2021) 118698. https://doi.org/10.1016/j.memsci.2020.118698.

[13] H.Z. Zhang, J.Y. Sun, Z.L. Zhang, Z.L. Xu, Hybridly charged NF membranes with MOF incorporated for removing low-concentration surfactants, Sep. Purif. Technol. 258 (2021) 118069. https://doi.org/10.1016/j.seppur.2020.118069.

[14] Z. Rahimi, A.A. Zinatizadeh, S. Zinadini, M. van Loosdrecht, A hydrophilic and antifouling nanofiltration membrane modified by citric acid functionalized tannic acid (CA-f-TA) nanocomposite for dye removal from biologically treated baker’s yeast wastewater, J. Environ. Chem. Eng. 9 (2021) 104963. https://doi.org/10.1016/j.jece.2020.104963.

[15] S.R. Mousavi, M. Asghari, N.M. Mahmoodi, Chitosan-wrapped multiwalled carbon nanotube as filler within PEBA thin film nanocomposite (TFN) membrane to improve dye removal, Carbohydr. Polym. 237 (2020) 116128. https://doi.org/10.1016/j.carbpol.2020.116128.

[16] B. Sasikumar, S. Bisht, G. Arthanareeswaran, A.F. Ismail, M.H.D. Othman, Performance of polysulfone hollow fiber membranes encompassing ZIF-8, SiO2/ZIF-8, and amine-modified SiO2/ZIF-8 nanofillers for CO2/CH4 and CO2/N2 gas separation, Sep. Purif. Technol. 264 (2021) 118471. https://doi.org/10.1016/j.seppur.2021.118471.

[17] Y.Y. Zhao, Y.L. Liu, X.M. Wang, X. Huang, Y.F. Xie, Impacts of Metal-Organic Frameworks on Structure and Performance of Polyamide Thin-Film Nanocomposite Membranes, ACS Appl. Mater. Interfaces. 11 (2019) 13724–13734. https://doi.org/10.1021/acsami.9b01923.

[18] W. Wu, M. Jia, J. Su, Z. Li, W. Li, Air–water interfacial synthesis of metal–organic framework hollow fiber membranes for water purification, AIChE J. 66 (2020). https://doi.org/10.1002/aic.16238.

[19] Y. Lukka Thuyavan, G. Arthanareeswaran, A.F. Ismail, P.S. Goh, M. V. Shankar, B.C. Ng, R. Sathish Kumar, K. Venkatesh, Binary metal oxides incorporated polyethersulfone ultrafiltration mixed matrix membranes for the pretreatment of seawater desalination, J. Appl. Polym. Sci. 138 (2021) 49883. https://doi.org/10.1002/app.49883.

[20] A. Nasir, F. Masood, T. Yasin, A. Hameed, Progress in polymeric nanocomposite membranes for wastewater treatment: Preparation, properties and applications, J. Ind. Eng. Chem. 79 (2019) 29–40. https://doi.org/10.1016/j.jiec.2019.05.052.

[21] Y. Zhang, S. Wei, Y. Hu, S. Sun, Membrane technology in wastewater treatment enhanced by functional nanomaterials, J. Clean. Prod. 197 (2018) 339–348. https://doi.org/10.1016/j.jclepro.2018.05.211.

[22] F. Yang, H. Sadam, Y. Zhang, J. Xia, X. Yang, J. Long, S. Li, L. Shao, A de novo sacrificial-MOF strategy to construct enhanced-flux nanofiltration membranes for efficient dye removal, Chem. Eng. Sci. 225 (2020) 115845.

https://doi.org/10.1016/j.ces.2020.115845.

[23] Y. Meng, L. Shu, L. Liu, Y. Wu, L.-H. Xie, M.-J. Zhao, J.-R. Li, A high-flux mixed matrix nanofiltration membrane with highly water-dispersible MOF crystallites as filler, J. Memb. Sci. 591 (2019) 117360. https://doi.org/10.1016/j.memsci.2019.117360.

[24] M.M. Baneshi, A.M. Ghaedi, A. Vafaei, D. Emadzadeh, W.J. Lau, H. Marioryad, A. Jamshidi, A high-flux P84 polyimide mixed matrix membranes incorporated with cadmium-based metal organic frameworks for enhanced simultaneous dyes removal: Response surface methodology, Environ. Res. 183 (2020) 109278. https://doi.org/10.1016/j.envres.2020.109278.

[25] Z.J. Parkerson, T. Le, P. Das, S.N. Mahmoodi, M.R. Esfahani, Cu-MOF-Polydopamine-Incorporated Functionalized Nanofiltration Membranes for Water Treatment: Effect of Surficial Adhesive Modification Techniques, ACS ES&T Water. (2020) acsestwater.0c00173. https://doi.org/10.1021/acsestwater.0c00173.

[26] Y. Xia, J.-J. Zhou, Y.-Y. Gong, Z.-J. Li, E.Y. Zeng, Strong influence of surfactants on virgin hydrophobic microplastics adsorbing ionic organic pollutants, Environ. Pollut. 265 (2020) 115061. https://doi.org/10.1016/j.envpol.2020.115061.

[27] J. Stanković, D. Milošević, D. Savić-Zdraković, G. Yalçın, D. Yildiz, M. Beklioğlu, B. Jovanović, Exposure to a microplastic mixture is altering the life traits and is causing deformities in the non-biting midge Chironomus riparius

Meigen (1804), Environ. Pollut. 262 (2020) 114248. https://doi.org/10.1016/j.envpol.2020.114248.

[28] K. Guesh, C.A.D. Caiuby, Á. Mayoral, M. Díaz-García, I. Díaz, M. Sanchez-Sanchez, Sustainable Preparation of MIL-100(Fe) and Its Photocatalytic Behavior in the Degradation of Methyl Orange in Water, Cryst. Growth Des. 17 (2017) 1806–1813. https://doi.org/10.1021/acs.cgd.6b01775.

[29] G. Gnanasekaran, S. Balaguru, G. Arthanareeswaran, D.B. Das, Removal of hazardous material from wastewater by using metal organic framework (MOF) embedded polymeric membranes, Sep. Sci. Technol. 54 (2019) 434–445. https://doi.org/10.1080/01496395.2018.1508232.

[30] P.F. Andrade, A.F. de Faria, S.R. Oliveira, M.A.Z. Arruda, M. do C. Gonçalves, Improved antibacterial activity of nanofiltration polysulfone membranes modified with silver nanoparticles, Water Res. 81 (2015) 333–342. https://doi.org/10.1016/j.watres.2015.05.005.

[31] D. Cheng, L. Zhao, N. Li, S.J.D. Smith, D. Wu, J. Zhang, D. Ng, C. Wu, M.R. Martinez, M.P. Batten, Z. Xie, Aluminum fumarate MOF/PVDF hollow fiber membrane for enhancement of water flux and thermal efficiency in direct contact membrane distillation, J. Memb. Sci. 588 (2019). https://doi.org/10.1016/j.memsci.2019.117204.

[32] A. Zirehpour, A. Rahimpour, S. Khoshhal, M.D. Firouzjaei, A.A. Ghoreyshi, The impact of MOF feasibility to improve the desalination performance and

antifouling properties of FO membranes, RSC Adv. 6 (2016) 70174–70185. https://doi.org/10.1039/c6ra14591d.

[33] Y. Kang, M. Obaid, J. Jang, M.-H. Ham, I.S. Kim, Novel sulfonated graphene oxide incorporated polysulfone nanocomposite membranes for enhanced-performance in ultrafiltration process, Chemosphere. 207 (2018) 581–589. https://doi.org/10.1016/j.chemosphere.2018.05.141.

[34] S. Abdi, M. Nasiri, Enhanced Hydrophilicity and Water Flux of Poly(ether sulfone) Membranes in the Presence of Aluminum Fumarate Metal-Organic Framework Nanoparticles: Preparation and Characterization, ACS Appl. Mater. Interfaces. 11 (2019) 15060–15070. https://doi.org/10.1021/acsami.9b01848.

[35] T.A. Makhetha, R.M. Moutloali, Antifouling properties of Cu(tpa)@GO/PES composite membranes and selective dye rejection, J. Memb. Sci. 554 (2018) 195–210. https://doi.org/10.1016/j.memsci.2018.03.003.

[36] F. Mohammadnezhad, M. Feyzi, S. Zinadini, A novel Ce-MOF/PES mixed matrix membrane; synthesis, characterization and antifouling evaluation, J. Ind. Eng. Chem. 71 (2019) 99–111. https://doi.org/10.1016/j.jiec.2018.09.032.

[37] J. Cao, Y. Su, Y. Liu, J. Guan, M. He, R. Zhang, Z. Jiang, Self-assembled MOF membranes with underwater superoleophobicity for oil/water separation, J. Memb. Sci. 566 (2018) 268–277. https://doi.org/10.1016/j.memsci.2018.08.068.

[38] J.S. Beril Melbiah, N.J. Kaleekkal, D. Nithya Rabekkal, D. Rana, A. Nagendran, D. Mohan, Improved permeation, separation and antifouling performance of

customized polyacrylonitrile ultrafiltration membranes, Chem. Eng. Res. Des. 159 (2020) 157–169. https://doi.org/10.1016/j.cherd.2020.04.014.

[39] R. Dai, X. Wang, C.Y. Tang, Z. Wang, Dually Charged MOF-Based Thin-Film Nanocomposite Nanofiltration Membrane for Enhanced Removal of Charged Pharmaceutically Active Compounds, Environ. Sci. Technol. 54 (2020) 7619–7628. https://doi.org/10.1021/acs.est.0c00832.

[40] H. Liu, M. Zhang, H. Zhao, Y. Jiang, G. Liu, J. Gao, Enhanced dispersibility of metal–organic frameworks (MOFs) in the organic phase via surface modification for TFN nanofiltration membrane preparation, RSC Adv. 10 (2020) 4045–4057. https://doi.org/10.1039/C9RA09672H.

[41] D. Ma, S.B. Peh, G. Han, S.B. Chen, Thin-Film Nanocomposite (TFN) Membranes Incorporated with Super-Hydrophilic Metal–Organic Framework (MOF) UiO-66: Toward Enhancement of Water Flux and Salt Rejection, ACS Appl. Mater. Interfaces. 9 (2017) 7523–7534. https://doi.org/10.1021/acsami.6b14223.

CHAPTER 6 SUMMARY AND RECOMMENDATIONS

6.1 Summary

This chapter describes the general conclusions of the overall thesis and recommendations of this work. This thesis mainly focuses on improving membrane properties by incorporating MOFs to remove hazardous pollutants from wastewater. We focused on the synthesis of MOF, incorporated it into polymeric membranes, and investigated to improve the filtration performances in possible ways. The first two chapters described polymeric membranes, MOF, MOF membranes, and materials/techniques used in the research work.

The novel MOF-5 was synthesized and incorporated into polyethersulfone membrane matrix to investigate the hazardous textile dyes' removal performances (methylene blue and indigo carmine) in Chapter-3. The PES/MOF-5 nanofiltration membranes show high rejection performance of methylene blue and indigo carmine dyes with high permeability. The effect of MOF-5 incorporation on the membrane was characterized by XRD, FT-IR, SEM, EDX TGA, and contact angle measurements.

Chapter 4 discusses the high water-stable MOF (MIL-100 (Fe)) incorporated into chitosan biopolymer to remove the hazardous anionic, cationic dyes, and salts from the textile wastewater. The prepared CS/MIL-100 (Fe) composite membrane attained improved water permeability from 4.2 to 52.5 L/m^2 h with a 99% rejection of both MB and MO dyes. Besides, the CS/MIL-100 (Fe) membrane displays a higher rejection of more than 98% of MB dye and 51.6% of Mg^{2+} and 52.5% of SO_4^{2-} ions from the feed solution of $MB+MgSO_4$ mixtures. In addition, the CS/MIL-100 (Fe) membranes show excellent rejection and antifouling performances with high recycling stability of 6 cycles at a feed solution of MB, MO, and $MB/MgSO_4$ mixture.

Chapter-5 discusses the MIL-100 (Fe) incorporated into polysulfone membrane matrix to remove microplastic adsorbed dye contaminants from textile wastewater. The membrane that contained an optimal amount of hydrophilic MIL-100 (Fe) in the PSF matrix (0.5 wt.%, the M0.5 membrane) offered high MB rejection, superior permeability, enhanced pore size, and delivered high anti-fouling performance. Moreover, the performance of the M0.5 membrane was outstanding for various dye and MPs concentrations and TMPs. In addition, the M0.5 membrane delivered good salt rejection performance and could be reused for six cycles of MB dye rejection.

6.2 Recommendation

Based on these works' outcomes, MOF incorporation opens the possibility of improving the properties of the membranes towards wastewater treatment. As for the following, the recommendation for future research works and perspective direction for developing new MOF membranes for wastewater treatments. The prepared MOF membranes should be investigated with industrial effluent and study the performance.

APPENDIX A: LIST OF PUBLICATIONS

First Author

- **Gnanaselvan Gnanasekaran,** Sasikumar Balaguru., Arthanareeswaran G., **Young Sun Mok** (2019). Performance of composite PES/MOF-5 membranes for the treatment of textile wastewater. Desalination and Water Treatment, 156, 220-228.
- **Gnanaselvan Gnanasekaran,** M.S.P.Sudhakaran, Dilafruz Kulmatova, Jeongho Han, G.Arthanareeswaran, EunjinJwa, **Young SunMok** (2021). Efficient removal of anionic, cationic textile dyes and salt mixture using a novel CS/MIL-100 (Fe) based nanofiltration membrane, 284, Chemosphere, 131244.

Co-Author

- Sudhakaran MSP, **Gnanaselvan Gnanasekaran**, Parthiban Pazhamalai, Surjit Sahoo, Md Mokter Hossain, Roshan Mangal Bhattarai, Sang-Jae Kim, **Young Sun Mok**, (2019) Hierarchically Porous Nanostructured Nickel Phosphide with Carbon Particles Embedded by Dielectric Barrier Discharge Plasma Deposition as a Binder-Free Electrode for Hybrid Supercapacitors, ACS Sustainable Chem. Eng., 7, 17, 14805–14814.
- Sudhakaran MSP, Md Hossain, **Gnanaselvan Gnanasekaran**, **Young Sun Mok**, (2019) Dry reforming of propane over γ-Al2O3 and nickel foam supported novel SrNiO3 perovskite catalyst, Catalysts, 9(1), 68.

- Sudhakaran Moopri Singer Pandiyarajan, Ganesh Kumar Veerasubramani, Roshan Mangal Bhattarai, **Gnanaselvan Gnanasekaran,** Sang Jae Kim, **Young Sun Mok**, (2021) Designing an Interlayer-Widened MoS_2-Packed Nitrogen-Rich Carbon Nanotube Core–Shell Structure for Redox-Mediated Quasi-Solid-State Supercapacitors, ACS Appl. Energy Mater, 4, 3, 2218–2230.

List of submitted papers

- **Gnanasekaran Gnanaselvan,** G. Arthanareeswaran, **Mok Young Sun**, "Novel MIL-100 (Fe) incorporated high-flux polysulfone nanofiltration membrane and its excellent removal performance of microplastics adsorbing dye from textile wastewater"- Separation and Purification Technology.

APPENDIX B: LIST OF CONFERENCES

Conference
Gnanaselvan Gnanasekaran, Sudhakaran MSP, **Young Sun Mok**, “Removal of anionic dyes from the wastewater by MIL-100 Fe incorporated into natural polymeric membranes” at The Korean Society of Industrial and Engineering Chemistry -May 2019 **(Best Poster Award)**
Gnanaselvan Gnanasekaran, Sudhakaran MSP, **Young Sun Mok**, “Preparation of high flux MOFs embedded polysulfone (PSF/MOF) nanofiltration membranes for effective dye removal from aqueous solution” at 30th anniversary of the 2020 Korea Industrial and Engineering Chemistry Conference-Oct 2020 **(Best Presenter Award)**
Gnanaselvan Gnanasekaran, Arthanareeswaran, G, **Young Sun Mok**, “A novel high flux MOFs embedded polysulfone nanofiltration membranes for effective anionic and cationic dye removal” at International Congress on Membranes & Membrane Processes - Dec 2020
Gnanaselvan Gnanasekaran, Arthanareeswaran, G, Dilyafruz **Young Sun Mok**, “Removal of anionic and cationic dyes from wastewater using a composite of natural polymer/metal-organic framework (MOFs) membranes” at 4th International Conference on Desalination using Membrane Technology, Dec-2019 Australia.

Gnanaselvan Gnanasekaran, Arthanareeswaran, G, **Young Sun Mok**,

“Enhanced performance and antifouling of MOF membranes of cellulose acetate with hydrophilic nanoparticles of MIL-100 (Fe) for textile wastewater treatment” at

KiChe-2021, Busan.

Gnanaselvan Gnanasekaran, Arthanareeswaran, G, **Young Sun Mok**,

“A novel MOF/Cellulose acetate nanofiltration membranes for effective removal of microplastics with adsorbed contaminants from the textile wastewater” at

KSIEC, Busan. 2021

Gnanaselvan Gnanasekaran, Sudhakaran MSP, **Young Sun Mok**,

“Anionic dyes removal from wastewater using MOFs (MIL-100 Fe) incorporated polysulfone nanofiltration membrane” at

KSCT, Daejeon- Sept 2019

Gnanaselvan Gnanasekaran, Sudhakaran MSP, **Young Sun Mok**,

“A novel high flux MOFs embedded polysulfone nanofiltration membranes for effective anionic and cationic dye removal” at

Korean Society for Clean Technology Fall Conference- 2020

DECLARATION

I, **Gnanaselvan Gnanasekaran**, hereby declare that the thesis entitled **“Metal-organic frameworks (MOFs) incorporated polymeric membranes for the removal of hazardous materials from wastewater”** submitted to the Jeju National University, in partial fulfillment of the requirements for the award of the Degree of Doctor of Philosophy in **Faculty of Applied Energy Systems, Major of Energy & Chemical Engineering** is a record of original and independent research work done and published by me during the period of September 2018 to August 2021 under the supervision and guidance of **Prof. Young Sun Mok**, Department of Chemical and Biological Engineering, Jeju National University. This thesis is solely based on our publication in reputed journals. It has not been formed to award any other Degree/ Diploma/ Associateship/ Fellowship to any candidate of any university.

Gnanaselvan Gnanasekaran